



**Marlin Jeannette Pedrozo Peñafiel**

**Development of electro-analytical methods using sensors modified with nanomaterials for determination of primaquine, INHHQ, thiomersal and creatinine**

**Tese de Doutorado**

Thesis presented to the Programa de Pós-graduação em Química of PUC-Rio in partial fulfillment of the requirements for the degree of Doutor em Química.

Advisor: Prof. Ricardo Queiroz Aucélio

Rio de Janeiro  
May 2020



**Marlin Jeannette Pedrozo Peñafiel**

**Development of electro-analytical methods using sensors modified with nanomaterials for determination of primaquine, INHHQ, thiomersal and creatinine**

Thesis presented to the Programa de Pós-graduação em Química of PUC-Rio in partial fulfillment of the requirements for the degree of Doutor em Química. Approved by the Examination Committee.

**Prof. Ricardo Queiroz Aucélio**

Advisor

Departamento de Química - PUC-Rio

**Prof. Andréa Fernandes Arruda**

UFG

**Prof. Felipe Silva Semaan**

UFF

**Dr. Jefferson Rodrigues De Souza**

UFES

**Prof<sup>a</sup>. Sonia Letichevsky**

Departamento de Engenharia Química e de Materiais - PUC-Rio

**Dra. Joseany Almeida**

Departamento de Química - PUC-Rio

**Prof. Jones Limberger**

Departamento de Química - PUC-Rio

Rio de Janeiro, May 13 2020

All rights reserved

## Marlin Jeannette Pedrozo Peñafiel

Doctorate candidate in Chemistry of the Pontifical Catholic University of Rio de Janeiro (PUC-Rio). She holds a Master's degree in Chemistry from the Pontifical Catholic University of Rio de Janeiro (2016). She holds a degree in Chemistry from the University of the Atlantic in (2013). Has experience in Instrumental Analytical Chemistry.

### Bibliographic data

Pedrozo Peñafiel, Marlin Jeannette

Development of electro-analytical methods using sensors modified with nanomaterials for determination of primaquine, INHHQ, thiomersal and creatinine / Marlin Jeannette Pedrozo Peñafiel ; advisor: Ricardo Queiroz Aucélio. – 2020.

169 f. : il. color. ; 30 cm

Tese (doutorado)–Pontifícia Universidade Católica do Rio de Janeiro, Departamento de Química, 2020.

Inclui bibliografia

1. Química – Teses. 2. Voltametria. 3. Sensores eletroquímicos. 4. Pontos quânticos de grafeno. 5. Nanotubos de carbono. 6. Fármacos. I. Aucélio, Ricardo Queiroz. II. Pontifícia Universidade Católica do Rio de Janeiro. Departamento de Química. III. Título.

CDD: 540

## Acknowledgment

I thank God for the strength He gives me every day.

I would like to express my sincere and immense gratitude to Dr. Ricardo Queiroz Aucélio for his guidance, patience and friendship. He is an excellent example of a researcher and advisor.

I thank to the examining members for making themselves available and accepting the invitation.

I thank my family, my motivation.

I thank my friends, my joy.

I thank the LEEA group for helping.

I thank the Chemistry Department at PUC-Rio for the opportunity they gave me and the support for this research.

I thank the professors in the Chemistry Department for their lessons.

I thank Fatima for her support.

I thank the Brazilian agencies, CNPq, CAPES and FAPERJ, for the doctoral scholarship.

I thank all the people who influenced me in some way and were not mentioned before.

This study was financed in part by the Coordenação de Aperfeiçoamento de Pessoal de Nível Superior - Brasil (CAPES) - Finance Code 001.

## Abstract

Pedrozo Peñafiel, Marlin Jeannette; Aucélio, Ricardo Queiroz (advisor). **Development of electro-analytical methods using sensors modified with nanomaterials for determination of primaquine, INHHQ, thiomersal and creatinine.** Rio de Janeiro, 2020. 169p. Tese de Doutorado- Departamento de Química, Pontifícia Universidade Católica do Rio de Janeiro.

The goal of this work was the development of electro-analytical methods using electrodes modified with carbon-based nanomaterials for determination of analytes of biological (creatinine) and pharmacological interest (primaquine, INHHQ, thiomersal).

The determination of primaquine (antimalarial) and INHHQ (potential drug for treatment of neurodegenerative diseases) was proposed using glassy carbon (GC) electrode modified with multi-walled carbon nanotubes (MWCNTs) that promoted significant improvement in faradaic current and better peak resolution obtained using square-wave voltammetry (SWV) in Britton-Robinson (BR) buffer  $0.02 \text{ mol L}^{-1}$ ; pH 7.00 and KCl ( $0.25 \text{ mol L}^{-1}$ ). Although several methods to quantify primaquine are reported, many of these depend on procedure considered complex and laborious, therefore, the proposed GC modification using MWCNTs is comparatively easy, leading to a robust modification that produce repetitive results also providing amplification of the electrochemical signal due to the increased active area and improved electron-transfer rate. The GC/MWCNTs also provided, when working on a proper pH, higher resolution in detecting the different electrochemical steps involved in the redox process of primaquine. The electrode

enabled limit of detection (LOD) of 28 nmol L<sup>-1</sup> for primaquine and, when associated with a simple developed procedure, relying of liquid-liquid extraction (LLE) and thin-layer chromatography (TLC), it was achieved the selectivity and the capability to determine the lower levels expected in urine samples. In the case of INHHQ, a method for quantification by SWV was reported for the first time. In addition to the use of GC/MWCNTs electrode, a previous TLC procedure, enabled the selectivity required to determine INHHQ in brain tissue from Wistar rats. The LOD was 0.85 μmol L<sup>-1</sup> and the linear dynamic range covered two orders of magnitude (10<sup>-6</sup> to 10<sup>-5</sup> mol L<sup>-1</sup>).

Graphene quantum dots (GQDs) was chosen to chemically modify electrodes used to determine thiomersal and creatinine. GQDs are nanometric fragments of graphene (present in dispersions as monolayer, few layer or multilayer) where electron transport is confined in their dimensions. GQDs are carbon-based structure that are bio-compatible and present low toxicity. The research presents a new approach for the determination of thimerosal (preservative in vaccines and cosmetics) in influenza vaccines using GQDs as a modifier of the GC electrode and exploring the synergistic effect between GQDs, visible radiation and the applied potential difference. This system promotes thiomersal oxidation, producing a significant increase in response (Hg/Hg<sup>2+</sup> redox pair) in terms of current intensity using SWV and BR buffer (0.02 mol L<sup>-1</sup>; pH 4.00 with KCl at 0.25 mol L<sup>-1</sup>). The LOD was 0.85 μmol L<sup>-1</sup> with linear dynamic range covering three orders of magnitude (10<sup>-6</sup> to 10<sup>-4</sup> mol L<sup>-1</sup>). For creatinine, a biomarker for the renal dysfunction, a GQDs-copper composite was used to modify a gold electrode. Determination of creatinine was made using SWV (BR buffer 0.02 mol L<sup>-1</sup>; pH 4.00 with KCl at 0.25 mol L<sup>-1</sup>). The method relied on the decreasing of the Cu<sup>2+</sup>/Cu

oxidation peak in the presence of creatinine, enabling LOD of  $50 \text{ nmol L}^{-1}$  and linear dynamic range covering three orders of magnitude ( $10^{-6}$  to  $10^{-4} \text{ mol L}^{-1}$ ). The SWV response of creatinine was attributed to the formation of creatinine- $\text{Cu}^{2+}$  complex being reasonably selective towards this analyte. All procedures developed by voltammetry were adequately compared with reference methods, being statistically compatible.

## **Keywords**

Voltammetry; Electrochemical sensors; Graphene quantum dots; Carbon nanotubes; Drugs.

## Resumo

Pedrozo Peñafiel, Marlin Jeannette; Aucélio, Ricardo Queiroz. **Desenvolvimento de métodos eletro-analíticos usando sensores modificados com nanomateriais para determinação de primaquina, INHHQ, tiomersal e creatinina.** Rio de Janeiro, 2020. 169p. Tese de Doutorado, Departamento de Química, Pontifícia Universidade Católica do Rio de Janeiro.

O objetivo deste trabalho foi o desenvolvimento de métodos eletro-analíticos utilizando eletrodos modificados com nanomateriais a base de carbono para determinação de analitos de interesse biológico (creatinina) e farmacológico (primaquina, INHHQ, tiomersal).

A determinação de primaquina (antimalárico) e de INHHQ (potencial medicamento para o tratamento de doenças neurodegenerativas) foi proposta usando eletrodo de carbono vítreo (GC) modificado com nanotubos de carbono de paredes múltiplas (MWCNTs) o qual promoveu uma melhora significativa na corrente faradaica e na resolução de pico obtida usando voltametria de onda quadrada (SWV) em tampão Britton-Robinson (BR)  $0.02 \text{ mol L}^{-1}$ ; pH 7.00 e KCl ( $0.25 \text{ mol L}^{-1}$ ). Embora vários métodos para quantificar primaquina estejam reportados, muitos deles dependem de procedimentos considerados complexos e trabalhosos, portanto, a modificação proposta de GC usando MWCNTs é comparativamente fácil, levando a uma modificação robusta que produz resultados repetitivos, fornecendo também amplificação do sinal eletroquímico devido à área ativa aumentada e a taxa de transferência eletrônica aprimorada. Os GC/MWCNTs também forneceram, ao trabalhar em um pH adequado, maior resolução na detecção das diferentes etapas eletroquímicas envolvidas no processo redox da primaquina.

O eletrodo permitiu o limite de detecção (LOD) de  $28 \text{ nmol L}^{-1}$  para a primaquina e, quando associado a um procedimento simples baseado na extração líquido-líquido (LLE) e cromatografia em camada fina (TLC), foi alcançada a seletividade e a capacidade de determinar os níveis mais baixos esperados em amostras de urina. No caso do INHHQ, um método para quantificação por SWV foi relatado pela primeira vez. Além do uso do eletrodo GC/MWCNTs um prévio procedimento de TLC, permitiu a seletividade necessária para determinar o INHHQ no tecido cerebral de ratos Wistar. O LOD foi de  $0.85 \text{ } \mu\text{mol L}^{-1}$  e a faixa dinâmica linear cobriu duas ordens de magnitude ( $10^{-6}$  a  $10^{-5} \text{ mol L}^{-1}$ ).

Os pontos quânticos de grafeno (GQDs) foram escolhidos para modificar quimicamente os eletrodos utilizados para determinar tiomersal e creatinina. GQDs são fragmentos nanométricos de grafeno (presentes em dispersões como monocamada, poucas camadas ou multicamadas) onde o transporte de elétrons é confinado em suas dimensões. GQDs são estruturas baseadas em carbono que são biocompatíveis e apresentam baixa toxicidade. A pesquisa apresenta uma nova abordagem para a determinação de tiomersal (conservante em vacinas e cosméticos) em vacinas contra influenza usando GQDs como modificador do eletrodo de GC e explorando o efeito sinérgico entre GQDs, radiação visível e a diferença de potencial aplicado. Este sistema promove a oxidação do tiomersal, produzindo um aumento significativo na resposta (par redox  $\text{Hg}/\text{Hg}^{2+}$ ) em termos de intensidade de corrente usando SWV e tampão BR ( $0.02 \text{ mol L}^{-1}$ ; pH 4.00 com KCl a  $0.25 \text{ mol L}^{-1}$ ). O LOD foi de  $0.85 \text{ } \mu\text{mol L}^{-1}$  e a faixa dinâmica linear cobriu três ordens de grandeza ( $10^{-6}$  a  $10^{-4} \text{ mol L}^{-1}$ ). Para a creatinina (um biomarcador para a disfunção renal), um composto de GQDs-cobre foi usado para modificar um eletrodo de ouro. A determinação da creatinina foi realizada utilizando SWV

(tampão BR 0.02 mol L<sup>-1</sup>; pH 4.00 com KCl a 0.25 mol L<sup>-1</sup>). O método contou com a diminuição do pico de oxidação Cu/Cu<sup>2+</sup> na presença de creatinina, permitindo LOD de 50 nmol L<sup>-1</sup> e faixa dinâmica linear, cobrindo três ordens de magnitude (10<sup>-6</sup> a 10<sup>-4</sup> mol L<sup>-1</sup>). A resposta SWV da creatinina foi atribuída à formação do complexo creatinina-Cu<sup>2+</sup>, sendo razoavelmente seletiva em relação a este analito. Todos os procedimentos desenvolvidos por voltametria foram adequadamente comparados com métodos de referência, sendo estatisticamente compatíveis.

## **Palavras-chave**

Voltametria; Sensores eletroquímicos; Pontos quânticos de grafeno; Nanotubos de carbono; Fármacos.

## Table of contents

1	Introduction	23
1.1	Contextualization of work	23
1.2	Thesis structure	26
1.3	Objectives	27
1.3.1	General objective	27
1.3.2	Specific objectives	28
2	Theoretical fundamentals	30
2.1	Chemically modified electrodes	30
2.2	Electrochemical sensor based on nanomaterials	33
2.2.1	Carbon nanotubes	34
2.2.2	Quantum dots	36
2.2.2.1	Production of graphene quantum dots	37
2.2.2.2	Analytical approaches through the use of graphene quantum dots as modifiers in electro-analytical sensors	40
2.3	Electrochemical techniques	41
2.3.1	Cyclic voltammetry	41
2.3.2	Square-wave voltammetry	43
3	Materials and methods	46
3.1	Instrumentation	46
3.2	Reagents and materials	49
3.3	Preparation of supporting electrolyte	50
3.4	Preparation of nanomaterials used as electrode modifiers	50
3.4.1	Preparation of graphene quantum dots	50
3.4.2	Preparation of graphene quantum dots modified with $\text{Cu}(\text{NO}_3)_2$	51
3.4.3	Synthesis of $\text{Cu}(\text{OH})_2$	51
3.5	Modifications of the different electrodes for the determination of the analytes	51
3.5.1	Dispersion of MWCNTs and its use as modifier for the determination of primaquine and INHHQ	51
3.5.2	Modification of the glassy carbon electrode (GCE) with GQDs for determination of thiomersal	53
3.5.3	Modification of the gold electrode with GQDs-Cu for determination of creatinine	54

3.6 Preparation of samples, voltammetric measurements and other procedures	54
3.6.1 Procedures for primaquine	54
3.6.1.1 Standard solutions, voltammetric measurements for primaquine determination	54
3.6.1.2 Liquid-liquid extraction and thin-layer chromatography for determination of primaquine	55
3.6.1.3 High-performance liquid chromatographic analysis of primaquine	56
3.6.2 Procedures for INHHQ	56
3.6.2.1 Standard solutions, voltammetric measurements procedures for INHHQ determination	56
3.6.2.2 Rats' brain samples treatment and thin-layer chromatography for determination of INHHQ	57
3.6.2.3 High-performance liquid chromatographic analysis of INHHQ	58
3.6.3 Procedures for thiomersal	58
3.6.3.1 Standard solutions, voltammetric measurements, mercury cold vapor atomic absorption measurements.	58
3.6.3.2 Analytical procedure for determination of Hg by multipass-cold vapor-AAS	59
3.6.3.2.1 Mercury cold vapor atomic absorption measurements	59
3.6.3.2.2 Vaccine analysis by mercury cold vapor atomic absorption	60
3.6.4 Procedures for creatinine	60
3.6.4.1 Standard solutions, voltammetric measurements and HPLC procedure for creatinine determination	60
3.6.4.2 High-performance liquid chromatographic analysis of creatinine	61
4 Square-wave voltammetric determination of primaquine in urine using a multi-walled carbon nanotube modified electrode	62
4.1 Primaquine and analytical methods for its determination	62
4.2 Results and discussion	65
4.2.1 Electrochemical studies	65
4.2.2 Optimization of measurement conditions	71
4.2.3 Analytical characteristics	73
4.2.4 Strategy for the application of the method in the analysis of urine	75
4.3 Partial conclusion	79

5 Square-Wave voltammetric determination of INHHQ, a promising metal-protein attenuating compound for the treatment of Alzheimer's disease, using a MWCNT modified glassy carbon electrode	80
5.1 INHHQ and analytical methods for its determination	80
5.2 Results and discussion	83
5.2.1 Electrochemical properties of INHHQ on a glassy carbon electrode modified with MWCNTs	83
5.2.2 Electrochemical behavior of INHHQ and precursors at GC/MWCNTs electrode	87
5.2.3 Square-wave voltammetry for INHHQ using the GC/MWCNTs electrode	89
5.2.4 Analytical performance	92
5.2.5 Determination of INHHQ in wistar rats' brains	95
5.3 Partial conclusion	97
6 Indirect voltammetric determination of thiomersal in influenza vaccine using photo-degradation and graphene quantum dots modified glassy carbon electrode	98
6.1 Thiomersal and analytical methods for its determination	98
6.2 Results and discussion	102
6.2.1 Characterization of GQDs in aqueous dispersion and modification of the GC	102
6.2.2 Cyclic voltammogram of thiomersal onto the GQDs-modified GC electrode	104
6.2.3 Stability of the GC/GQDs electrode	108
6.2.5 Electrochemical behavior of thiomersal on GC/GQDs electrode	111
6.2.6 Square-wave voltammetry using the GC/GQDs electrode: study of synergetic effect between applied potential and sample irradiation	112
6.2.7 Analytical performance	117
6.2.8 Determination of thiomersal in influenza vaccines	118
6.3. Partial conclusion	119
7 Voltammetric determination of creatinine using a gold electrode modified with Nafion mixed with graphene quantum dots/copper	121
7.1 Creatinine and analytical methods for its determination	121
7.2 Results and discussion	129
7.2.1 Characterization of GQDs and GQDs-Cu in aqueous dispersion	129

7.2.2 Cyclic Voltammograms of creatinine using a gold electrode modified with Nafion-GQDs-Cu	132
7.2.3 Effect of Nafion and graphene quantum dots on the electrode surface	136
7.2.4 Influence of pH	138
7.2.5 Analytical performance	142
7.2.6 Interference study	145
7.2.7 Determination of creatinine in urine	146
7.3 Partial conclusion	148
8 General conclusion	149
9 Future work	151
10 Reference	152
11 Attachment	168
A Published papers	168
B Participation in congress	170

## List of figures

- Figure 2.1.** Illustration of a potential application in SWV, where:  $a$  is the pulse width;  $\Delta E_s$  is the scan increment and  $\tau$  is the time. Source: Adapted from [56,55]. 45
- Figure 3.1.** Electrochemical cell: (A) Platinum auxiliary electrode; (R) Reference electrode of Ag|AgCl<sub>(sat)</sub>; (W) Working electrode. 46
- Figure 3.2.** Schematic of the set-up used for the photo-reactor coupled to the electrochemical system. 47
- Figure 3.3.** General methodology for the modification of electrodes with nanomaterials. 52
- Figure 3.4.** (A) Cyclic voltammograms of 1.0 mmol L<sup>-1</sup> K<sub>3</sub>[Fe(CN)<sub>6</sub>] in 0.5 mol L<sup>-1</sup> KNO<sub>3</sub> solution at the (a) bare unmodified GC electrode and (b) MWCNT-modified GC electrode at 100 mV s<sup>-1</sup>. (B) Cyclic voltammograms of 1.0 mmol L<sup>-1</sup> K<sub>3</sub>[Fe(CN)<sub>6</sub>] in 0.5 mol L<sup>-1</sup> KNO<sub>3</sub> solution at MWCNT-modified GC electrode at sweep rates: (a) 10 (b) 30 (c) 50 (d) 70 (e) 100 mV s<sup>-1</sup> (C)  $I_{pa}$  versus square root of sweep rate. 53
- Figure 4.1.** Structure of primaquine (8- [4-amino-1-methyl butylamino]) - 6-methoxyquinoline). 62
- Figure 4.2.** (A) Scanning electron microscopy of MWCNTs onto GC. (B) CV response from primaquine: (a) GC/MWCNTs electrode and (b) bare GC electrode. (C) CV response from primaquine using GC/MWCNTs electrode: (a) 1<sup>st</sup> scan, (b) 2<sup>nd</sup> scan at 100 mV s<sup>-1</sup>. (D) Study of the amount of MWCNTs onto the surface of GC. Experimental conditions: Britton-Robinson Buffer 0.02 mol L<sup>-1</sup> with KCl 0.25 mol L<sup>-1</sup> and pH 7.0. 68
- Figure 4.3.** CV response from primaquine ( $2 \times 10^{-4}$  mol L<sup>-1</sup>) using (a) GC/MWCNTs electrode and (b) bare GC electrode at: (A) pH 4.0 (B) pH 7.0 and (C) pH 9.0. BR Buffer 0.02 mol L<sup>-1</sup> with KCl 0.25 mol L<sup>-1</sup> and 100 mV s<sup>-1</sup> scan rate. 69
- Figure 4.4.** (A) Plot of  $E_p$  (main oxidation peak) versus pH using the GC/MWCNTs electrode. (B) Redox pair at lower potential range (peak 1/peak 3). (C)  $E_p$  as a function of scan rate. (D)  $I_p$  as a function of  $v^{1/2}$ : (a) Lower rates ( $R^2 = 0.979$  from 20 to 100 mV s<sup>-1</sup>) and (b) higher rates ( $R^2 = 0.995$  from 200 to 1000 mV s<sup>-1</sup>). BR Buffer 0.02 mol L<sup>-1</sup> with KCl 0.25 mol L<sup>-1</sup>. Primaquine at  $2 \times 10^{-4}$  mol L<sup>-1</sup>. 71

**Figure 4.5.** SWV studies for primaquine ( $1 \times 10^{-4} \text{ mol L}^{-1}$ ) using MWCNTs. (A) voltammograms at: a) pH 4.0, b) pH 7.0 and c) pH 9.0. (B)  $I_p$  in function of  $f$  for main oxidation peak ( $R^2 = 0.996$ ); C)  $E_p$  in function of the log  $f$  ( $R^2 = 0.996$ ). BR Buffer  $0.02 \text{ mol L}^{-1}$  with KCl  $0.25 \text{ mol L}^{-1}$ .

72

**Figure 4.6.** (A) SWV of primaquine using GC/MWCNTs electrode: a) 0, b)  $5 \times 10^{-7}$ , c)  $1 \times 10^{-6}$ , d)  $1.5 \times 10^{-6}$ , e)  $2 \times 10^{-6}$ , f)  $2.5 \times 10^{-6}$ , g)  $3 \times 10^{-6}$ , h)  $3.5 \times 10^{-6}$ , i)  $4 \times 10^{-6}$ , j)  $4.5 \times 10^{-6}$ , k)  $5 \times 10^{-6} \text{ mol L}^{-1}$  and (B) Analytical curve:  $I_p (\mu\text{A}) = (2.08 \pm 0.04) \times 10^6 C_{\text{primaquine}} + (1.19 \pm 0.10)$ , ( $R^2 = 0.999$ ). (C) SWV response of primaquine using bare GC: a) 0, b)  $3 \times 10^{-5}$ , c)  $6 \times 10^{-5}$ , d)  $9 \times 10^{-5}$ , e)  $1.2 \times 10^{-4}$ , f)  $1.5 \times 10^{-4}$ , g)  $1.3 \times 10^{-4} \text{ mol L}^{-1}$ . (D) Analytical curve:  $I_p (\mu\text{A}) = (8.92 \pm 0.50) \times 10^4 C_{\text{primaquine}} + (7.11 \pm 0.25)$ , ( $R^2 = 0.984$ ). BR buffer  $0.04 \text{ mol L}^{-1}$  with KCl  $0.5 \text{ mol L}^{-1}$  at pH 7.0.

74

**Figure 4.7.** SWV voltammograms at GCE/MWCNTs (a) Urine control after deproteinization, LEE and TLC; (b) Urine fortified with primaquine ( $1.0 \times 10^{-5} \text{ mol L}^{-1}$ ) after LEE and TLC; (c) Urine control sample only after deproteinization.

78

**Figure 5.1.** INHHQ structure (8-hydroxyquinoline-2-carboxaldehyde isonicotinoyl hydrazone).

81

**Figure 5.2.** Cyclic voltammograms from INHHQ using (A) different quantities of MWCNTs onto electrode surface (peak current at +209 mV in detail). (B) a) Blank solution at GC/MWCNTs electrode ( $30 \mu\text{g}$  MWCNTs) b) GC/MWCNTs electrode ( $30 \mu\text{g}$  MWCNTs) with INHHQ: Peak 1 at -47 mV, peak 2 at +209 mV, peak 3 at +926 mV, peak 4 at -215 mV, peak 5 at -966 mV, peak 6 at -1267 mV. (C) Bare GC electrode: Peak 1' at +418 mV, peak 2' at +867 mV, peak 3' at -590 mV. INHHQ at  $2 \times 10^{-4} \text{ mol L}^{-1}$ , BR buffer ( $0.02 \text{ mol L}^{-1}$ ; pH 11.0 in KCl  $0.25 \text{ mol L}^{-1}$ ) and  $100 \text{ mV s}^{-1}$  scan rate.

84

**Figure 5.3.** Cyclic voltammograms of INHHQ at  $1 \times 10^{-4} \text{ mol L}^{-1}$ : (A) at pH 7 (peak 1 at +160 mV, peak 2 at +438 mV, peak 3 at +1070 mV, peak 4 at -67 mV, peak 5 at -781 mV, peak 6 at -1127 mV). (B) at pH 9 (peak 1 at +47 mV, peak 2 at +297 mV, peak 3 at +1029 mV, peak 4 at -100 mV, peak 5 at -872 mV, peak 6 at -1248 mV). (C) at pH 11 (peak 1 at -47 mV, peak 2 at +209 mV, peak 3 at +926 mV, peak 4 at -215 mV, peak 5 at -966 mV, peak 6 at -1267 mV). (D) Cyclic voltammogram of INHHQ using different potential ranges at pH 11. Britton-Robinson Buffer  $0.02 \text{ mol L}^{-1}$  with KCl  $0.25 \text{ mol L}^{-1}$  and scan rate at  $100 \text{ mV s}^{-1}$ .

86

**Figure 5.4.** Cyclic voltammograms of (A) INHHQ at  $6 \times 10^{-4} \text{ mol L}^{-1}$ . (B) 8-hydroxyquinoline-2-carboxaldehyde at the  $6 \times 10^{-4} \text{ mol L}^{-1}$ . (C) isoniazid at  $6 \times 10^{-4} \text{ mol L}^{-1}$  and 8-

hydroxyquinoline at the  $6 \times 10^{-4} \text{ mol L}^{-1}$  using BR Buffer (pH 11.0;  $0.02 \text{ mol L}^{-1}$  with KCl  $0.25 \text{ mol L}^{-1}$ ) and scan rate at  $100 \text{ mV s}^{-1}$ . 89

**Figure 5.5.** (A) Anodic square-wave voltammogram of INHHQ at  $4 \times 10^{-5} \text{ mol L}^{-1}$  at  $f = 30 \text{ Hz}$ . (B) Histogram of the effect of pH on the INHHQ SWV peak current at  $+303 \text{ mV}$  at  $f = 30 \text{ Hz}$ . (C)  $I_p$  in function of  $f$  for the peak at  $+303 \text{ mV}$  ( $R^2 = 0.997$ ). (D)  $E_p$  in function of the  $\log f$  ( $R^2 = 0.990$ ). Britton-Robinson Buffer  $0.02 \text{ mol L}^{-1}$  with KCl  $0.25 \text{ mol L}^{-1}$  at pH 11.0 and sweep rate was  $100 \text{ mV s}^{-1}$ . 90

**Figure 5.6.**  $I_p$  versus scan rate of INHHQ (peak at  $+209 \text{ mV}$  or peak 2 of Fig. 3B) at higher (A) and at lower (B) scan rates, using GC/MWNTCs.  $I_p$  versus scan rate of (peak at  $+418 \text{ mV}$  or peak 1 of Fig. 3C) at higher (C) and at lower (D) scan rates, using bare GC electrode. Solution containing  $2 \times 10^{-4} \text{ mol L}^{-1}$  of INHHQ. BR Buffer  $0.02 \text{ mol L}^{-1}$  with KCl  $0.25 \text{ mol L}^{-1}$  and sweep rate was  $100 \text{ mV s}^{-1}$  and pH 11. 92

**Figure 5.7.** (A) Analytical curve (peak current at  $+303 \text{ mV}$ ) for INHHQ at a GC-MWNTCs electrode ( $R^2 = 0.996$ ). (B) Square-wave voltammetric response of INHHQ using GC-MWNTCs electrode: (a) 0, (b)  $3.0 \times 10^{-6}$  (c)  $9.2 \times 10^{-6}$ , (d)  $2.2 \times 10^{-5}$ , (e)  $3.5 \times 10^{-5}$ , (f)  $4.2 \times 10^{-5}$ , (g)  $5.7 \times 10^{-5}$ , (h)  $6.4 \times 10^{-5} \text{ mol L}^{-1}$ . BR Buffer  $0.02 \text{ mol L}^{-1}$  with KCl  $0.25 \text{ mol L}^{-1}$  at pH 11 and  $100 \text{ mV s}^{-1}$  scan rate. (C) TLC  $R_f$  values of INHHQ and related compounds. 94

**Figure 6.1.** Thiomersal structure (sodium ethylmercurithiosalicylate). 99

**Figure 6.2.** (A) Photoluminescence spectrum emission GQDs in aqueous dispersion (excitation at  $357 \text{ nm}$ ). (B) Raman spectra of GQDs. (C) Scanning transmission electronic microscopy image of GQDs. (D) Size distribution of GQDs in aqueous dispersion obtained by DLS with insert showing  $\xi$ -potential of GQDs in aqueous dispersion in function of pH. 103

**Figure 6.3.** Cyclic voltammograms of thiomersal (at  $3.5 \times 10^{-4} \text{ mol L}^{-1}$ ) using a) GC/GQDs electrode and bare b) GC electrode: Peak 1 at  $+189 \text{ mV}$ ; peak 2 at  $+1004 \text{ mV}$ ; peak 3 at  $-33 \text{ mV}$ . BR buffer pH 4.0 ( $0.02 \text{ mol L}^{-1}$ ; KCl  $0.25 \text{ mol L}^{-1}$ ) and  $100 \text{ mV s}^{-1}$  scan rate. 105

**Figure 6.4.** Cyclic voltammogram of the blank solution using the GC/GQDs electrode. BR buffer ( $0.02 \text{ mol L}^{-1}$ ; pH 4.0 in KCl  $0.25 \text{ mol L}^{-1}$ ) and  $100 \text{ mV s}^{-1}$  scan rate. 105

Figure 6.5. (A) Mechanism oxidation of thiomersal reported by da Silva *et al.* [113] (B) Redox process concerning ethylmercury

106

**Figure 6.6.** Cyclic voltammograms using GC/GQDs electrode. (A)  $\text{Hg}^{2+}$  ( $2 \times 10^{-4} \text{ mol L}^{-1}$ ). (B) Thiosalicylic acid ( $3 \times 10^{-3} \text{ mol L}^{-1}$ ). (C) Dithiobenzoic acid ( $3 \times 10^{-3} \text{ mol L}^{-1}$ ). BR buffer pH 4.0 ( $0.02 \text{ mol L}^{-1}$ ;  $\text{KCl } 0.25 \text{ mol L}^{-1}$ ) and  $100 \text{ mV s}^{-1}$  scan rate.

107

**Figure 6.7.** (A) Contact angle image of the surface of glassy carbon electrode modified with GQDs dispersed in water and in 1,4-dioxane. (B) Histogram of the electrochemical response of thiomersal ( $n = 4$ ) using GC electrode modified with GQDs obtained by hydro-exfoliation in water and then dispersed in either 1,4-dioxane and in water. (C) Peak current (at +189 mV) in function of the amount of GQDs, produced by hydro-exfoliation of different masses of citric acid, deposited onto the GC. (D) Cyclic voltammograms of thiomersal at different pH. a) pH 2,  $E_p = +184.1 \text{ mV}$ , b) pH 3,  $E_p = +184.3 \text{ mV}$ , c) pH 4,  $E_p = +189.0 \text{ mV}$ , d) pH 5,  $E_p = +177.1 \text{ mV}$ , e) pH 6,  $E_p = +175.6 \text{ mV}$ , f) pH 7,  $E_p = +174.3 \text{ mV}$ , g) pH 8,  $E_p = +169.8 \text{ mV}$ , h) pH 9,  $E_p = +169.4 \text{ mV}$ , i) pH 10, no signal. BR buffer  $0.02 \text{ mol L}^{-1}/\text{KCl } 0.25 \text{ mol L}^{-1}$  (scan rate at  $100 \text{ mV s}^{-1}$ ).

110

**Figure 6.8.** (A) Cyclic voltammograms of thiomersal (at  $2 \times 10^{-4} \text{ mol L}^{-1}$ ) using the GC/GQDs electrode at different scan rates (10 to  $900 \text{ mV s}^{-1}$ ). (B) peak current ( $I_p$ ) in function of square root of the scan rate ( $v^{1/2}$ ) with  $R^2 = 0.990$ . (C) Cyclic voltammogram of thiomersal performed within the limited potential range between  $-200$  and  $+600 \text{ mV}$ . (D)  $I_{p1}/I_{p3}$  ratio in function of the scanning rate for the redox pair (peak 1 and 3) obtained in CV. Experiments made with BR buffer pH 4.0 ( $0.02 \text{ mol L}^{-1}/\text{KCl } 0.25 \text{ mol L}^{-1}$ ).

112

**Figure 6.9.** SWV response from thiomersal ( $2 \times 10^{-4} \text{ mol L}^{-1}$ ) using GC/GQDs electrode. (A) Measurements made (a) in the dark and (b) under exposition to visible radiation. (B) Measurements made (a) in the dark, (b) in the dark after 20 cyclic voltammetric cycles and (c) under exposition to visible radiation after 20 cyclic voltammetric cycles. (C) Comparative of analytical signals obtained by SWV using different experimental conditions. BR Buffer  $0.02 \text{ mol L}^{-1}$  (pH 4.0) with  $\text{KCl } 0.25 \text{ mol L}^{-1}$ ; SWV scanning rate at  $100 \text{ mV s}^{-1}$  and CV cycles at  $100 \text{ mV s}^{-1}$  from  $\pm 300 \text{ mV}$ .

114

**Figure 6.10.** Square-wave voltammetric signal measured under sample irradiation using different number of previous voltammetric cycles.

115

**Figure 6.11.** Absorption time profiles and concentrations of measured mercury cold vapor obtained from solutions added to the reaction cell ( $\text{SnCl}_2$  20 %) coupled to the cold vapor-AAS system: a) BR buffer solution ( $7 \text{ ng L}^{-1}$ ); b) thiomersal in BR buffer solution ( $12 \text{ ng L}^{-1}$ ); c) thiomersal in BR buffer solution after voltammetric cycles and SWV using bare GC electrode ( $17 \text{ ng L}^{-1}$ ); d) thiomersal in buffer solution after voltammetric cycles and SWV using GC/GQDs electrode in the dark ( $58 \text{ ng L}^{-1}$ ); e) thiomersal in buffer solution after voltammetric cycles and SWV using GC/GQDs electrode and exposition to visible radiation ( $112 \text{ ng L}^{-1}$ ). 116

**Figure 6.12.** (A) SWV of thiomersal using GC/GQDs electrode: a) 0, b)  $4 \times 10^{-6}$ , c)  $8 \times 10^{-6}$ , d)  $1.2 \times 10^{-5}$ , e)  $1.6 \times 10^{-5}$ , f)  $2 \times 10^{-5}$ , g)  $2.4 \times 10^{-5}$ , h)  $2.8 \times 10^{-5}$ , i)  $3.2 \times 10^{-5} \text{ mol L}^{-1}$ , and (B) analytical curve:  $I_p = (6.47 \pm 0.23) \times 10^5 C_{\text{thiomersal}} + (11.1 \pm 4.4)$  ( $R^2=0.991$ ). 118

**Figure 7.1.** Creatinine structure (2-Amino-1-methyl-5H-imidazol-4-one). 121

**Figure 7.2.** (A) Photoluminescence emission GQDs and GQDs-Cu (excitation at 337 nm). (B) Raman spectra of GQDs and GQDs-Cu. (C) STEM image of GQDs, (D) STEM image of GQDs-Cu. (E) Size distribution obtained by DLS for GQDs and  $\zeta$ -potential of GQDs in function of pH. (F) Size distribution obtained by GQDs-Cu and  $\zeta$ -potential of GQDs-Cu in function of pH. 131

**Figure 7.3.** (A) XPS general survey spectra of GQDs-Cu. (B) High resolution C 1s peaks with a and b corresponding to C-C  $\text{sp}^2$  e  $\text{sp}^3$ , and COOH groups, respectively. (C) High resolution Cu 2p peaks with profile corresponding to copper(I) oxide or Cu metal. 132

**Figure 7.4.** Cyclic voltammograms using Au/Nafion-GQDs-Cu electrode for a solution without creatinine (grey) and with creatinine (black). Experimental conditions: BR buffer ( $0.02 \text{ mol L}^{-1}$ ; pH 4.0 in KCl  $0.25 \text{ mol L}^{-1}$ ) and  $100 \text{ mV s}^{-1}$  scan rate. Creatinine at  $4 \times 10^{-5} \text{ mol L}^{-1}$ . 134

**Figure 7.5.** Cyclic voltammograms using the Au/Nafion-GQDs-Cu electrode and sequential additions of creatinine. (a) blank, (b) creatinine addition. Experimental conditions: BR buffer ( $0.02 \text{ mol L}^{-1}$ ; pH 4.0 in KCl  $0.25 \text{ mol L}^{-1}$ ) and  $100 \text{ mV s}^{-1}$  scan rate. 136

**Figure 7.6.** (A) Cyclic voltammograms using the Au/Nafion-GQDs-Cu electrode and sequential additions of creatinine. (a) blank, (b) creatinine addition. (B) Study of proportion of Nafion: GQDs-Cu dispersion. Experimental conditions: BR

buffer (0.02 mol L<sup>-1</sup>; pH 4.0 in KCl 0.25 mol L<sup>-1</sup>) and 100 mV s<sup>-1</sup> scan rate. 137

**Figure 7.7.** (A) Cyclic voltammograms of creatinine at different scan rates (10 to 800 mV s<sup>-1</sup>), using Au/Nafion-GQDs-Cu electrode. Experimental conditions: BR Buffer pH 4.0; 0.02 mol L<sup>-1</sup> in KCl 0.25 mol L<sup>-1</sup>. Solution containing 4 × 10<sup>-5</sup> mol L<sup>-1</sup> of creatinine. (B) Peak current (*I<sub>p</sub>*) measured at *E<sub>p</sub>* = +350 mV in function of the scan rate. 138

**Figure 7.8.** Voltammetric responses using SWV) and the Au/Nafion-GQDs-Cu electrode. (A) without addition of creatinine at different pH values. (B) at pH 3 without (a) and with (b) creatinine. (C) at pH 4 without (a) and with (b) creatinine. (D) at pH 5 without (a) and with (b) creatinine. (E) at pH 6 without (a) and with (b) creatinine. (F) at pH 7 without (a) and with (b) creatinine. BR Buffer 0.02 mol L<sup>-1</sup> with KCl 0.25 mol L<sup>-1</sup> with creatinine addition (4 × 10<sup>-5</sup> ml L<sup>-1</sup>). 140

**Figure 7.9.** Effect of Nafion-GQDs-Cu on the Au electrode surface in terms of the relative current produced in absence and in the presence of creatinine. Experimental conditions: BR Buffer pH 4.0; 0.02 mol L<sup>-1</sup> in KCl 0.25 mol L<sup>-1</sup>. 142

**Figure 7.10.** (A) Square-wave voltammetric responses of creatinine using Au/Nafion-GQDs-Cu electrode (peak current at *E<sub>p</sub>* = +415 mV). (B) Blank (in grey) and linear responses for creatinine (in black): (a) Lower concentration range (5 × 10<sup>-8</sup> to 1 × 10<sup>-6</sup> mol L<sup>-1</sup>) and (b) higher concentration range (5 × 10<sup>-6</sup> to 4.5 × 10<sup>-4</sup> mol L<sup>-1</sup>) with  $I_{p0}/I_{p(cre)} = (6.56 \pm 0.16) \times 10^3 C_{creatinine} + (1.48 \pm 0.03)$  and R<sup>2</sup> = 0.990. Experimental conditions: BR Buffer pH 4.0; 0.02 mol L<sup>-1</sup> in KCl 0.25 mol L<sup>-1</sup>. 144

## List of tables

<b>Table 4.1.</b> Summary of characteristics of analytical methods for primaquine in different samples	65
<b>Table 4.2.</b> Evaluation of interference imposed by urine components in the signal from primaquine	78
<b>Table 6.1.</b> Analysis results of thiomersal in vaccines using the proposed SWV method and by using cold vapor-AAS. Standard deviation for $n = 3$ . Confidence limit of 95%; two tails, each with $\alpha/2 = 0.025$ .	119
<b>Table 7.1.</b> Summary of characteristics of analytical methods for creatinine.	126
<b>Table 7.2.</b> Summary of characteristics of electrochemical methods for creatinine in different samples	128
<b>Table 7.3.</b> Quantification study after urine samples fortification with creatinine for the estimation of the original analyte content.	147
<b>Table 7.4.</b> Analysis results of creatinine in urine samples using the proposed SWV method and by HPLC. Standard deviation for $n = 3$ . Confidence limit of 95%; two tails, each with $\alpha/2 = 0.025$ .	148

## List of abbreviations

$\Delta E_s$	Scan Increment
2-D	Two-Dimensional
<i>a</i>	Amplitude
$A\beta$	Proteína $\beta$ -amiloide
AAS	Atomic Absorption Spectrometry
AuNPs	Gold Nanoparticles
Au electrode	Gold Electrode
CFs	Carbon Nanofibers
CMEs	Chemically Modified Electrodes
CNDs	Carbon Nano Dots
CNTs	Carbon Nanotubes
CQDs	Carbon Quantum Dots
CV	Cyclic Voltammetry
D	Diffusion Coefficient
DLS	Dynamic Light Scattering
DPV	Diferential Pulse Voltammetry
$E_{pa}$	Anodic Peak Potential
$E_{pc}$	Cathodic Peak Potential
<i>f</i>	Frequency
GCE	Glassy Carbon Electrode
GC	Glassy Carbon Electrode
GO	Graphene Oxide
GQDs	Graphene Quantum Dots
HPLC	High Performance Liquid Chromatography
INHHQ	8-Hydroxyquinoline-2-Carboxaldehyde Isonicotinoyl Hydrazone
$I_{pa}$	Anodic Peak Current
$I_{pc}$	Cathodic Peak Current
LLE	Liquid-Liquid Extraction
LOD	Limit of Detection
LOQ	Limit of Quantification
MPAC	Metal Protein Attenuating Compounds
MWCNTs	Multi-walled Carbon Nanotubes
STEM	Scanning Transmission Electron Microscopy
SWCNTs	Single-walled Carbon Nanotubes
SWV	Square-Wave Voltammetry
PDs	Polymer Dots
QDs	Quantum Dots
<i>v</i>	Scanning speed
$\tau$	Time
TLC	Thin Layer Chromatography
XPS	X-ray photoelectron Spectroscopy

# 1

## Introduction

### 1.1

#### Contextualization of work

Considering the great versatility, sensitivity, and precision provided by electrochemical techniques, the development of methods based on voltammetry is attractive for the pharmaceutical and biomedical areas. The choice of the sensor is fundamental to enable a sensitive analytical response, reproduction of measured signals and selective response in function of the applied potential.

Nanomaterials have become essential in designing electrochemical sensors because of their electrocatalytic properties, large surface area, and high-speed electron transport. The development of electro-analytical methods using sensors modified with nanomaterials may provide advantages to analytical detection when compared to traditional electrodes and chemical modified electrodes. Carbon-based nanomaterials, such as carbon nanotubes (CNTs) and graphene quantum dots (GQDs), show remarkable properties after functionalization or as composites, being flexible to design sensors for specific applications.

Primaquine is a drug used to treat malaria caused by *Plasmodium vivax* and *Plasmodium ovale* (parasitic single-celled microorganisms). This drug may be also used to treat *Pneumocystis pneumonia* that often affects people with HIV. Primaquine is prescribed with care because of its strong side effects. Since

primaquine is photo-chemically unstable, forming a myriad of products, the toxicity of the drug may be related to some of their photo-derivatives.

INHHQ (8-hydroxyquinoline-2-carboxaldehyde isonicotinoyl hydrazine) is a potential drug for the treatment of neurodegenerative diseases. Alzheimer's patients commonly have developed extracellular senile plaques, composed of aggregates of the amyloid- $\beta$  peptide ( $A\beta$ ), and intracellular neurofibrillary tangles, primarily consisting of hyperphosphorylated tau protein. Some studies indicate that the interaction of amyloid- $\beta$  peptide with metals, such as copper and zinc, may be involved in the oxidative stress and processes leading to peptide oligomerization and aggregation because these ions have been found in amyloid plaques. INHHQ has demonstrated in recent works as it was capable of blocking the interactions of  $Zn^{2+}$  and  $Cu^{2+}$  with the  $A\beta$  protein.

The determination of primaquine and INHHQ was proposed using glassy carbon electrode (GC) modified with multi-walled carbon nanotubes (MWCNTs) that promoted significant improvement in faradaic current and better peak resolution obtained using square-wave voltammetry (SWV). A method for the quantification of INHHQ by SWV is reported for the first time in this work. On the other hand, several methods to quantify primaquine are reported, but, many of these depend on procedure considered complex and laborious, therefore, the proposed GC modification using MWCNTs is comparatively easy leading to a robust modification that produces repetitive results also providing amplification of the electrochemical signal due to the increased active area and producing in very sensitive method.

Thiomersal is an organomercury derivative widely used in topical pharmaceutical preparations and as a preservative in vaccines and cosmetics. Thiomersal structure comprises 49.55 % (w/w) of mercury and its degradation produces thiosalicylic acid, dithiobenzoic acid, and ethylmercury. Despite the fact that thiomersal is a very effective preservative, its inclusion in vaccines is controversial as some studies indicate the presence of mercury seriously affects health.

Creatinine is a decomposition product from creatine phosphate in muscles. Creatinine is excreted at a relatively constant rate that has been shown to be proportional to the individual's muscle mass. It is removed from circulation by glomerular filtration and excreted in the urine. Creatinine levels in blood and urine can be used as an important biomarker for the diagnosis of renal, thyroid and muscle malfunctions.

Graphene quantum dots (GQDs) were chosen to chemically modify electrodes used to determine thiomersal and creatinine and, in the case of thiomersal, exploring the synergistic effect between GQDs, visible radiation and the applied potential difference. The electroanalysis has great advantages such as easy portability, low costs of implementation and maintenance of the equipment used and the use of nanomaterials as electrode modifiers leads to low limits of detection in the range of  $\mu\text{g L}^{-1}$  and  $\text{ng L}^{-1}$ , in addition to reducing the cost, the analysis time and increasing the selectivity of the electro-analytical methods presented in this work. The present thesis is the first of this research group that relies on the use of electrochemical sensors based on nanomaterials.

## 1.2 Thesis structure

This thesis is structured in eight chapters. In Chapter 1, contextualization and the objectives of the work are presented. In chapter 2, a bibliographical review is made to present some of the nanomaterials used as electrode modifiers. In addition, a short review of theoretical fundamentals on the employed electro-analytical techniques is shown.

Chapter 3 contains detailed information on instrumentation and materials used in this work and procedures for preparing solutions, MWCNT dispersion, preparation of graphene quantum dots dispersed in aqueous solutions and preparation of the modified electrodes. The detailed procedures involving the development of the analytical methods are also presented.

The results are presented in four chapters (4, 5, 6 and 7) each of them referring to a work previously published in a scientific journal or a manuscript submitted for publication. A short introduction on each of the analytes, the full description of the results and a partial conclusion regarding each chapter is also presented.

Chapter 4 is referred to the square-wave voltammetry (SWV) determination of primaquine using MWCNTs on glassy carbon electrode. In addition, the method validation and application in fortified urine samples is shown.

In Chapter 5 the results concerning the determination of INHHQ using MWCNTs on glassy carbon electrode by SWV is presented. The application of this method in Wistar rats' brains fortified with INHHQ also is presented.

The development of the SWV based analytical method for the determination of thiomersal in influenza vaccines using GQDs as a modifier of the GC electrode is presented in the Chapter 6, showing the synergistic effect between GQDs, visible radiation and the applied potential difference in providing a strong measured signal to be used for quantitative purposes in vaccine samples.

In Chapter 7 the results concerning the determination by SWV of creatinine using gold electrode modified with a composite made of Nafion and GQDs modified with copper is presented, showing their application in urine samples.

In all the chapters referring to results, the studies of optimization of different experimental conditions, the analytical figures of merit and a study of potential interferences on the analytical signal also are presented. Finally, in Chapter 8 the overall conclusion of the thesis is made, as well as directions for future works.

## **1.3 Objectives**

### **1.3.1 General objective**

The proposal of this thesis was the development of voltammetric methods using sensors modified with nanomaterials (MWCNTs and GQDs) for the determination of primaquine, INHHQ, thiomersal, and creatinine.

### 1.3.2 Specific objectives

- Adjust conditions for dispersion of multi-walled carbon nanotubes (MWCNTs) and for the preparation of graphene quantum dots (GQDs) and graphene quantum dots functionalized with copper (GQDs-Cu);
- Characterization of the nanomaterials by spectroscopic and microscopic techniques;
- Selection of the base electrode for chemical modification and evaluate methods of chemical modification of electrodes;
- Study conditions that provide adequate electrochemical responses for the determination of analytes;
- Investigate the interaction of the sensors with analytes and the redox processes;
- Adjust instrumental parameters to obtain the best possible analytical response;
- Study of selectivity in terms of possible interferences that may exist in samples of interest;
- Obtain the analytical figures of merit of the developed methods;
- Apply the proposed methods in real and/or simulated/fortified samples to determine the analytes;

- Study strategies to eliminate interferences imposed by sample matrices;
- Compare the performance of the developed methods with traditional methods reported in the literature.

## 2 Theoretical fundamentals

### 2.1 Chemically modified electrodes

An electrochemical sensor contains two major components being one the recognition element that enables the selective response to a particular analyte or a group of analytes, thus minimizing interferences from other sample components. The other main component is the transducer or the detector device that produces a signal [1]. In this context, the electrode materials play a critical role in the construction of high-performance electrochemical sensing platforms for detecting target molecules through various analytical principles [2].

The term Chemically Modified Electrodes (CMEs) was introduced in electrochemistry by Murray *et al.* in 1975 [3] to designate electrodes with chemically active species, conveniently immobilized on their surfaces. Such a modification can alter the reactivity and selectivity of the electrode (substrate), favoring it for various purposes and applications [2,4]. For instance, CMEs can be used in the detection of natural markers for the diagnosis of diseases and in the monitoring and control of drugs [5].

In general, electrodes are evaluated both on their ability to detect the target in complex media (selectivity), and to detect very small amounts of it (sensitivity). Thus, to justify the use of CMEs the selectivity and sensitivity of an electroanalytical method should increase markedly [6].

The preparation and use of CMEs have expanded considerably helping electroanalysis to stand out as one of the most active areas in analytical chemistry. However, CMEs have been used for other non-analytical purposes, including in electrocatalysis, in membrane permeation, in electroorganic synthesis and in photoelectrochemistry [7]. The preparation of a CMEs is, ideally, determined by the desired analytical characteristics of the sensor. The choice of material for the base electrode, whose surface will undergo modification, is a very important step in preparing a CMEs and must be suitable for the approach of immobilization. Conventional materials include gold, platinum, glassy carbon and carbon paste, being reticulated glassy carbon, carbon fibers, conductive plastic material and conductive glasses among the less common substrates [6].

The most important methods used for the introduction of a modifying agent on the base electrode consist of direct irreversible adsorption, covalent bonding to specific sites on the electrode surface, coating with polymeric films or even the preparation of electrodes based on carbon paste mixed with a modifier sparingly soluble in water [8]. Adsorption or chemisorption consists of dissolving the modifying agent in an appropriate solvent and exposing the electrode surface, in general by immersion, to this solution. It also involves placing this solution with the aid of a micro-pipette, on the electrode surface, with subsequent evaporation of the solvent (creating an ink). Graphite and glassy carbon electrodes are mostly used for this type of modification [9]. Carbon electrodes have a particular ability to chemisorb reagents that have extended  $\pi$ -electron systems, such as aromatic organic compounds. Such adsorption is due to the strong interaction between the basal plane of the carbon electrode and the  $\pi$ -electron system of the aromatic molecule. The adsorption technique is widely used, given its simplicity and efficiency in many

cases. However, it has the disadvantage of producing as much as one monolayer of the immobilized modifier, which generally limits the linear response range. Desorption of the modifier in the medium during its use may also occur, resulting in loss of reproducibility and reduction of the CMEs useful life [8].

Another way to immobilize the modifying agent is through covalent bonding, in which the modifier is covalently attached to the electrode substrate, for instance by silanization involving organosilanes and the oxides present on the electrode surface. Most metallic electrodes, when oxidized in an acid medium, are covered with a thin layer of oxide that can be silanized and later reacted with another molecule, containing an appropriate functional group. Silane then acts as a bridge to fix a specific functional groups to the electrode surface. As the carbon-based electrodes have functional group containing oxygen, the modification of carbon-based electrodes is based on manipulating the reactivity of their oxygenated functional groups, against reagents such as amines, thionyl chloride, organosilanes and others [9]. Electrodes modified via covalent bond are more stable compared to those obtained by the other methods, however, such type of modification is more difficult to make and, as the adsorption modification, it tends to generate one monolayer of the immobilized modifier [9].

The polymer film coating technique consists on covering the electrode surface with polymeric films that are conductive or permeable to both the supporting electrolyte and the species of interest. Unlike the modification by adsorption or covalent bonding, the modification with polymeric membranes allows the immobilization of many layers of the active species on the modified surface, which results in the amplification of the electrochemical response. Polymeric films

coating has been used in chemically modified electrodes and employed to the development of sensors to protect the electrode surface from impurities, to block interferers [10], to immobilize biocomponents [11], to incorporate mediators and to provide biocompatibility [12].

These polymeric films are classified into four classes: conductive, non-conductive, ion-exchange and composite membranes. Conductive polymeric films are used to increase the speed of electron transfer. Non-conductive polymers are often used for their permselective characteristics. Generally, polymeric ion-exchange films have an active redox component, which is a counterion of a polyonic film such as polyvinylpyridine or Nafion. Composite materials are formed by combining two or more phases of different nature [8]. Each phase maintains its individual characteristics, but the mixture may have new physical, chemical or biological characteristics. This technique is suitable for modifying powder-based carbon electrodes such as carbon paste and graphite-epoxy electrodes.

## 2.2

### **Electrochemical sensor based on nanomaterials**

Nowadays, nanomaterials are one of the essential materials in designing electrochemical sensors and biosensors. Carbon nanomaterials including nanoparticles, nanowires, and nanotubes, owing to their peculiar physical and chemical properties, are particularly interesting in the design of modified electrodes for electrochemical sensing [13]. Graphene is the basic structure of all graphitic materials, is a two-dimensional (2-D) sheet of carbon atoms in a hexagonal configuration with atoms bonded by  $sp^2$  bonds. The electron configuration is the reason for the extraordinary properties of graphene, which include high mechanical

strength, high elasticity and thermal conductivity [14] besides the very large surface area [15].

### 2.2.1

#### Carbon nanotubes

The carbon nanotubes (CNT) consist of a graphene sheet rolled up to form a tube with remarkable electronic, chemical and mechanical properties [16]. CNT are particularly attractive for electrochemistry due to easily promote electron transfer between the electroactive species and the electrode surface as a result of their unique long and tubular geometry. The use of CNT as electrode modifiers can lead to a decrease of the overpotential, a decrease in response time, enhanced electrocatalytic activity, and an increase in available active surface area in comparison with conventional carbon electrodes [1]. The electrocatalytic effect of CNTs has been attributed to the activity of edge-plane-like graphite sites at the CNT ends, and it can be further increased by the functionalization of CNTs. CNTs also reduce the fouling of the electrode, which can greatly improve the reusability of such sensors [1].

CNT can be divided into single-wall carbon nanotubes (SWCNTs) and multi-wall carbon nanotubes (MWCNTs). A single-walled carbon nanotube (SWCNTs) can be formed by rolling a graphene sheet into a cylinder and a multi-walled nanotube (MWCNTs) is composed of concentric graphene cylinders with an interlayer spacing of 0.34 nm [17,18]. MWCNTs have attracted considerable attention in the field of material science for electrode modification due to improving the sensitivity and anti-interference properties of electrodes.

### 2.2.1.1

#### Analytical sensors based on the use of carbon nanotubes

The electrocatalytic effect of CNTs has been attributed to the activity of edge-plane-like graphite sites at the CNT extremes [19]. It has been demonstrated that the electrocatalytic activity of MWCNTs strongly depended on the CNTs synthesis and on the dispersing agent used to immobilize them on the electrode surface [20].

Literature has reported modified electrodes obtained by the incorporation of a small volume of a CNTs dispersion onto a glassy carbon substrate [21][22][23] but modification is most usually carried out by coating or preparing CNTs-binder composites. Fayemi *et al.* reported the electrochemical response of serotonin using MWCNTs doped with metal oxide nanoparticles (of nickel, zinc or iron) coated glassy carbon. The dynamic linear range, using SWV, was between  $0.005 \mu\text{mol L}^{-1}$  to  $62.8 \mu\text{mol L}^{-1}$  with limit of detection (LOD) 118, 129 and  $166 \text{ nmol L}^{-1}$  for GCE/MWCNT-NiO, GCE/MWCNT-ZnO and GCE/MWCNT-Fe<sub>3</sub>O<sub>4</sub> sensors respectively. The developed sensors were found to be stable and selective towards serotonin in urine samples [24]. Sipa *et al.* modified a glassy carbon electrode with  $\beta$ -cyclodextrins and MWCNTs and applied for the square-wave adsorptive stripping voltammetric determination of the pesticide dichlorophen. A linear response was achieved in the concentration range from  $0.05 \mu\text{mol L}^{-1}$  to  $2.9 \mu\text{mol L}^{-1}$ . The LOD of  $0.014 \mu\text{mol L}^{-1}$  was achieved with quantitative analysis river water samples [25]. Hudari *et al.* developed a voltammetric sensor based on a GC electrode modified with MWCNTs for the simultaneous determination of the diuretics hydrochlorothiazide and triamterene with oxidation observed at, respectively, 1.01 and 1.17 V, allowing up to 10-fold improvement intensity

compared to the unmodified electrode, enabling LOD in the nmol level. The electrode was applied in the analysis of hemodialysis samples [26]. Santos *et al.* developed a composite electrode based on MWCNTs and a polyurethane resin. The device was used for the determination of hydroquinone in a cosmetic formulation by differential pulse voltammetry with a linear dynamic range from 0.05 to 1.12 mmol L<sup>-1</sup> and a LOD of 12 μmol L<sup>-1</sup> [27]. Dogan-Topal *et al.* investigated the voltammetric oxidation of valganciclovir hydrochloride, an antiviral drug, using GC electrode modified with MWCNTs by cyclic and differential pulse voltammetry. The results revealed that the oxidation of analyte is irreversible and pH-dependent process in an adsorption-controlled mechanism. The results show that the oxidation signal was remarkably enhanced providing linear response in the concentration range from 7.5 nmol L<sup>-1</sup> to 1.0 μmol L<sup>-1</sup> with the LOD of 1.5 nmol L<sup>-1</sup> [28].

### 2.2.2 Quantum dots

Quantum dots (QDs) are monocrystalline colloidal semiconductors that have sizes typically in the range 1-12 nanometer (nm) in diameter [29]. The properties of the QDs depend largely on their size behaving differently from bulk solids due to quantum confinement effects [30]. Quantum confinements are responsible for the notable optoelectronic properties exhibited by QDs, including high emission quantum yields, size-tunable emission profiles, and narrow spectral bands [29].

Most literature on using QDs have focused on their use in microelectronics and opto-electrochemistry, however, some researchers have shown the potential of QDs as highly sensitive fluorescent biomarkers and bio-chemical probes. It has also

been shown the surface modification of QDs can increase their luminescent quantum yields [30].

The QDs are divided into Carbon Nano Dots (CNDs), Polymer Dots (PDs), and Carbon Quantum Dots (CQDs). Carbon Quantum Dots (CQDs) possess abundant atoms of oxygen and nitrogen in functional groups in their structures, such as carboxyl, hydroxyl, aldehyde, and amino groups [31]. CQDs have strong photoluminescence but, lower quantum yields, when compared to inorganic QDs. The size of CQDs, the chemical surface groups and doping with other elements modify their photoluminescence [32,33].

Graphene quantum dots (GQDS) is categorized as one of the subdivisions of CQDs. GQDs are nanometric fragments of graphene where electron transport is confined in their dimensions. GQDs present special optical and catalytic properties, due to quantum confinement, that can be accessed in the visible range of the electromagnetic spectrum. GQDs have sizes typically smaller than 100 nm [34,35] but typically varying from 10 nm to 60 nm [36], depending on the preparation method and conditions used [31]. While graphene does not have a band-gap, graphene quantum dots are semiconductors, thus presenting band-gap, not necessarily size-dependent as inorganic QDs but leading to peculiar properties that can be explored in terms of technological applications.

#### **2.2.2.1**

##### **Production of graphene quantum dots**

Different methods have been proposed for the preparation of GQDs and they can generally be classified into top-down and bottom-up methods. Top-down methods include cutting large graphene-based materials in nanometric systems,

while bottom-up approaches involve the preparation of GQDs from organic molecules as carbon source.

In top-down methods, a suitable carbon precursor is decomposed into small-sized GQDs via chemical, electrochemical, and physical approaches. Carbonic compound such as graphene oxide (GO), carbon fibers (CFs) or graphite was cutting down through acidic exfoliation and oxidation, beam irradiation, ultrasonic-assisted synthesis, electrochemical oxidation, and other techniques [37]. The first stage of acid oxidation includes chemical exfoliation of carbon source by inorganic acids. Production of GQDs by the top-down method has some advantages as starting materials are abundant and cheap raw carbon materials also due to the simple preparation allowing mass production. However, quality of nanomaterials tends to be poor.

Dong *et al.* prepared an electrochemical sensor for determination of tyrosine enantiomers using GQDs and  $\beta$ -cyclodextrin composites. For this, they used natural graphite submitted to acid treatment ( $\text{H}_2\text{SO}_4/\text{HNO}_3$ ) and chemical exfoliation [38]. Nirala *et al.* presented the electrochemical synthesis of nearly uniform size (about 5 nm) graphene quantum dots from wood charcoal, applying them as a peroxidase enzyme mimetic [39]. Zhuo *et al.* presented an ultrasonic route for the fabrication of GQDs that exhibit an excitation-independent downconversion and upconversion photoluminescent behavior [40]. Jiang *et al.* prepared luminescent GQDs by a photo-Fenton reaction and subsequent hydrothermal process using graphene oxide sheets as the precursor. These GQDs were of sizes ranging from 2.3 to 6.4 nm and emitted intense green luminescence in water [41]. Liu *et al.* presented a chemical exfoliation route for the synthesis of GQDs using graphite as precursor to produce

homogeneous GQDs in organic solvents such as N-methyl-pyrrolidone, N,N-dimethylformamide and dimethyl sulfoxide. The produced GQDs had diameters of less than 4 nm with the blue emission [42].

A bottom-up approach is used to link elements together to form larger subsystems. In bottom-up strategy, GQDs could be prepared via a series of chemical reactions, starting from small organic molecules, through several techniques like hydrothermal exfoliation, pyrolysis, microwave-assisted processes, step-wise organic synthesis, and by cage-opening of C<sub>60</sub> and of silica nanospheres [37]. Bottom-up methods offer opportunities to get a high degree of control over the size, shape, and morphology. However, these methods require complicated multi steps and the sizes of the GQDs are usually very small [37].

Solvothermal synthesis involves the use of a solvent under moderate to high pressure (usually between 1 atm and 10,000 atm) and temperature between 100°C and 1000°C, that facilitates the interaction of precursors during synthesis. If water is used as solvent, the method is called hydrothermal synthesis. Bayat *et al.* synthesized green-photoluminescent single layer graphene quantum dots with deionized water and glucose as precursor using a hydrothermal method [43]. Pyrolysis methods also belongs to bottom-up strategy being cost-effective and allowing size control of the product. A variety of small organic molecules can be selected as starting materials in such approach. Dong *et al.* developed a synthetic method by carbonizing citric acid and dispersing the carbonized products into alkaline solutions [44] while Wu *et al.* used L-glutamic acid [45]. Microwave heating technique is also used in the synthesis of nanomaterials. Through controlling the specific microwave parameters such as temperature (and

temperature ramp), pressure and choice of solvents can be prepared the desired nanomaterial. For example, Zheng *et al.* presented an ammonia-driven microwave-assisted synthesis of high-quality nitrogen-doped graphene quantum dots (NGQDs) at room temperature and atmospheric pressure. The as-synthesized NGQDs consisted of one to three graphene monolayers exhibited highly crystalline quality [46].

#### 2.2.2.2

#### **Analytical approaches through the use of graphene quantum dots as modifiers in electro-analytical sensors**

Most of literature concerning the use of GQDs in analytical chemistry has been focused on optical probes in photoluminescence-based applications. Nevertheless, applications in designing electrochemical sensors have been reported owing to its easy functionalization, large surface area, accessible edges and highly efficient electron transport. Roushani *et al.* produced an electrochemical sensor based on graphene quantum dots/riboflavin modified GC electrode for the amperometric detection of persulfate ( $S_2O_8^{2-}$ ). LOD of  $0.2 \mu\text{mol L}^{-1}$  and linear concentration range from  $1 \mu\text{mol L}^{-1}$  to  $1 \text{mmol L}^{-1}$  were achieved [47]. Pang *et al.* determined dopamine by differential pulse voltammetry using a mixture of GQDs and Nafion as a modifier of a GC electrode. Nafion was used as an anchoring agent to increase the robustness of GQDs on the electrode surface enabling sensor stability and response reproducibility. The response toward dopamine exhibited linear range of  $5 \text{nmol L}^{-1}$  to  $100 \text{nmol L}^{-1}$  and a LOD of  $0.45 \text{nmol L}^{-1}$  [48].

Dong *et al.* developed an electrochemical sensor using composites of GQDs and  $\beta$ -cyclodextrins functionalized glassy carbon electrode for determination and recognition of tyrosine enantiomers (biomarker of depression) in blood serum

samples. Cyclic voltammetry was used for quantification. The LOD of L-Tyrosine and D-Tyrosine were  $6.0 \text{ nmol L}^{-1}$  and  $100 \text{ nmol L}^{-1}$  respectively [38]. Ting *et al.* conjugated GQDs and gold nanoparticles (AuNPs) for electrochemical detection of  $\text{Hg}^{2+}$  and  $\text{Cu}^{2+}$  with GC used as base electrode. LOD of  $0.02 \text{ nmol L}^{-1}$  for  $\text{Hg}^{2+}$  and  $0.05 \text{ nmol L}^{-1}$  for  $\text{Cu}^{2+}$  were achieved using anodic stripping voltammetry [49]. Arvand and Hemmati fabricated a nanocomposite based on GQDs and  $\text{Fe}_3\text{O}_4$  nanoparticles to functionalize multi-walled carbon nanotubes that was used to modify GC substrate. The electrocatalytic properties of the modified electrode toward the oxidation of progesterone were studied. The peak current for progesterone varies linearly in two ranges, the first from  $0.01$  to  $0.5 \text{ } \mu\text{mol L}^{-1}$  and the second from  $0.5$  to  $3.0 \text{ } \mu\text{mol L}^{-1}$ . The method was applied for the analysis of progesterone in human serum samples [50]. Cai *et al.* reported a polyaniline functionalized GQDs composite to modify GC, fabricating an electrochemical sensor for the determination of calycosin in the samples of traditional Chinese medicine. Differential pulse voltammetry technique was used and the proposed sensor exhibited a detection range of  $11.0$  to  $352 \text{ } \mu\text{mol L}^{-1}$  with a LOD of  $9.8 \text{ } \mu\text{mol L}^{-1}$  [51].

## 2.3

### Electrochemical techniques

#### 2.3.1

##### Cyclic voltammetry

Cyclic voltammetry (CV) is a simple and direct method for measuring the formal potential of a half reaction when both oxidized and reduced forms are stable during the time required to obtain the voltammogram (current-potential curve). CV

offers quick information about the thermodynamics of redox processes, the kinetics of heterogeneous electron transfer reactions and chemical reactions coupled to adsorptive processes [52].

In CV, a potential is applied at a constant rate, producing a linear potential variation as a function of time, starting from an initial potential value, until reaching a final one, when the potential sweep is reversed until the starting potential is reached again. These two scan steps produce a cycle that may be repeated as many times as necessary. As the current, measured during the process, is plotted in function of the applied potential, the so-called cyclic voltammogram is obtained.

The type of voltammogram generated depends on the type of redox mechanism that the compound undergoes on the electrode, which makes CV a valuable tool for mechanistic studies. The oxidation and reduction processes of the target chemical species occur at the working electrode and produce, in a reversible redox system, features represented by the anodic peak current ( $I_{pa}$ ) that occur at a maximum anodic peak potential ( $E_{pa}$ ) and the cathodic peak current ( $I_{pc}$ ) that occur at a maximum anodic peak potential ( $E_{pc}$ ). The peak current values ( $I_p$ ) depend upon different parameters indicated in Eq. 1, where  $n$  is the number of electrons involved in the process,  $A$  is the electrode area ( $\text{cm}^2$ ),  $D$  is the diffusion coefficient ( $\text{cm}^2 \text{s}^{-1}$ ) and  $C$  is the concentration of the species in solution ( $\text{mol L}^{-1}$ ),  $\nu$  is the scanning speed ( $\text{V s}^{-1}$ ).

$$I_p = (2.686 \times 10^5) n^{3/2} ACD^{1/2} \nu^{1/2} \quad (\text{Eq. 1})$$

Through the use of Eq. 1, it is also possible to calculate the electrode area of the working electrode. Through linearity between the peak current and the square

root of the scan rate, information about the nature of the involved electrochemical process is found. When electron transfer at the electrode surface is slow compared to mass transport, the process is termed “electrochemically irreversible”. Slow electrode kinetics necessitate significantly more negative applied potentials for appreciable current to flow [53].

A process is defined as electrochemically reversible when the rate of the electron transfer is higher than the rate of the mass transport. For a reversible reaction the peak current varies linearly with the square root of the scan rate. Processes occurring in the transition zone between reversible and irreversible behaviour are called *quasi*-reversible [54]. For a diffusion-controlled mass transport, the linear relationship is established between the value of current peak (cathodic or anodic) and the square root of the potential scan velocity. In systems with mass transport controlled by adsorption, such a relationship is not linear.

### 2.3.2

#### **Square-wave voltammetry**

Square-wave voltammetry (SWV) is an electrochemical technique suitable for mechanistic study of electrode processes and electrokinetic measurements. It is considered as one of the most advanced voltammetric techniques, representing the advantages of pulse techniques (high sensitivity), cyclic voltammetry (elucidation of the electrode mechanisms) and impedance techniques (kinetic information of very fast electrode processes) [55].

Another great advantage of this technique is the speed of data acquisition. Frequencies from 1 to 100 square-wave cycles per second allow the use of

extremely fast potential sweep speeds. While in differential pulse voltammetry the scanning speed varies from 1 to 10  $\text{mV s}^{-1}$ , in SWV this speed varies from 100 to 1000  $\text{mV s}^{-1}$ , this decreases the analysis time (from 3 - 5 minutes to 3 -10 seconds) without loss of peak resolution.

SWV is a technique in which the acquisition of the current resulting from the redox process comes from the overlapping of a square-shaped pulse over a potential linear ramp, forming a ladder with a characteristic pulse amplitude ( $a$ ), scan increment ( $\Delta E_s$ ) and duration ( $\tau$ ). In Fig. 2.1 the form of application of the potential in square-wave voltammetry is presented. The frequency of the square-wave, in Hz, is equal to  $1/\tau$ . Current measurement is performed at two points along the square-wave pulse. The first measurement (position 1 in Fig. 2.1) is at the end of the direct pulse (direct scanning) and the second measurement (position 2 in Fig. 2.1) is made in the reverse direction of the scanning [56].

SWV possesses high analytical sensitivity and speed of measurements. The excitation signal, that is, potential modulation in the course of the voltammetric measurement, enables the electrode reaction to be driven in both oxidative and reductive directions repeatable at each step of the staircase potential, thus providing an insight into the mechanistic aspects of the studied electrode reaction [57]. SWV is suited to analyse reversible or quasireversible electrode processes and electrode processes coupled with fast chemical reactions. In SWV, an irreversible system is characterized by a linear relationship between the peak current ( $I_p$ ) and the frequency ( $f$ ) of the pulses. While a linear relationship between  $E_p$  and the logarithm of the frequency ( $\log f$ ) is found. In reversible systems, the linear relationship occurs when the peak current is monitored as a function of the square-root of  $f$ . In quasi-

reversible redox systems, no linear behavior is found in the relationship between  $I_p$  and frequency of pulse. The SWV mathematical models also can be used to calculate important parameters such as the number of electrons involved in the redox process.

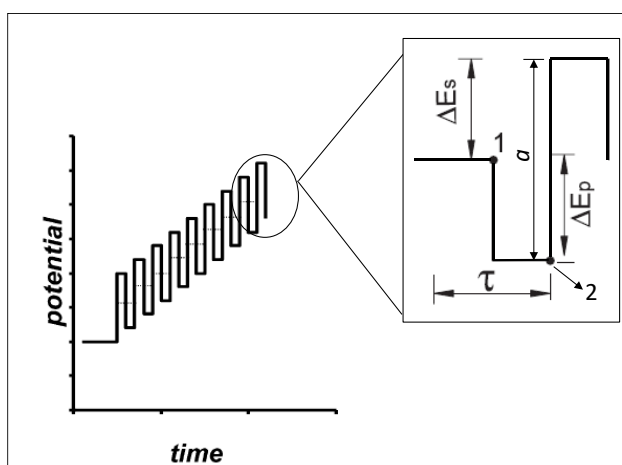


**Figure 2.1.** Illustration of a potential application in SWV, where:  $a$  is the pulse width;  $\Delta E_s$  is the scan increment and  $\tau$  is the time. Source: Adapted from [56,55].

### 3 Materials and methods

#### 3.1 Instrumentation

Electrochemical studies for primaquine e INHHQ were performed on a BAS CV 50W analyzer (USA) operating in the voltammetric square-wave and cyclic voltammetric modes and electrochemical experiments for thiomersal and creatinine were made using a potentiostat  $\mu$ -AUTOLAB Type III (Metrohm, The Netherlands) operating in SWV and CV modes.

The electrochemical cell (15 mL volume) is made of Pyrex glass with a Teflon cap with four hole-positions (Fig. 3.1) to place the purging gas and the three electrodes; the auxiliary electrode (Pt wire), a reference electrode (Ag|AgCl(KCl<sub>(sat)</sub>)) and the working electrode. The working electrodes used were: i) Glassy carbon electrode (GCE), ii) Gold electrode (Au electrode).

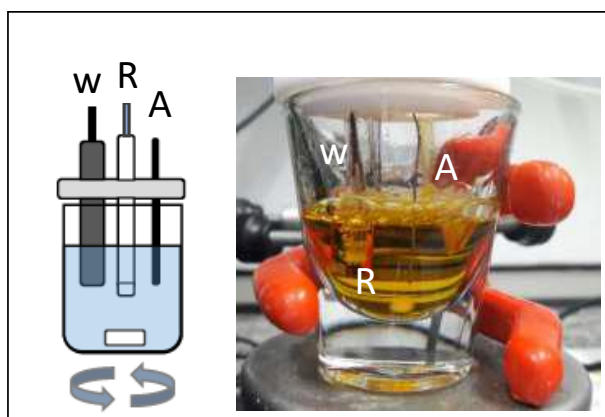


**Figure 3.1.** Electrochemical cell: (A) Platinum auxiliary electrode; (R) Reference electrode of Ag|AgCl<sub>(sat)</sub>; (W) Working electrode.

For the determination of thiomersal, it was used the laboratory-made photochemical reactor consisted of six commercial fluorescent lamps (6 W each, emitting in the visible spectral range) set on the internal wall of a PVC tube (20 cm diameter  $\times$  30 cm width) fixed onto a wood box, as a base that contain a magnetic stirrer which promotes mass transport within the electrochemical cell. A scheme of the experimental set-up used for the determination of thiomersal is presented in Fig. 3.2.

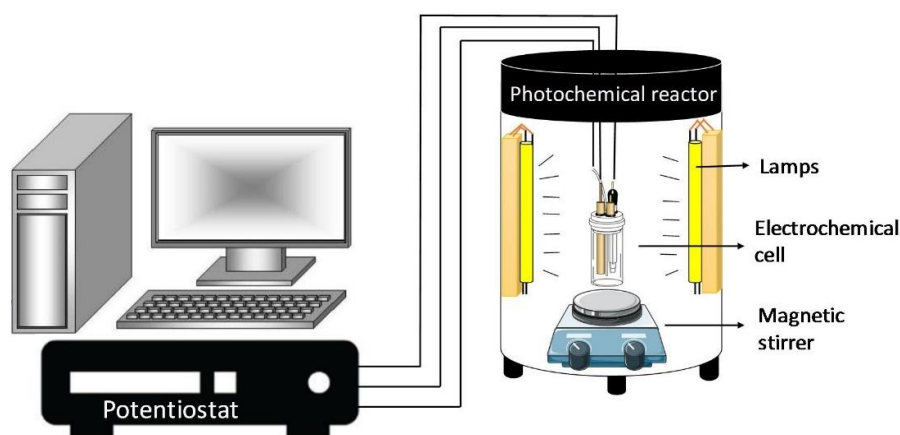


**Figure 3.2.** Schematic of the set-up used for the photo-reactor coupled to the electrochemical system.

Mercury measurements were made by atomic absorption spectrometry (AAS) using a mercury cold vapor dedicated system with a multi-path length cell (multipass-cold vapor-AAS), model RA-915 (LUMEX, Russia), equipped with Zeeman background correction and connected to an RP-92 accessory for chemical reduction in aqueous solution. HPLC was an Agilent 1200 series system (Agilent, Japan) with a G1315C model diode-array type absorption photometric detector and an auto-sampler. Total Organic Carbon measurements were made on a carbon

analyzer model TOC-VCPN (Shimadzu, Japan). Photoluminescence measurements were made on a model LS 55 luminescence spectrometer (Perkin-Elmer) (600 nm  $\text{min}^{-1}$  scan rate, 10.0 nm spectral bandpass and 1 cm optical path length quartz cuvettes).

Images from the GQDs and GQDs-Cu were made using a field emission scanning electron microscope (JEOL, model JSM-7800F, Japan) operated in the scanning transmission electron microscopy (STEM) mode at 30 kV. Raman spectroscopy was performed using a confocal Raman microscope (WITec Alpha 300R, Germany) equipped with an electron multiplying charge coupled device detector and an air cooled solid-state laser. Raman measurements were obtained using a 532 nm laser source, a monochromator with a 600 line/mm grating and 1 mW of laser radiation power. Dynamic light scattering (DLS) and zeta-potential measurements were made on a nanoparticle analyzer model SZ-100 (Horiba, Japan). Zeta potential measurement were made using an acrylic electrochemical cell containing a flat carbon electrode (6 mm thickness) and DLS measurements were obtained using glass cuvettes with 1 cm optical path length. The contact angle measurements were made using drop shape analyzer- Kruss Advance. X-ray photoelectron spectroscopy analysis was performed in ultrahigh vacuum ( $\sim 10^{-9}$  mbar) using a surface analysis chamber equipped with a VG Thermo Alpha 110 hemispherical analyser and using non-monochromatized Al- $K_{\alpha}$  line as the x-ray source.

The pH measurements were made on a pHmeter model mPA 210 (Tecnopon, Brazil) with a glass membrane electrode conjugated with a Ag|AgCl (KCl(sat)) reference electrode. Sonication was performed by the use of an

ultrasonic bath (9 L, NSC 2800 model, Unique, Brazil). The introduction of standard and samples in voltammetric analyzes were made using a manual micropipete (from Brand, Germany) with adjustable volumes from 10 to 100  $\mu\text{L}$  and from 100 to 1000  $\mu\text{L}$ .

### 3.2

#### Reagents and materials

Ultrapure water (18.2  $\text{M}\Omega\text{ cm}$ ) was obtained from the Milli-Q gradient A10 ultra-purifier (Milipore, USA). Primaquine diphosphate, 8-hydroxy-2-quinolinecarboxaldehyde, isoniazid, thiomersal, thiosalicylic acid, 2,2'-dithiodibenzoic acid, creatinine, Nafion solution (5% v/v) and MWCNTs (110–170 nm diameter and 5–9  $\mu\text{m}$  length) were from Sigma- Aldrich (USA). Ethylmercury was from Brooks Rand Instruments (USA). Acetonitrile (HPLC grade) was obtained from J.T. Baker (USA). Citric acid, Sodium hydroxide (98.0%, m/m), acetic acid (65.0% m/v), boric acid (99.8% m/m), phosphoric acid (85.0%, m/v), potassium chloride and sodium acetate were obtained from Merck (Germany). The 1,4-Dioxane was from Tedia (USA). Nitric acid, dimethyl sulfoxide, methanol, chloroform, Tin chloride ( $\text{SnCl}_2$ ) and ammonium hydroxide were purchased from Vetec (Brazil). Aluminum oxide (1.0  $\mu\text{m}$ ) was obtained from Fortel, Brazil. Nitrogen gas (99.999%) was supplied from Linde-gases (Brazil). Thinlayer chromatography (TLC) plates (60 F254) were purchased from Merck. PTFE syringe filters (0.45  $\mu\text{m}$ ) were from Whatman (UK). Dialysis membrane (retained molecular weight of 3.5 kDa) was from Spectrum Laboratories Inc. (USA).

### 3.3

#### Preparation of supporting electrolyte

The supporting electrolyte consisted of a mixture of the Britton-Robinson (BR) buffer solution (final concentration in the cell of  $0.02 \text{ mol L}^{-1}$ ) and KCl solution ( $0.25 \text{ mol L}^{-1}$  final concentration in the cell). BR buffer stock solution were prepared by mixing acetic acid, boric acid and phosphoric acid and adjusting pH with aliquots of NaOH ( $1 \text{ mol L}^{-1}$ ).

### 3.4

#### Preparation of nanomaterials used as electrode modifiers

##### 3.4.1

#### Preparation of graphene quantum dots

The GQDs were produced by the pyrolysis and hydro-exfoliation of citric acid (2 g). First, 2 g of citric acid was placed into a 5 mL beaker and heated to about  $240 \text{ }^{\circ}\text{C}$  using a heating plate. As citric acid melted (with color changing from colorless to pale yellow and then to brown) within 2 to 5 min, the hot molten material was added into 25 mL of ultrapure water, at room-temperature, in order to obtain (after filtering on a  $0.22 \text{ }\mu\text{m}$  syringe filter) a clear pale yellow aqueous dispersion that was further dialyzed, for 24 h, in order to obtain the so called GQDs aqueous synthesis dispersion. GQDs dispersions were also prepared by adding the molten material into HCl ( $0.1 \text{ mol L}^{-1}$ ) and NaOH ( $0.25 \text{ mol L}^{-1}$ ) aqueous solutions at room-temperature.

### 3.4.2

#### Preparation of graphene quantum dots modified with $\text{Cu}(\text{NO}_3)_2$

Graphene quantum dots modified with  $\text{Cu}(\text{NO}_3)_2$  (GQDs-Cu) were produced by the pyrolysis of citric acid with a small amount of  $\text{Cu}(\text{NO}_3)_2 \cdot 3\text{H}_2\text{O}$ . First, 0.6 g of citric acid was placed into a 5 mL beaker and heated to about 240 °C using a heating plate. As citric acid became molten (with color changing from colorless to pale yellow and then to light brown) within 2 to 5 min, 0.09 g  $\text{Cu}(\text{NO}_3)_2 \cdot 3\text{H}_2\text{O}$  was added to the molten and mixed using a glass stick. After about 4 min, the hot melted mixture (dark-brown molten) was added into 20 mL of ultrapure water, at room-temperature, in order to obtain (after filtering on a 0.22  $\mu\text{m}$  syringe filter) a clear pale aqueous dispersion.

### 3.4.3

#### Synthesis of $\text{Cu}(\text{OH})_2$

The synthesis of  $\text{Cu}(\text{OH})_2$  was carried out, adding dropwise  $\text{NaOH}$  1 mol  $\text{L}^{-1}$  to  $\text{Cu}(\text{NO}_3)_2$ , 0.1 mol  $\text{L}^{-1}$ , until pH 10 is obtained (at room temperature constant stirring and). Then, it was filtered and washed with ethanol (10 mL) and water (10 mL) to remove impurities.

### 3.5

#### Modifications of the different electrodes for the determination of the analytes

#### 3.5.1

##### Dispersion of MWCNTs and its use as modifier for the determination of primaquine and INHHQ

MWCNTs dispersion was prepared by mixing 3 mg of the nanomaterial in 1 mL of 1,4-dioxane and, after vortex agitation, the mixture was placed in an ultrasonic bath (20 min) and then stored at room-temperature.

Prior to modification, GC surface was polished using 1.0  $\mu\text{m}$  alumina paste (abrasive powder wet with water) and then washed with water. Modification consisted on adding 10  $\mu\text{L}$  of the MWCNTs dispersion (previously homogenized in an ultrasonic bath for 20 min) onto the GC (Fig. 3.3). After evaporation of 1,4-dioxane (using an infrared lamp) a homogeneous layer of the nanoparticle was obtained [58].

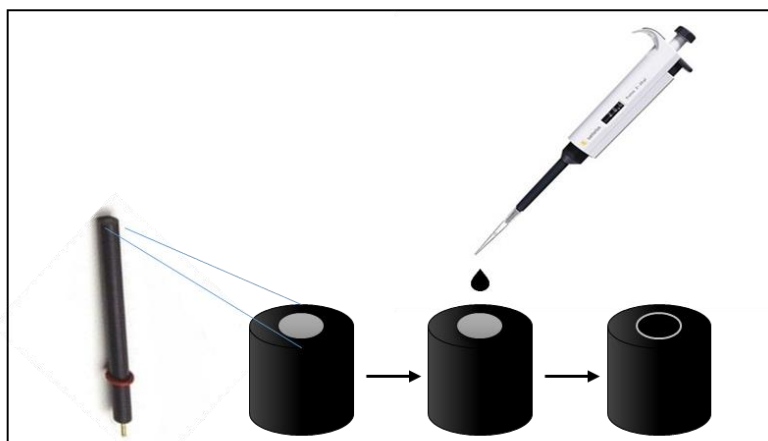


**Figure 3. 3.** General methodology for the modification of electrodes with nanomaterials.

GC electrode areas were estimated by cyclic voltammetric measurements of a solution of  $[\text{Fe}(\text{CN})_6]^{3-}$  ( $1.0 \times 10^{-3} \text{ mol L}^{-1}$ ) in a KCl ( $0.5 \text{ mol L}^{-1}$ ) aqueous solution (Fig. 3.4A). The scanning rate was varied from 10 to  $100 \text{ mV s}^{-1}$  and a relationship between peak current ( $I_p$ ) and the square root of the scan velocity ( $v^{1/2}$ ) was constructed. Using the diffusion coefficient ( $D$ ) of  $[\text{Fe}(\text{CN})_6]^{3-}$  ( $6.32 \times 10^{-6} \text{ cm}^2$

$s^{-1}$ ) and considering 1 mol of electrons per 1 mol of species involved in the redox process, the concentration of the electroactive species ( $C^*$ ) was  $1.0 \times 10^{-6} \text{ mol cm}^{-3}$ . Substituting these values in the equation  $I_p / v^{1/2} = (2.686 \times 10^5) n^{3/2} AC^*D^{1/2}$  and using the slope obtained from the curve of  $I_{pa}$  versus  $v^{1/2}$  (Fig. 3.4C), the active electrode area (A) found for the bare GC electrode was  $0.063 \text{ cm}^2$  and the one for the GC/MWCNTs electrode was  $0.27 \text{ cm}^2$  or 4.3 times larger.

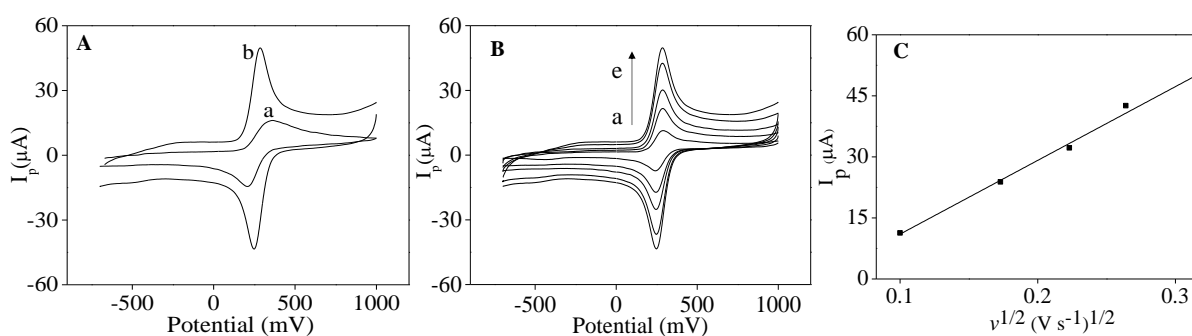


**Figure 3.4.** (A) Cyclic voltammograms of  $1.0 \text{ mmol L}^{-1} K_3[Fe(CN)_6]$  in  $0.5 \text{ mol L}^{-1} KNO_3$  solution at the (a) bare unmodified GC electrode and (b) MWCNT-modified GC electrode at  $100 \text{ mV s}^{-1}$ . (B) Cyclic voltammograms of  $1.0 \text{ mmol L}^{-1} K_3[Fe(CN)_6]$  in  $0.5 \text{ mol L}^{-1} KNO_3$  solution at MWCNT-modified GC electrode at sweep rates: (a) 10 (b) 30 (c) 50 (d) 70 (e)  $100 \text{ mV s}^{-1}$ . (C)  $I_{pa}$  versus square root of sweep rate.

### 3.5.2

#### Modification of the glassy carbon electrode (GCE) with GQDs for determination of thiomersal

The GQDs aqueous synthesis dispersion ( $25 \text{ mL}$ ) was evaporated to about  $200 \mu\text{L}$ , then  $2 \text{ mL}$  of 1,4-dioxane was added and the mixture was briefly vortex agitated. After ultrasonic agitation, for  $20 \text{ min}$ , the dispersion was stored at room temperature. The GC electrode surface was polished with alumina then, washed with ultra-pure water prior to modification. Modification consisted on adding  $10 \mu\text{L}$  of the GQDs dispersed in dioxane (previously homogenized in an ultrasonic bath for  $20 \text{ min}$ ) onto the GC surface (Fig. 3.3). The 1,4 dioxane rapidly evaporated,

at room temperature, allowing the formation of a homogeneous layer of GQDs on the electrode surface.

### 3.5.3

#### **Modification of the gold electrode with GQDs-Cu for determination of creatinine**

The gold electrode surface was polished with 1.0  $\mu\text{m}$  aluminum oxide suspension then with 1.0  $\mu\text{m}$  diamond polish slurry, finally washed with ultra-pure water prior to modification. The GQDs-Cu aqueous original dispersion (20 mL) was evaporated until about 2 mL, then an aliquot of 100  $\mu\text{L}$  was mixed with 100  $\mu\text{L}$  of a Nafion solution (5% m/v) and the mixture was vortex agitated. After ultrasonic agitation, for 25 min, 1  $\mu\text{L}$  of this dispersion was placed onto the gold electrode (Fig. 3.3) and it was dried using an infrared lamp (5 min).

### 3.6

#### **Preparation of samples, voltammetric measurements and other procedures**

##### 3.6.1

##### **Procedures for primaquine**

###### 3.6.1.1

##### **Standard solutions, voltammetric measurements for primaquine determination**

Primaquine diphosphate standard solutions were prepared ( $1.0 \times 10^{-2}$  mol  $\text{L}^{-1}$  and  $1.0 \times 10^{-4}$  mol  $\text{L}^{-1}$ ) by direct dissolution in water. For the treatment of urine samples, in order to reduce protein content, a volume of 60 mL of human fresh urine, fortified with primaquine diphosphate, was mixed with 10 mL of methanol/acetonitrile (50/50% v/v). After vortex mixing (5 min) and centrifugation (15 min at 1000 RFC) urine sample supernatant was collected.

Diagnostic studies of the redox process for determination of primaquine were performed using CV with a scanning speed varying from 100 to 1200  $\text{mV s}^{-1}$  in the potential range from -900 mV to +1200 mV. The supporting electrolyte used was BR Buffer; 0.02  $\text{mol L}^{-1}$  in KCl 0.25  $\text{mol L}^{-1}$  in the pH range from 3 to 10. SWV was employed to study the redox process and to perform determination of primaquine. Quantification was performed by measuring peak height after scanning from 0 to +1000 mV at 30 Hz using 20 mV step potential and 40 mV pulse amplitude.

### 3.6.1.2

#### **Liquid-liquid extraction and thin-layer chromatography for determination of primaquine**

For the liquid-liquid extraction and thin-layer chromatography, in an amber-glass separation funnel (250.00 mL), the urine supernatant (50.00 mL) was mixed with water (50 mL) and the pH adjusted to about 9 (with NaOH solution). Primaquine was extracted three times with 10 mL of chloroform with aliquots combined in one single volume. Chloroform was evaporated on a hot plate (60 °C) and the residue was re-dissolved with 1 mL of water with pH adjusted to about 4 (by adding HCl solution). From this solution, aliquots of 10  $\mu\text{L}$  were spotted on the TLC plates (10 spots per plate) allowing spots to dry at room-temperature. Plates were placed into a developing tank containing a mobile phase constituted by 98 parts methanol and 2 parts of ammonia solution (15  $\text{mol L}^{-1}$ ). After separation of primaquine, the areas of the TLC plate containing the analyte spots ( $R_f = 0.4 \pm 0.5$  cm) were removed and the analyte was extracted with 3 mL of water at pH 4 (under 20 min of ultrasonic agitation). The mixture was filtered in a syringe filter, then, 3 mL water was passed through the filter to wash it. These solutions were collected

in the same vial and evaporated (in a glycerin-bath at 70 °C) until a dry residue was obtained. The residue was re-dissolved in water (1.00 mL) and transferred to the electrochemical cell, in order to perform voltammetric measurements.

### 3.6.1.3

#### **High-performance liquid chromatographic analysis of primaquine**

Analyzes by HPLC were made based on literature [59] using isocratic elution and mobile phase consisting of sodium acetate buffer (0.01 mol L<sup>-1</sup>; pH 5.6) and acetonitrile at 45/55% v/v. The two components of the mobile phase were previously filtered and then degassed in an ultrasonic bath. Chromatography was performed at 1.0 mL min<sup>-1</sup>, at 27 °C, and the introduced sample volume was 20 µL. The retention time of primaquine was 3.6 min. Analytical curves were constructed using three replicates and absorciometric detection at 265 nm.

### 3.6.2

#### **Procedures for INHHQ**

##### 3.6.2.1

#### **Standard solutions, voltammetric measurements procedures for INHHQ determination**

The INHHQ and precursors standard solutions were prepared at concentration levels equal to  $1.0 \times 10^{-2}$  mol L<sup>-1</sup> and  $1.0 \times 10^{-4}$  mol L<sup>-1</sup> in dimethyl sulfoxide. The brains of certified pathogen-free male Wistar rats were used in the analytical measurements. The rat brains were donated by the LABSO-Bio after declaring that the performed experiments were approved by the University Ethics Committee and from appropriate committees from the collaborating universities (Protocol CEUA/036/2013) in conformity with the Ethical Principles in Animal Experimentation adopted by the Brazilian Science Society and with the Guide of

the North American Society of Neuroscience and Behavior for the care and the use of laboratory animals.

CV was performed to characterize the redox process of INHHQ by the variation of scan rate from 100 to 1000  $\text{mV s}^{-1}$  across a potential range between -1200 mV and +1200 mV. The supporting electrolyte used was BR Buffer ( $0.02 \text{ mol L}^{-1}$ ) in KCl  $0.25 \text{ mol L}^{-1}$  in the pH range from 3 to 12. SWV was employed to characterize the redox process and to carry out the quantitative determination of the INHHQ analyte. The quantitative determination was performed by the measurement of the peak height through the use of anodic scanning from 0 to 1000 mV at a frequency of 30 Hz, a 20 mV step potential and a 40 mV pulse amplitude.

### 3.6.2.2

#### **Rats' brain samples treatment and thin-layer chromatography for determination of INHHQ**

A mass of 0.1 g of a lyophilized rat brain sample was suspended in 2 mL of dimethyl sulfoxide and were fortified at INHHQ concentrations equal to  $5.0 \times 10^{-5} \text{ mol L}^{-1}$  and  $9.0 \times 10^{-6} \text{ mol L}^{-1}$ . After a vigorous vortex mixing procedure for 10 min and centrifugation for 15 min at 1008 RFC, the supernatant was separated from the solid pellet at the bottom of the centrifuge tube.

Aliquots equal to 200  $\mu\text{L}$  of supernatant were spotted upon the TLC plates that were allowed to dry at room temperature. Next, the plates were placed into a developing tank containing a mobile phase composed of a mixture of methanol/phosphate buffer ( $0.001 \text{ mol L}^{-1}$  pH 7.0) at 30/70% (v/v). Following the separation, the area of the TLC plate containing the INHHQ spot centered at  $R_f$  equal to 0.82 was characterized by the use of iodine vapor. A similar procedure was employed to identify chromatographic spots of precursors, related compounds and

the rat brain matrix. The silica plate around the INHHQ was removed and the analyte was subsequently extracted by 300  $\mu\text{L}$  of dimethyl sulfoxide and 3.0 mL of Britton-Robinson buffer (pH 11; 0.02 mol  $\text{L}^{-1}$ ) in 0.25 mol  $\text{L}^{-1}$  KCl by the use of 20 min of ultrasonic agitation. The mixture was passed through a syringe filter, followed by 2.0 mL of Britton-Robinson buffer (pH 11; 0.02 mol  $\text{L}^{-1}$ ) in 0.25 mol  $\text{L}^{-1}$  KCl to wash the filter. A volume of 5 mL of the filtered solution was collected and added to the electrochemical cell in order to carry out the voltammetric measurements.

### 3.6.2.3

#### **High-performance liquid chromatographic analysis of INHHQ**

The HPLC analysis was performed based on the work of Cukierman *et al.* [60] with some changes in the method by the use of isocratic elution of a mobile phase composed of a mixture of methanol/ phosphate buffer (pH 7.5; 0.001 mol  $\text{L}^{-1}$  70/30% (v/v) and at a flow rate of 1 mL  $\text{min}^{-1}$ . The liquid chromatography was performed at a flow rate of 0.8 mL  $\text{min}^{-1}$  at 35 °C. The introduced sample volume was equal to 20  $\mu\text{L}$ . Under these conditions, the retention time for the INHHQ analyte was 4.6 min. The analytical curve was constructed by the introduction of 20  $\mu\text{L}$  of INHHQ standard solutions at concentrations from  $5.0 \times 10^{-7}$  mol  $\text{L}^{-1}$  (146.1  $\mu\text{g L}^{-1}$ ) to  $5.0 \times 10^{-5}$  mol  $\text{L}^{-1}$  (14.6 mg  $\text{L}^{-1}$ ) using three replicate measurements and absorciometric detection at a wavelength of 290 nm.

### 3.6.3

#### **Procedures for thiomersal**

##### 3.6.3.1

**Standard solutions, voltammetric measurements, mercury cold vapor atomic absorption measurements.**

Thiomersal and ethylmercury were prepared ( $1.0 \times 10^{-2}$  mol L<sup>-1</sup> and  $1.0 \times 10^{-4}$  mol L<sup>-1</sup>) by direct dissolution in water. Thiosalicylic acid and 2,2'-dithiodibenzoic acid solutions were prepared in methanol. The influenza vaccine with thiomersal, GC Flu Multi (Split virion, inactivated) Green Cross, was obtained from the Colombian public health system, and contained originally 0.01 % m/v ( $100 \mu\text{g mL}^{-1}$ ) of thiomersal according to the vaccine instruction. The influenza vaccines (FluQuadri<sup>®</sup>), used in the Brazilian public health system, was fortified with thiomersal at  $2.47 \times 10^{-4}$  mol L<sup>-1</sup> ( $97.1 \mu\text{g mL}^{-1}$ ). Each vaccine sample was diluted in ultrapure water prior to the addition of the electro-analytical analytical cell.

The redox process of thiomersal was studied using CV with a scanning velocity varying from 10 to 900 mV s<sup>-1</sup> in the  $\pm 1500$  mV potential range. The supporting electrolyte used was BR Buffer ( $0.02$  mol L<sup>-1</sup>) in KCl  $0.25$  mol L<sup>-1</sup> within the pH range from 2 to 10. SWV was employed to study the redox process and to perform quantitative determination of thiomersal. Quantification was performed by measuring peak height, at +158 mV, using anodic scanning within  $\pm 1500$  mV at 25 Hz using 20 mV step potential and 40 mV pulse amplitude.

### 3.6.3.2

#### **Analytical procedure for determination of Hg by multipass-cold vapor-AAS**

##### 3.6.3.2.1

#### **Mercury cold vapor atomic absorption measurements**

The cold vapor multipass-AAS system was used to measure the mercury formed during the electrochemical process. In order to do this, samples collected from the electrochemical cell (5 mL) were diluted 1000 times and aliquots (10 mL)

were transferred to the bubbler of the cold vapor-AAS system (containing 2 mL SnCl<sub>2</sub> (20% v/v) to perform chemical reduction and the absorbance measurement of the mercury cold vapor produced from the reduction of Hg<sup>2+</sup>.

### **3.6.3.2.2**

#### **Vaccine analysis by mercury cold vapor atomic absorption**

Vaccine analysis by multipass-cold vapor-AAS were made based on literature [61]. Sample solutions (100 µL) were transferred to glass test tubes containing 10.0 mL of a H<sub>2</sub>O<sub>2</sub> (1%) solution (with pH previously adjusted to 4.5), also containing 17 µL of the dispersion of GQDs. The test tube content was transferred to a glass reaction cell containing 2 mL of a SnCl<sub>2</sub> aqueous solution (20% v/v) in order to provide a rapid reduction to Hg, that was transferred, by an air flow passing through the solution, to the multipass-cold vapor-AAS system operating in a continuous acquisition mode.

### **3.6.4**

#### **Procedures for creatinine**

##### **3.6.4.1**

#### **Standard solutions, voltammetric measurements and HPLC procedure for creatinine determination**

The creatinine standard solutions were prepared at concentration levels equal to  $1.0 \times 10^{-3} \text{ mol L}^{-1}$  and  $1.0 \times 10^{-5} \text{ mol L}^{-1}$  in water. For the treatment of urine samples, in order to reduce protein content, a volume of 60 mL of human fresh urine was treated to reduce protein content by adding 10 mL of methanol/acetonitrile (50/50% v/v). After vortex mixing (5 min) and centrifugation (15 min at 1000 RFC), urine sample supernatant was collected. Other urine samples were fortified with creatinine.

In the case of creatinine, CV were made with a scanning velocity from 10 to 900  $\text{mV s}^{-1}$  in the  $\pm 1000$  mV potential range. The supporting electrolyte used was BR Buffer;  $0.02 \text{ mol L}^{-1}$  in KCl  $0.25 \text{ mol L}^{-1}$  in the pH range from 3 to 7. SWV was employed to study the redox process and to perform quantitative determination of creatinine. Quantification was performed by measuring peak height, at the potential  $E_P = +415$  mV, using anodic scanning from -1000 to +1000 mV at 20 Hz using 10 mV step potential and 20 mV pulse amplitude.

#### 3.6.4.2

##### **High-performance liquid chromatographic analysis of creatinine**

Analyzes by HPLC were made based on literature [62] using isocratic elution of a mobile phase consisting of a mixture of water/acetate buffer (pH 4.2;  $0.1 \text{ mol L}^{-1}$ ) 60/40% v/v. Chromatography was performed at a flow rate of  $0.8 \text{ mL min}^{-1}$ , at  $25 \text{ }^\circ\text{C}$ , and the introduced sample volume was  $20 \text{ }\mu\text{L}$ . Under these conditions, the retention time of creatinine was 2.4 min. Analytical curve was constructed by introducing  $20 \text{ }\mu\text{L}$  of the standard solutions of creatinine from  $1 \times 10^{-6} \text{ mol L}^{-1}$  ( $113.1 \text{ }\mu\text{g L}^{-1}$ ) to  $1 \times 10^{-4} \text{ mol L}^{-1}$  ( $11.3 \text{ mg L}^{-1}$ ) using three replicates and absorciometric detection at 220 nm.

## 4

### Square-wave voltammetric determination of primaquine in urine using a multi-walled carbon nanotube modified electrode

Paper published in *Microchemical Journal*, 2019, 150, 104201.

DOI: 10.1016/j.microc.2019.104201.

#### 4.1

##### Primaquine and analytical methods for its determination

Malaria is endemic in tropical and subtropical regions and it was responsible for, at least, half a million deaths in 2016 [63]. The disease is caused by parasitic single-celled microorganisms belonging to the *Plasmodium* group, and transmitted to humans by infected *Anopheles* mosquitoes [64]. These parasites travel to the liver where they mature and reproduce.

Primaquine (Fig. 4.1) is used to treat malaria caused by *Plasmodium vivax* and *Plasmodium ovale* [65] probably acting at the DNA level [66]. This drug may be used to treat *Pneumocystis pneumonia* that often affects people with HIV [67]. Primaquine is prescribed with care because of its short therapeutic window and strong side effects [68]. Since primaquine is photo-chemically unstable, forming a myriad of products, the toxicity of the drug may be related to some of the photo-derivatives [69].

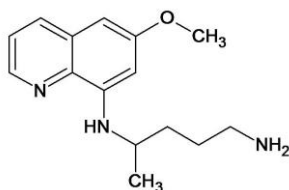


**Figure 4.1.** Structure of primaquine (8- [4-amino-1-methyl butylamino]) - 6-methoxyquinoline).

The procedure indicated by the Pharmacopoeia for the determination of primaquine in pharmaceutical formulations involves potentiometric titration with perchloric acid [70]. Reverse-phase high performance liquid chromatography (HPLC) with the direct absorciometric detection of primaquine has been preferably used for pharmaceuticals [70,71]. The use chromogenic agents such as 2,6-dichloroquinone chlorimide or 1,2-naphthoquinone-4-sulfonate have been reported to enable stronger absorbance in the visible range and spectrophotometric determinations at the  $\text{mg L}^{-1}$  range with very short linear ranges [72]. Fluorimetric methods were also developed after derivatization with fluorescamine (397/480 nm), enabling limit of quantification (LOQ) of  $150 \mu\text{g L}^{-1}$  [73]. Primaquine is metabolized forming several species but the major ones are carboxyprimaquine and glucuronide conjugates [74]. Primaquine, in its original form, was detected, at the  $\mu\text{g L}^{-1}$  level, in blood of patients submitted to multiple oral dose treatment [75]. In urine, a small percent of the drug is still in the original form at the  $\text{ng L}^{-1}$  level [76]. HPLC with absorciometric detection has been employed to monitor primaquine and its derivatives in blood of people infected with malaria [77], also in rabbit plasma [78], at concentrations down to  $20 \mu\text{g L}^{-1}$  after liquid-liquid extraction (LLE) and pre-concentration [78]. Concerning the determination of lower levels (residues of drug), solid phase extraction and HPLC with mass spectrometry have been used to determine primaquine in human whole blood [79] and in blood plasma [80] at  $\mu\text{g L}^{-1}$  levels.

Electrochemical methods have been developed for quantification of primaquine. For instance, HPLC with amperometric detection enabled determinations in calf plasma with limit of detection (LOD) of  $10 \mu\text{g mL}^{-1}$  [81].

Differential pulse voltammetry (DPV) and square-wave voltammetry (SWV) were used to determine primaquine in commercial tablets using a glassy carbon (GC) electrode (buffer at pH 4.0), enabling LOD of  $4.2 \text{ mg L}^{-1}$  (DPV) and  $1.8 \text{ mg L}^{-1}$  (SWV) [65]. The determination of primaquine was also made by DPV with a carbon paste electrode modified with  $\text{Cu(OH)}_2$  nanowires, enabling LOD of  $250 \text{ } \mu\text{g L}^{-1}$  (buffer at pH 5.5) [82]. SWV with a GC electrode, modified with gold nanourchins, allowed LOQ of  $3.3 \text{ nmol L}^{-1}$  ( $1.5 \text{ } \mu\text{g L}^{-1}$ ) for primaquine, which was used for the analysis of urine diluted in buffer (pH 7.2) [83]. Finally, a molecularly imprinted polymer-based electrochemical sensor, using functionalized fullerene as a nanomediator, 2,4,6 trisacrylamido-1,3,5-triazine as a functional monomer and primaquine diphosphate as template, was proposed for selective determinations in human blood plasma and urine (LOD at  $1 \text{ nmol L}^{-1}$  or  $0.45 \text{ } \mu\text{g L}^{-1}$ ) [84]. In Table 4.1, a list of electro-analytical methods is shown, comparing type of analyzed samples and key figure of merits.

The present work, an electro-analytical method for primaquine was developed using a GC modified with multi-walled carbon nanotubes (MWCNTs) that promoted significant improvement in faradaic current (obtained using SWV) as well as better peak resolution. MWCNTs are enormously interesting due to their structure and properties, such as large specific surface area, high electrical conductivity and the ability to promote the electron-transfer reactions [85,86]. A procedure based on the combined use of LLE and thin-layer chromatography (TLC) enabled selectivity and pre-concentration factor for the detection of primaquine in human urine sample.

**Table 4.1.** Summary of characteristics of analytical methods for primaquine in different samples

Sample	Technique <sup>a</sup>	Electrode	Range	Limit of detection <sup>b</sup>	Ref.
Pharmaceutical formulation	SWV	GCE	$3 \times 10^{-5}$ to $1 \times 10^{-2}$ mol L <sup>-1</sup>	1.8 µg mL <sup>-1</sup> ( $6.9 \times 10^{-6}$ mol L <sup>-1</sup> )	[65]
Pharmaceutical formulation	DPV	GCE	$3 \times 10^{-5}$ to $1 \times 10^{-4}$ mol L <sup>-1</sup>	4.2 µg mL <sup>-1</sup> $1.6 \times 10^{-5}$ mol L <sup>-1</sup>	[65]
Pharmaceutical formulation	DPV	Cu(OH) <sub>2</sub> nano-wire modified carbon paste electrode	$2.2 \times 10^{-6}$ to $2.3 \times 10^{-5}$ mol L <sup>-1</sup>	0.25 µg mL <sup>-1</sup> ( $9.6 \times 10^{-7}$ mol L <sup>-1</sup> )	[82]
Urine, pharmaceutical formulation	DPV	Au-nanourchins modified GCE	$1 \times 10^{-8}$ to $1 \times 10^{-6}$ mol L <sup>-1</sup>	$3.5 \times 10^{-9}$ mol L <sup>-1</sup>	[83]
Urine, pharmaceutical formulation	SWV	Au-nanourchins modified GCE	$1 \times 10^{-9}$ to $1 \times 10^{-6}$ mol L <sup>-1</sup>	$0.9 \times 10^{-9}$ mol L <sup>-1</sup>	[83]
Blood Plasma	DPV	Vinylic-C60 modified PGE	$4.2 \times 10^{-9}$ to $8.2 \times 10^{-7}$ mol L <sup>-1</sup>	$1.2 \times 10^{-9}$ mol L <sup>-1</sup>	[84]
Urine	DPV	Vinylic-C60 modified PGE	$3.4 \times 10^{-9}$ to $7.9 \times 10^{-7}$ mol L <sup>-1</sup>	$1.2 \times 10^{-9}$ mol L <sup>-1</sup>	[84]
Pharmaceutical formulation	DPV	Vinylic-C60 modified PGE	$4.8 \times 10^{-9}$ to $8.0 \times 10^{-7}$ mol L <sup>-1</sup>	$1.2 \times 10^{-9}$ mol L <sup>-1</sup>	[84]
Urine	SWV	GCE/MWCNTs	$5.0 \times 10^{-7}$ to $5.0 \times 10^{-6}$ mol L <sup>-1</sup>	$28 \times 10^{-9}$ mol L <sup>-1</sup>	This work

<sup>a</sup>DPV, differential pulse voltammetry; SWV, square-wave voltammetry; GCE, glassy carbon electrode; PGE, pyrolytic graphite electrode.

<sup>b</sup>Some original LOD and LOQ values were converted in mol L<sup>-1</sup>.

## 4.2

### Results and discussion

#### 4.2.1

##### Electrochemical studies

The electrochemical behavior of primaquine on GC has been previously studied and reported in literature [65,87,88]. At low concentrations, oxidation of primaquine has been investigated by CV and only one irreversible anodic peak,

within +550 to +700 mV range, depending on the pH, was observed with no cathodic peak in the reversed scan [65]. The process was found to be controlled by diffusion, involving transfer of two-electrons [87,88]. Peak potential ( $E_p$ ) of the oxidation process shifted linearly towards less negative values at more acidic conditions ( $2 < \text{pH} < 4$ ) with involvement of hydrogen ions in electrode reaction [88]. At this more acidic range, a new less intense redox process (oxidation/reduction pair) is reported at less positive potentials and attributed to the formation of a product from the main oxidation process. In an intermediary pH range ( $4.5 < \text{pH} < 9.0$ ), the main oxidation peak potential becomes pH independent, as the electrochemical process occurs with no pre-protonation, showing that the neutral form of primaquine is more easily oxidized than the deprotonated form [88]. Above pH 9.0, the shifting towards lesser negative potentials is observed [65,87,88]. It was concluded that the oxidation of primaquine in aqueous solution involves the quinolinic ring, since aliphatic amines are oxidized at very positive potentials. In addition,  $E_p$  becomes independent upon pH in the range limited to values that clearly corresponds to the  $\text{pK}_{a1}$  (about 4), related to the acid-base equilibrium between the protonated form of the quinolinic ring, and to the  $\text{pK}_{a2}$  (about 9) related to the quinolone/quinolinate pair.

Initial electrochemical studies were made comparing the primaquine oxidation peak observed using bare GC and the GC with the surface modified with MWCNTs whose scanning electron microscopy is shown in Fig. 4.2A. The experiment was made at pH 7.0 (BR buffer at  $0.02 \text{ mol L}^{-1}$ /KCl  $0.25 \text{ mol L}^{-1}$ ) with the CV scanning within a broad interval (between  $-1200$  and  $+1200$  mV). In such conditions, the  $I_p$  of the oxidation peak ( $E_p$  at  $+551$  mV), achieved using the GC/MWCNTs electrode, was about 7 times more intense than the one ( $E_p$  at  $+631$

mV) observed using the bare GC (Fig. 4.2B). By using the GC/MWCNTs electrode, the redox pair, observed at less positive potential by La Scalea *et al.* only at pH 4.0 [87,88], became apparent even at pH 7.0. It is also observed a decreasing in  $I_p$  during a second voltammetric cycle, minimizing reposition of the analyte in the electrode-solution interface by convective mass transport, which is in agreement with the irreversible character of the process (Fig. 4.2C). It is known that the presence of the MWCNTs largely improved electrode area, also increasing electrontransfer rate and promoting electrocatalytic activity [17].

A study was made to adjust the amount of MWCNTs to be added to the surface of the GC (from 15  $\mu\text{g}$  to 90  $\mu\text{g}$ ). It was observed that as the amount of MWCNTs increased the analyte signal ( $I_p$  measured at +551 mV) also increased (Fig. 4.2D) with no further shift in  $E_p$ . However, it was decided to use 30  $\mu\text{g}$  (by means of 10  $\mu\text{L}$  of a 3  $\text{mg mL}^{-1}$  MWCNTs dispersion) since drying of the electrode was faster and better mechanical stability of the modification onto de GC surface was obtained.

Cyclic voltammograms (Fig. 4.3) were also made at three different pH values (4.0, 7.0 and 9.0) and, in all cases, the electrochemical processes were more intense in the GC-MWCNTs when compared to the ones observed using bare GC. The complexity of the electrochemical processes can be also better observed using the GC/MWCNTs (better resolution) allowing even the main process, occurring in the more positive range (above +400 mV), to appear as a more than one-step event (except at pH 9.0, in which coalescence of peaks occurs). The study concerning the main oxidation peak (Fig. 4.4A) indicated that  $E_p$  does not significantly change in function of the pH in the shorter range from pH 6.0 to 9.0.

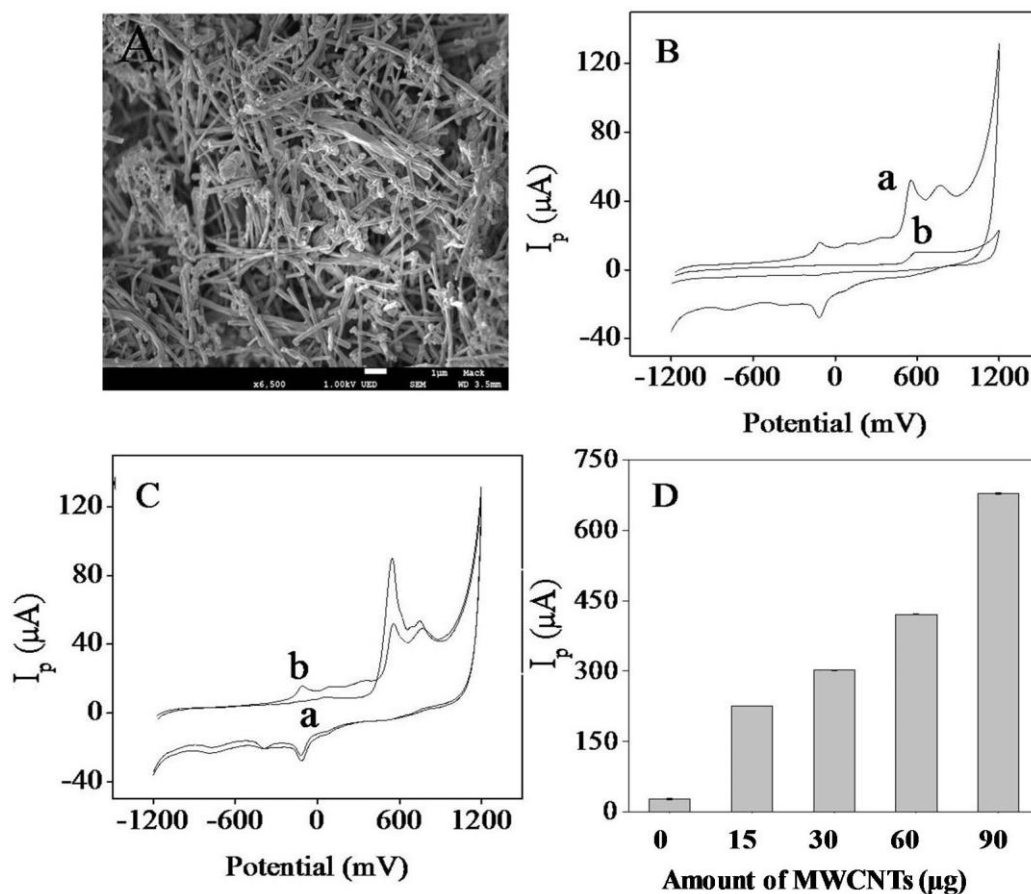


**Figure 4.2.** (A) Scanning electron microscopy of MWCNTs onto GC. (B) CV response from primaquine: (a) GC/MWCNTs electrode and (b) bare GC electrode. (C) CV response from primaquine using GC/MWCNTs electrode: (a) 1<sup>st</sup> scan, (b) 2<sup>nd</sup> scan at  $100 \text{ mV s}^{-1}$ . (D) Study of the amount of MWCNTs onto the surface of GC. Experimental conditions: Britton-Robinson Buffer  $0.02 \text{ mol L}^{-1}$  with KCl  $0.25 \text{ mol L}^{-1}$  and pH 7.0.

As the  $E_p$  (from the CV experiment) remained constant in the range from pH 6.0 and 9.0 (indicating robust condition for signal measurement), the chosen condition for the analytical studies using the GC/MWCNTs was pH 7.0. In such condition, cyclic voltammogram presented two oxidation peaks (anodic scan) with the less intense one (peak 1) with at about +78 mV ( $E_{p1}$ ) and the main peak (peak 2) at +551 mV ( $E_{p2}$ ). As the scan was reversed (cathodic scan), a reduction peak ( $E_{p3}$  at  $-108 \text{ mV}$ ) was found (peak 3) establishing a redox pair with peak 1 (Fig.

4.4B). As a second voltammogram was made from  $-1200$  to  $+1200$  mV, with minimized convective transport, a significantly reduction of the intensity of all peaks (especially peak 1) was observed (Fig. 4.2C).

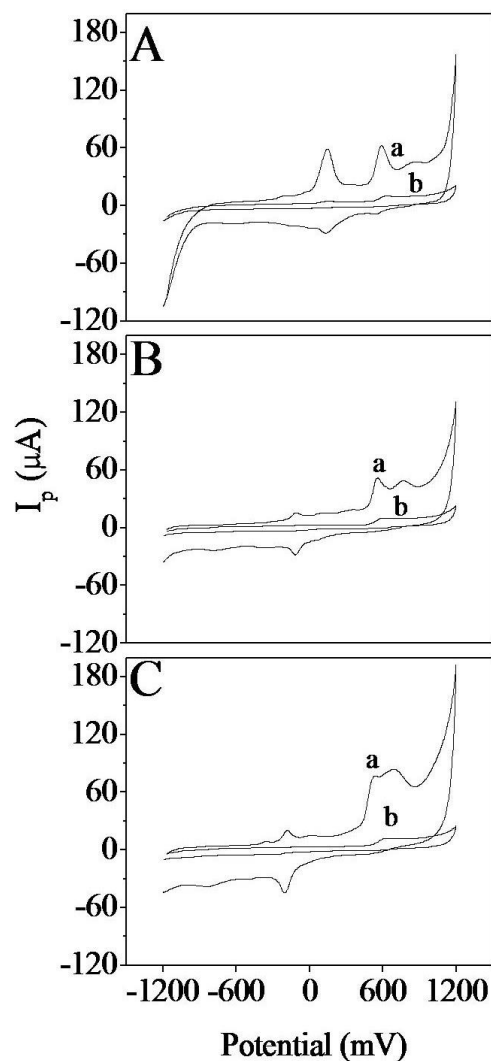


**Figure 4.3.** CV response from primaquine ( $2 \times 10^{-4}$  mol L $^{-1}$ ) using (a) GC/MWCNTs electrode and (b) bare GC electrode at: (A) pH 4.0 (B) pH 7.0 and (C) pH 9.0. BR Buffer 0.02 mol L $^{-1}$  with KCl 0.25 mol L $^{-1}$  and 100 mV s $^{-1}$  scan rate.

It was verified that the redox pair (peaks 1 and peak 3) is dependent upon each other as shown by the experiment made in a limited potential range ( $-1200$  to  $+100$  mV) that still produces this specific electrochemical process (Fig. 4.4B). In

contrast with literature, the result may indicate that the redox pair is not necessarily due to a product of the oxidation that occurs at higher potentials. The peak potential of peak 2 ( $E_{p2}$ ) varied to more positive values as the scanning rate ( $v$ ), obtained by CV, increased from 20 to 1000  $\text{mV s}^{-1}$  (Fig. 4.4C), confirming the irreversible oxidation and suggesting a chemical reaction coupled to the electrochemical process. The experiment also indicated two linear regions when  $I_{p2}$  was plotted in function of the square root of  $v$  (Fig. 4.4D): one at lower scanning rates ( $R^2 = 0.979$  from 20 to 100  $\text{mV s}^{-1}$ ) and another at higher scanning rates ( $R^2 = 0.995$  from 200 to 1000  $\text{mV s}^{-1}$ ). In addition, the relationship between  $\log(I_{p2})$  and the  $\log(v)$  has a linear tendency ( $R^2 = 0.90$ ). These results combined indicate that a mixed diffusion-adsorption controlled processes are taking place [89].

Square-wave voltammograms for primaquine using the GC/MWCNTs electrode confirms a more complex redox process at more acidic pH, with a less positive redox event (at +160 mV) and a main electrochemical peak occurring at higher positive potential (at +620 mV). At higher pH values, the only relevant peak observed using SWV is the one at the more positive potential (+577 mV at pH 7.0 and +607 mV at pH 9.0) as seen in Fig. 4.5A. The relationship between  $I_{p2}$  and the applied frequency ( $f$ ) in SVW was found to be linear ( $R^2 = 0.996$ ), which confirms that the oxidation that occurs at more positive potential is irreversible (Fig. 4.5B). Irreversible reactions are characterized by the linear relationship ( $R^2 = 0.996$ ) between  $E_p$  and the  $\log(f)$  [89] (Fig. 4.5C).

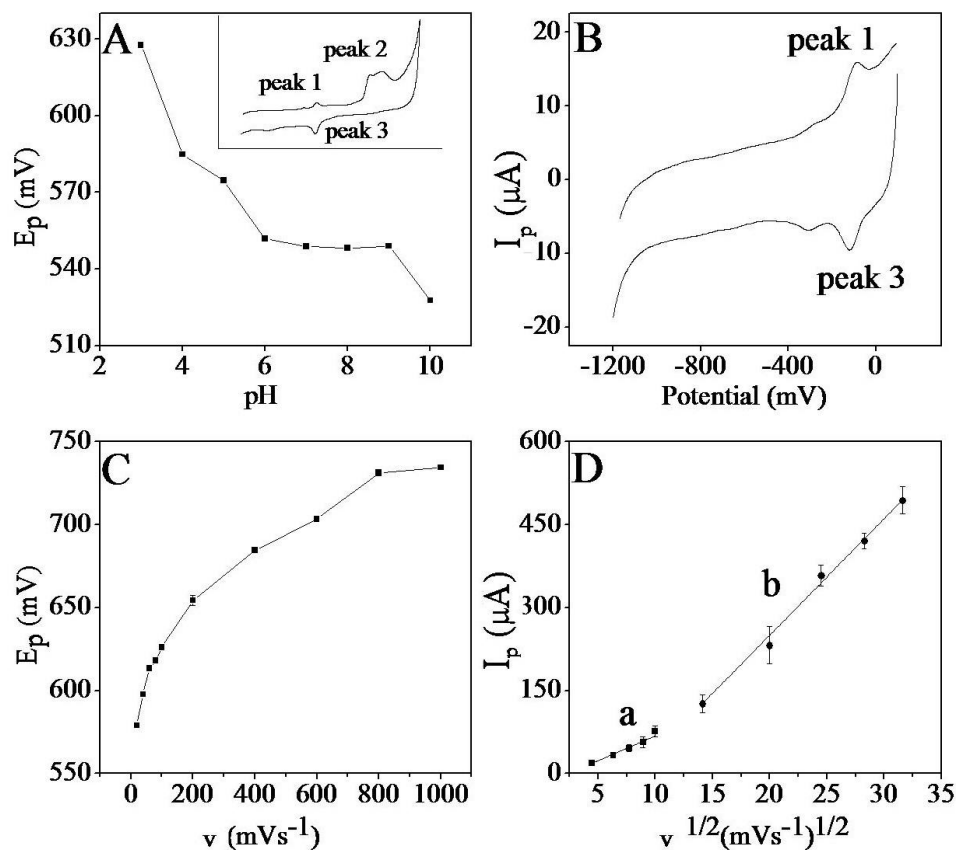


**Figure 4.4.** (A) Plot of  $E_p$  (main oxidation peak) *versus* pH using the GC/MWCNTs electrode. (B) Redox pair at lower potential range (peak 1/peak 3). (C)  $E_p$  as a function of scan rate. (D)  $I_p$  as a function of  $v^{1/2}$ : (a) Lower rates: ( $R^2 = 0.979$  from 20 to 100  $\text{mV s}^{-1}$ ) and (b) higher rates ( $R^2 = 0.995$  from 200 to 1000  $\text{mV s}^{-1}$ ). BR Buffer 0.02  $\text{mol L}^{-1}$  with KCl 0.25  $\text{mol L}^{-1}$ . Primaquine at  $2 \times 10^{-4}$   $\text{mol L}^{-1}$ .

#### 4.2.2 Optimization of measurement conditions

A systematic study was made to obtain best experimental and instrumental conditions for the determination of primaquine using SWV with the GC/MWCNT electrode, taking into account the critical parameters that affect the intensity, stability and reproducibility of the main oxidation peak ( $I_p$  at +577 mV). The supporting electrolyte consisted of BR buffer (pH 7.0; 0.02  $\text{mol L}^{-1}$ ) and KCl (0.25  $\text{mol L}^{-1}$ ). The signal intensity steadily increased as the pulse amplitude was varied

(from 30 to 100 mV) with 40 mV selected due to the better relationship between peak sharpness and intensity. Pulse frequency of 30 Hz was a compromise between  $I_p$  and peak width within the 5 to 200 Hz range studied. The potential step was directly proportional to  $I_p$  up to 20 mV, remaining constant after 30 mV. Pre-concentration of primaquine on the working electrode was attempted by applying different lower potentials, for 30 s, before scanning the potential towards +1000 mV but no increasing of  $I_p$  was observed.

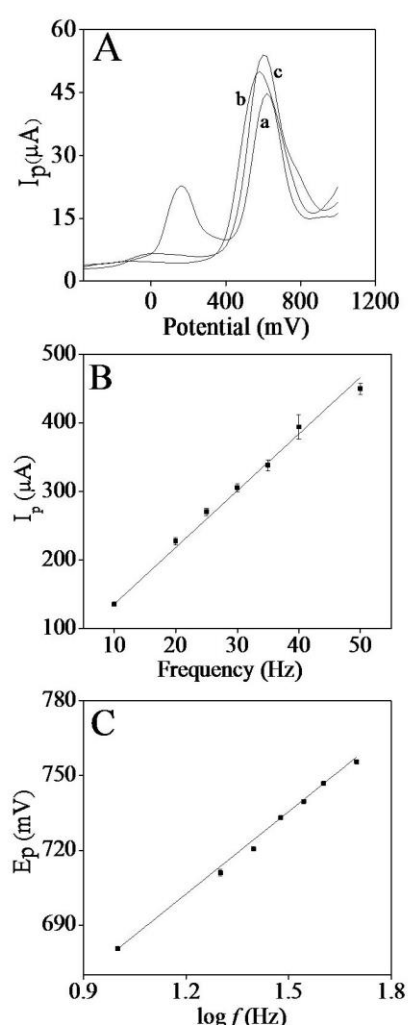


**Figure 4.5.** SWV studies for primaquine ( $1 \times 10^{-4} \text{ mol L}^{-1}$ ) using MWCNTs. (A) voltammograms at: a) pH 4.0, b) pH 7.0 and c) pH 9.0. (B)  $I_p$  in function of  $f$  for main oxidation peak ( $R^2 = 0.996$ ); C)  $E_p$  in function of the  $\log f$  ( $R^2 = 0.996$ ). BR Buffer  $0.02 \text{ mol L}^{-1}$  with KCl  $0.25 \text{ mol L}^{-1}$ .

### 4.2.3 Analytical characteristics

The analytical curve was constructed by sequential addition of increasing concentration of analyte into the electrochemical cell (Fig. 4.6A and B). The linear dynamic range of primaquine on GC/MWCNTs was in the range from 0.1 to 5.0  $\mu\text{mol L}^{-1}$ . In order to compare the performance of the GC/MWCNTs electrode ( $I_p$  at +577 mV), a set of square-wave voltammograms and the analytical curve was also obtained by using the bare GC electrode ( $I_p$  at +660 mV) as seen in Fig. 4.6C and D. The sensitivity using the GC/MWCNTs electrode ( $2.08 \text{ A L mol}^{-1}$ ) was almost 24 times higher than the one obtained using the bare GC electrode ( $0.089 \text{ A L mol}^{-1}$ ), which is an increasing factor five times larger than the one based only upon surface active area, indicating that an electro-catalytic process is probably taking place onto the surface of the MWCNTs.

Instrumental LOD and LOQ were calculated respectively as  $3sb m^{-1}$  and  $10sb m^{-1}$ , where  $sb$  is the standard deviation ( $n=10$ ) of the  $I_p$  measured for the lowest concentration of the analytical curve and  $m$  is the sensitivity of the curve. For the GC/MWCNTs electrode, the instrumental LOD was  $28 \text{ nmol L}^{-1}$  ( $7.26 \mu\text{g L}^{-1}$ ) and the instrumental LOQ was  $93 \text{ nmol L}^{-1}$  ( $24.1 \mu\text{g L}^{-1}$ ) of primaquine. As a comparison, the instrumental LOD and LOQ values obtained using the bare GC electrode were respectively  $1.6 \mu\text{mol L}^{-1}$  ( $0.41 \text{ mg L}^{-1}$ ) and  $5.4 \mu\text{mol L}^{-1}$  ( $1.4 \text{ mg L}^{-1}$ ).

Precision was evaluated as the coefficient of variation of  $I_p$  obtained from 10 consecutive SWV scans, at a given analyte concentration, using the same GC/MWCNTs electrode. Prior to each scanning, mechanical stirring of solution

was made to replenish the solution–electrode interface. Precision at  $1 \times 10^{-6} \text{ mol L}^{-1}$  ( $0.25 \text{ } \mu\text{g mL}^{-1}$ ) was 4.2% while at  $1 \times 10^{-5} \text{ mol L}^{-1}$  ( $2.59 \text{ } \mu\text{g mL}^{-1}$ ) it was 3.8%.

The stability of MWCNTs was evaluated by obtaining 20 repetitive cyclic voltammograms of  $200 \text{ } \mu\text{mol L}^{-1}$  of primaquine, using the same modified electrode. The measured average peak currents for primaquine were  $47.6 \text{ } \mu\text{A}$  with the relative standard deviation of 2%, indicating that MWCNTs modification onto the GC electrode surface is stable after several measurements.

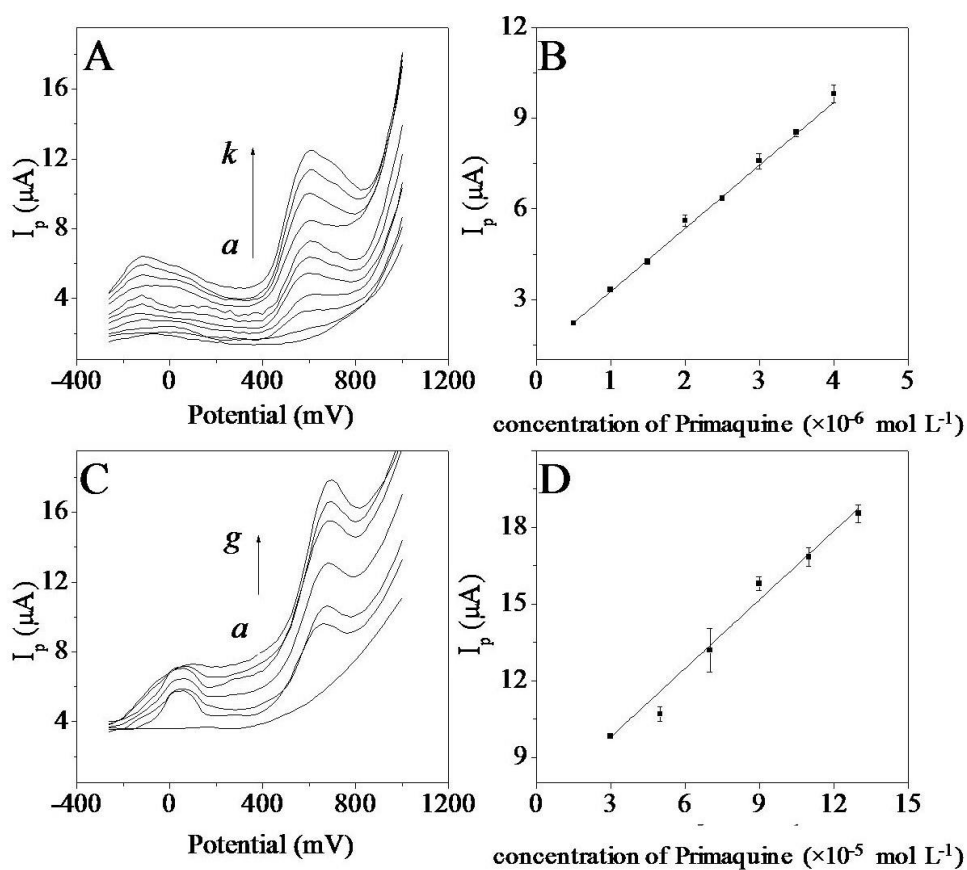


**Figure 4.6.** (A) SWV of primaquine using GC/MWCNTs electrode: a) 0, b)  $5 \times 10^{-7}$ , c)  $1 \times 10^{-6}$ , d)  $1.5 \times 10^{-6}$ , e)  $2 \times 10^{-6}$ , f)  $2.5 \times 10^{-6}$ , g)  $3 \times 10^{-6}$ , h)  $3.5 \times 10^{-6}$ , i)  $4 \times 10^{-6}$ , j)  $4.5 \times 10^{-6}$ , k)  $5 \times 10^{-6} \text{ mol L}^{-1}$  and (B) Analytical curve:  $I_p$  ( $\mu\text{A}$ ) =  $(2.08 \pm 0.04) \times 10^6 C_{\text{primaquine}} + (1.19 \pm 0.10)$  ( $R^2 = 0.999$ ). (C) SWV response of primaquine using bare GC: a) 0, b)  $3 \times 10^{-5}$ , c)  $6 \times 10^{-5}$ , d)  $9 \times 10^{-5}$ , e)  $1.2 \times 10^{-4}$ , f)  $1.5 \times 10^{-4}$ , g)  $1.3 \times 10^{-4} \text{ mol L}^{-1}$

L<sup>-1</sup>. (D) Analytical curve:  $I_p$  ( $\mu\text{A}$ ) =  $(8.92 \pm 0.50) \times 10^4 C_{\text{primaquine}} + (7.11 \pm 0.25)$  ( $R^2 = 0.984$ ). BR buffer  $0.04 \text{ mol L}^{-1}$  with KCl  $0.5 \text{ mol L}^{-1}$  at pH 7.0.

#### 4.2.4

##### Strategy for the application of the method in the analysis of urine

Studies were conducted to evaluate the potential interference imposed by some of the urine components in the electro-analytical signal of primaquine. Interference was evaluated by the ratio between the signal from a solution containing only the analyte and the signal measured from a solution containing the analyte and a substance typical of urine matrix, in this case, the analyte concentration was the same in both solutions ( $4 \times 10^{-6} \text{ mol L}^{-1}$  or  $1.04 \mu\text{g mL}^{-1}$ ).

These  $I_{\text{analyte}}/I_{(\text{analyte} + \text{urine component})}$  values near unity did not indicate interference. Values below unity indicated the increasing of the measured signal due to the contribution from the other urine component. These tests were carried out at two different analyte:urine component molar ratios (1:1 and 1:2). Measurements were performed in triplicate and the calculations were based on the peak height.

Urea, uric acid, phenylalanine, histidine, valine,  $\text{HCO}_3^-$ ,  $\text{Na}^+$ ,  $\text{K}^+$  did not impose any interference. In contrast, cysteine, tryptophan and creatinine were found to interfere as they also produce measurable signal at the potential range chosen to determine primaquine as indicated by the  $I_{\text{analyte}}/I_{(\text{analyte} + \text{urine component})}$  values lower than unity (Table 4.2). The voltammogram produced by a urine sample not containing primaquine (after deproteinization) is shown in Fig. 4.7 with a large redox profile probably composed by the contribution of oxidation of several substances.

In order to eliminate interferences, a combined procedure involving LLE and TLC was developed to enable separation and some level of analyte pre-concentration aiming the determination of primaquine at the expected levels ( $\text{ng L}^{-1}$ ) found in urine samples of people under treatment. LLE procedure involved the use of chloroform and urine sample (after deproteinization) diluted and at pH adjusted to about 9 (to guarantee that the major fraction of the drug is in the unprotonated form). LLE efficiency to remove primaquine (at  $1 \times 10^{-5} \text{ mol L}^{-1}$ ) was evaluated by means of three replicates (3 extractions per replicate that were combined altogether before solvent evaporation). The percent recovery, calculated based on the amount of primaquine (fortification), was  $(94.6 \pm 3.8)\%$  and the pre-concentration factor was 50 times. The same test was made using urine sample fortified with a standard solution of primaquine diphosphate (final concentration in sample of  $1 \times 10^{-5} \text{ mol L}^{-1}$ ). The recovery was  $(133.1 \pm 8.3)\%$  ( $n=3$ ) indicating that small fractions of other components in urine were also extracted along primaquine.

Because of the extraction of other sample components, an additional separation procedure was performed by TLC, based on a procedure from literature for chloroquine [90] that employed methanol/ammonia as mobile phase. A previous test was made to evaluate the chromatographic elution of primaquine and of three other urine components along the chromatographic plate. The procedure provided a retention factor ( $R_f$ ) for primaquine of 0.42.  $R_f$  values for cysteine, tryptophan and creatinine were respectively 0.65, 0.69 and 0.63 meaning that in a mixture these substances are concentrated in the same spot and far from the one of primaquine.

In order to maximize the use of the extracted material, 10 sample spots per TLC plate (side by side) were made. After separation, the area of the plate was removed ( $\pm 0.5 \text{ cm}$  around the  $R_f$  of primaquine) and transferred to a vial to be re-

dissolved in acidified water (about pH 4), filtrated and then dried again before it was re-dissolved with 1.00 mL water that was then quantitatively transferred to the analytical cell. The same procedure was made using a plate without primaquine and no signal was observed concerning any TLC plate constituent that could impose interference.

The analysis was performed using urine fortified with primaquine diphosphate at  $1.09 \times 10^{-5} \text{ mol L}^{-1}$ . The recovery obtained, after combination of LLE and TLC, was  $(1.21 \pm 0.10) \times 10^{-5} \text{ mol L}^{-1}$  (percent recovery of  $111 \pm 8.9\%$ ). The voltammogram of the analyte after LLE/TLC is shown in Fig. 4.7 along with the voltammogram of the control non-fortified urine that did not indicate a defined signal over the potential range measured (not producing systematic signal contribution). Considering the complexity of the matrix and the concentration level of primaquine, the result can be considered satisfactory. The same sample was also analyzed by HPLC, using a method from literature [59], and recovery was  $(1.16 \pm 0.03) \times 10^{-5} \text{ mol L}^{-1}$  (percent recovery of  $106.4 \pm 2.6\%$ ). *Student t*-test for different variances (previously verified using the *Fisher-Snedecor* test) was used to compare the mean values of the results of each method. The statistical test considered a confidence limit of 95% (two tails, each with  $\alpha/2=0.025$ ). The test indicated that results are in statistical agreement ( $t_{\text{experimental}}=0.7 < t_{\text{critical}}=4.3$ ). The simplicity of the electrode modification procedure, the facile sample pre-treatment and the combined use of LLE and thin layer chromatography (TLC) are part of the advantages of this work, besides the low detection limits, which correspond to the same order of magnitude of the best ones reported in literature (Table 4.1).

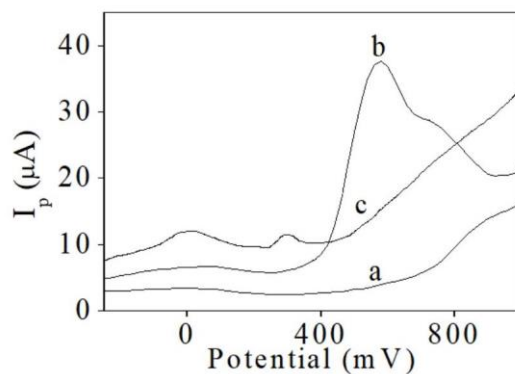


**Figure 4.7.** SWV voltammograms at GCE/MWCNTs (a) Urine control after deproteinization, LEE and TLC; (b) Urine fortified with primaquine ( $1.0 \times 10^{-5}$  mol  $L^{-1}$ ) after LEE and TLC; (c) Urine control sample only after deproteinization.

**Table 4.2.** Evaluation of interference imposed by urine components in the signal from primaquine

Urine component	Proportion (primaquine/urine component)	$I_{PQ}/I_{(PQ + \text{urine components})} \pm S_{ratio}^b$
Cysteine	1:0	$1.00 \pm 0.11$
	1:1	$0.80 \pm 0.04$
	1:2	$0.66 \pm 0.11$
Tryptophan	1:0	$1.00 \pm 0.03$
	1:1	$0.82 \pm 0.05$
	1:2	$0.60 \pm 0.04$
Creatinine	1:0	$1.00 \pm 0.15$
	1:1	$0.75 \pm 0.13$
	1:2	$0.73 \pm 0.12$

<sup>b</sup>The standard deviation of  $I_{analyte}/I_{(analyte + \text{other urine components})}$ .

### 4.3

#### Partial conclusion

The modification of the GC using a layer of MWCNTs provided amplification of the electrochemical signal measured from primaquine by SWV due to the increased active area and improved electron-transfer rate. GC/MWCNTs also provided, when working on a proper pH, higher resolution in detecting the different electrochemical steps involved in the redox process of primaquine. The electrode enabled low LOD for primaquine and when associated with a simple developed procedure, relying of LLE associated with TLC, enabled selectivity and capability to determine the lower levels expected in urine samples. In a standard malaria treatment, one tablet of primaquine (containing 26 mg of primaquine diphosphate) is administrated per day during 15 days [91] and between 1 and 5% of primaquine is excreted in its original form (within 24 h). Therefore, the developed method enabled the determination at the required  $\text{ng L}^{-1}$ , since LOD of the method, including pre-concentration factor, was  $250 \text{ ng L}^{-1}$ .

## 5

### **Square-Wave voltammetric determination of INHHQ, a promising metal-protein attenuating compound for the treatment of Alzheimer's disease, using a MWCNT modified glassy carbon electrode**

Paper published as “*Square-Wave Voltammetric Determination of 8-Hydroxyquinoline-2-Carboxaldehyde Isonicotinoyl Hydrazone (INHHQ), a Promising Metal-Protein Attenuating Compound for the Treatment of Alzheimer's Disease, Using a Multiwalled Carbon Nanotube (MWCNT) Modified Glassy Carbon Electrode (GCE)*”

Paper published in Analytical Letters, 2020.

DOI: 10.1080/00032719.2020.1741603

#### 5.1

##### **INHHQ and analytical methods for its determination**

Alzheimer's disease is a progressive neurodegenerative disorder that is characterized by cognitive and memory dysfunctions [92]. The disease is most commonly diagnosed in people above 65 years of age, although it may occur earlier [93]. Alzheimer's patients commonly have developed extracellular senile plaques, composed of aggregates of the amyloid- $\beta$  peptide ( $A\beta$ ), and intracellular neurofibrillary tangles, primarily consisting of hyperphosphorylated tau protein [94].

The human brain is able to concentrate metal ions, whose levels increase as a normal consequence of aging. Some studies indicate that the interaction of amyloid- $\beta$  peptide with metals, such as copper and zinc, may be involved in the oxidative stress and processes leading to peptide oligomerization and aggregation because these ions have been found in amyloid plaques [95][96][97]. Moreover, soluble amyloid- $\beta$  peptide oligomers are considered to be potent synaptotoxins [98]. Considering the putative importance of some metal ions in the development

of Alzheimer's disease, the prevention of amyloid- $\beta$  peptide oligomerization in the brain is considered to be a potential treatment strategy [99].

Metal protein attenuating compounds (MPACs) are therapeutic agents presenting a high potential for the treatment of amyloidogenic pathologies [100]. They compete with the aggregating peptide or protein for the binding of metal ions, avoiding oligomerization, decreasing oxidative stress and restoring metal homeostasis [95]. The 8-hydroxyquinoline-2-carboxaldehyde isonicotinoyl hydrazone or INHHQ (Fig. 5.1) has demonstrated *in vitro* metal protein attenuating activity in recent works [101][60] as it was capable of blocking the interactions of  $Zn^{2+}$  and  $Cu^{2+}$  with the Ab protein.

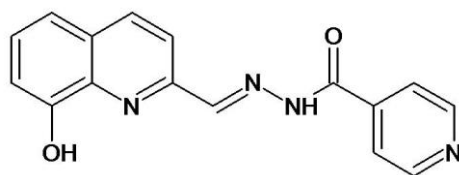


**Figure 5.1.** INHHQ structure (8-hydroxyquinoline-2-carboxaldehyde isonicotinoyl hydrazone).

*In vivo* studies have showed no lethality in acute exposure at high doses, up to 300 mg per kg of body weight in healthy rats [101], and suggested that an innocuous dose of 1mg per kg of body weight that was intraperitoneally injected in physiologic solution containing 10% dimethyl sulfoxide is adequate to prevent memory loss in an Alzheimer's disease mouse model [102]. In addition to the 8-hydroxyquinoline group, INHHQ also contains an isoniazid group, resulting in a ligand capable of coordinating metal ions of biological importance through different donor atoms including nitrogen and oxygen [103].

High concentrations of INHHQ are difficult to dissolve in water, forming primarily suspensions. However, at the *in vivo* tested active dose ( $0.1 \text{ mg mL}^{-1}$ ) the compound is stable and efficiently solubilized at physiological pH. Acidic aqueous media, on the other hand, enhance the hydrolysis of the hydrazine moiety of the INHHQ [104].

As there is no analytical method reported so far in the literature for determination of INHHQ in biological matrices, the present work describes how the modification of the glassy carbon electrode (GCE) with multi-walled carbon nanotubes (MWCNTs) promoted a large Faradaic current utilizing square-wave voltammetry (SWV).

The MWCNTs are characterized by high electrical conductivity, high surface area, good chemical stability, as well as relative chemical inertness in most electrolyte solutions in addition to a wide operation potential window. Further, they exhibit electro-catalytic properties due to their significant mechanical strength [17]. The MWCNTs have been widely employed in electrochemistry for the modification of electrodes. For example, the modification of the glassy carbon electrode surface using multiwalled carbon nanotubes provided amplification of the electrochemical signal measured utilizing square-wave voltammetry from an antimalarial (primaquine) due to the enhancement in the active area and the increased electron transfer rate [105]. By the use of this approach, a procedure has been developed for the detection of primaquine in human urine samples based on the combined use of liquid liquid extraction and thin-layer chromatography (TLC) to provide suitable selectivity. Based on this protocol, a square-wave voltammetric method using a glassy carbon modified with multiwalled carbon nanotubes was developed for the determination of INHHQ. A thin-layer chromatography (TLC) procedure was

involved to enhance the selectivity required to determine INHHQ in the brain tissue obtained from Wistar rats.

## 5.2

### Results and discussion

#### 5.2.1

#### Electrochemical properties of INHHQ on a glassy carbon electrode modified with MWCNTs

The results showed that an increase of the mass of MWCNTs onto the glassy carbon electrode, up to 30  $\mu\text{L}$  of dispersion (90  $\mu\text{g}$  of MWCNTs), improved current peak intensity obtained from the INHHQ cyclic voltammogram as shown in Fig. 5.2A for the current measured at +209 mV. However, 10  $\mu\text{L}$  of dispersion, corresponding to 30  $\mu\text{g}$  of MWCNTs, provided best mechanical stability of the modified electrode and most reproducible response as a function of time. The measurements also revealed that the glassy carbon electrode modified with MWCNTs (GC/MWCNTs) produced a notable increase in the electrochemical response of INHHQ as compared to the unmodified bare glassy carbon electrode. This effect can be observed in the cyclic voltammograms in Fig. 5.2B and C obtained at 100  $\text{mV s}^{-1}$  and using sustaining electrolyte consisting of 0.02  $\text{mol L}^{-1}$  pH 11.0 Britton-Robinson buffer solution 0.25  $\text{mol L}^{-1}$  KCl. The blank solution did not produce an electrochemical signal as shown in Fig. 5.2B.

The modification with MWCNTs provided a larger active surface area with enhanced contact between electrode and analyte in solution, leading to an approximate five-fold enhancement in the measured current of the redox processes concerning INHHQ with well-resolved peaks compared to the low intense and broad peaks observed using the bare glassy carbon electrode. The results also show

that the voltammetric peaks appear at lower potentials indicating that INHHQ is being easily reduced and oxidized at the MWCNT-modified glassy carbon electrode when compared to the unmodified electrode.

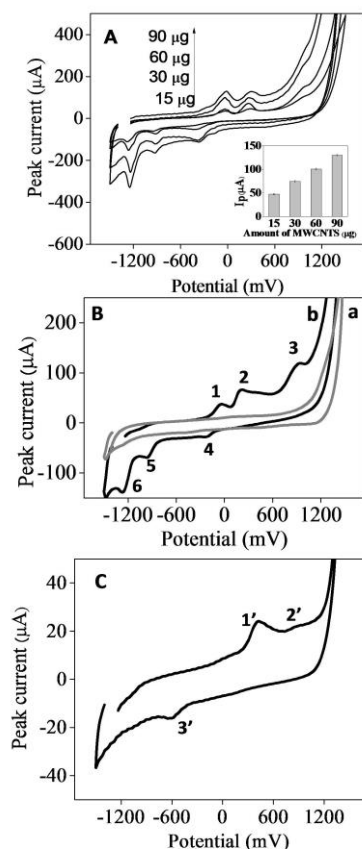


**Figure 5.2.** Cyclic voltammograms from INHHQ using (A) different quantities of MWCNTs onto electrode surface (peak current at +209 mV in detail). (B) a) Blank solution at GC/MWCNTs electrode (30  $\mu\text{g}$  MWCNTs) b) GC/MWCNTs electrode (30  $\mu\text{g}$  MWCNTs) with INHHQ: Peak 1 at -47 mV, peak 2 at +209 mV, peak 3 at +926 mV, peak 4 at -215 mV, peak 5 at -966 mV, peak 6 at -1267 mV. (C) Bare GC electrode: Peak 1' at +418 mV, peak 2' at +867 mV, peak 3' at -590 mV. INHHQ at  $2 \times 10^{-4} \text{ mol L}^{-1}$ , BR buffer ( $0.02 \text{ mol L}^{-1}$ ; pH 11.0 in KCl  $0.25 \text{ mol L}^{-1}$ ) and  $100 \text{ mV s}^{-1}$  scan rate.

On the basis of these observations, it can be postulated that the MWCNTs may promote a catalytic effect in the electrochemical oxidation of INHHQ, leading to a decrease in the overpotential and a remarkable enhancement of the anodic or

cathodic peak currents [82,106,107]. For example, peak 2, obtained using the MWCNT-modified glassy carbon electrode is a well-defined and sharp anodic peak at +209 mV. Its counterpart (peak 1'), obtained using the unmodified glassy carbon electrode, is a relatively broad and smaller anodic peak at +418 mV.

The choice of the pH to perform the cyclic voltammetry was based on the stability of the compound and the intensity of the electrochemical signal (Fig. 5.3) while also considering the solubility of INHHQ at a concentration of  $1 \times 10^{-4}$  mol L<sup>-1</sup> in aqueous solution. A volume of 100  $\mu$ L of a stock solution of  $1 \times 10^{-2}$  mol L<sup>-1</sup> INHHQ in dimethyl sulfoxide was placed in aqueous Britton-Robinson solutions at various pH values above neutral conditions (7.0, 9.0 and 11.0), because the literature has reported that in acidic conditions, INNHQ readily degrades back to its precursors [104]. After solubilizing the INNHQ at pH 7.0 and 9.0, turbidity was observed after a few minutes, probably due to the partial precipitation that occurs using INHHQ at the concentrations required to perform cyclic voltammetry. However, using the supporting electrolyte at pH 11.0, the analyte was shown to be stable and sufficiently soluble.

In Fig. 5.3C, the cyclic voltammogram at pH 11.0 (within  $\pm 1500$  mV) presented two main anodic peaks at -47 mV (peak 1) and +209 mV (peak 2) and another close to the limit of the potential window at +926 mV (peak 3). In addition, there are two main cathodic peaks at -215 mV (peak 4) and -966 mV (peak 5) along with a cathodic peak close to the negative limit of the electrode potential window at -1267 mV (peak 6). In order to evaluate the interdependence of the observed redox events, cyclic voltammograms of the analyte were obtained using shorter potential ranges at 100 mV s<sup>-1</sup> as shown in Fig. 5.3D which includes a more negative

potential range from -1500 mV to 0 mV, an intermediary potential range from -400 mV to +400 mV and a more positive potential range from 0 mV to +1500 mV. The profiles of voltammograms confirm a redox pair composed of the peak with a maximum at -47 mV and -215 mV (peaks 1 and 4). In contrast, the peak at +209 mV had no cathodic counterpart and the peak at -966 mV had no anodic counterpart.

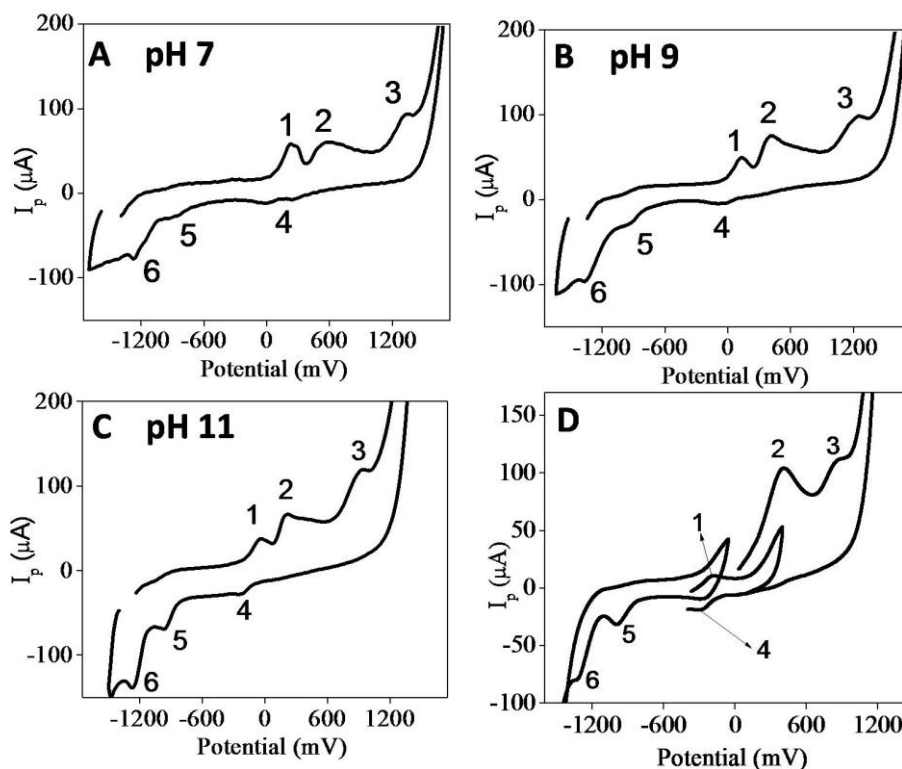


**Figure 5.3.** Cyclic voltammograms of INHHQ at  $1 \times 10^{-4} \text{ mol L}^{-1}$ : (A) at pH 7 (peak 1 at +160 mV, peak 2 at +438 mV, peak 3 at +1070 mV, peak 4 at -67 mV, peak 5 at -781 mV, peak 6 at -1127 mV). (B) at pH 9 (peak 1 at +47 mV, peak 2 at +297 mV, peak 3 at +1029 mV, peak 4 at -100 mV, peak 5 at -872 mV, peak 6 at -1248 mV). (C) at pH 11 (peak 1 at -47 mV, peak 2 at +209 mV, peak 3 at +926 mV, peak 4 at -215 mV, peak 5 at -966 mV, peak 6 at -1267 mV). (D) Cyclic voltammogram of INHHQ using different potential ranges at pH 11. Britton-Robinson Buffer 0.02 mol L<sup>-1</sup> with KCl 0.25 mol L<sup>-1</sup> and scan rate at 100 mV s<sup>-1</sup>.

### 5.2.2

#### Electrochemical behavior of INHHQ and precursors at GC/MWCNTs electrode

The electrochemical properties of 8-hydroxyquinoline have been extensively studied in the literature using carbon-based electrodes [108,109]. Cyclic voltammetry produced one primary oxidation peak across the range between -400 mV and +800 mV with maximum varying in the function of the pH of the solution, showing the influence of the acid-base equilibrium [108,109]. As the scan direction was reversed, a new reversible redox couple was present at less positive potentials, indicating that an electrochemical reaction gives rise to a molecule that is more easily oxidized than 8-hydroxyquinoline [108,109].

When the potential investigation was extended to +1400 mV, on subsequent cycles the voltammogram of 8-hydroxyquinoline exhibited one new reversible redox couple at less positive potentials involving the 1,4-naphthoquinone/1,4-naphtho-hydroquinone redox couple. The results showed that the oxidation of 8-hydroxyquinoline occurs at the phenolic group involving hydrogen bonding with the nitrogen heteroatom [108,109].

Stevic *et al.* employed cyclic voltammetry and semi-empirical computational methods to propose a two-electron irreversible oxidation peak in solutions across the pH range from 2 to 12 [109]. Single-electron oxidation leads to the formation of various free radical species depending on the solution pH that combine to produce dimers which, after being oxidized once more, produces quinonoid-type compounds. There is comparatively less information regarding the electrochemical characteristics of the isoniazid at carbon-based electrodes without the mixing or modification with chemical modifiers.

Cyclic voltammetric measurements for the direct oxidation from pH 2 to 11 at the carbon paste electrode showed a single well-defined irreversible anodic peak attributed to the two-electron oxidation of the amide moiety of the isoniazid molecule [110]. The peak current intensity was much higher across the pH range from 4 to 6 with the peak potential linearly shifting to less positive values with an increase in the pH upon the adsorption onto the carbon electrode and surface reactions.

In order to obtain further insights into the INHHQ redox processes, their precursors of isoniazid and 8-hydroxyquinoline or 8-hydroxyquinoline-2-carboxaldehyde, as well as 8-hydroxyquinoline which is structurally related to the 8-hydroxyquinoline-2-carboxaldehyde, were used as the reference standards evaluated by cyclic voltammetry using the MWCNT-modified glassy carbon electrode (Fig. 5.4) at concentration levels equal to  $6 \times 10^{-4} \text{ mol L}^{-1}$  in pH 11.0  $0.02 \text{ mol L}^{-1}$  Britton-Robinson buffer with  $0.25 \text{ mol L}^{-1}$  KCl at a scan rate of  $100 \text{ mV s}^{-1}$ . The INHHQ in Fig. 5.4A seems to present features from both 8-hydroxyquinoline-2-carboxaldehyde in Fig. 5.4B and isoniazid in Fig. 5.4C, but the maximum peak potentials differ from those of the reference standards, although they may represent similar redox processes.

The peaks recorded during the cathodic scan were generally obtained at more negative potentials than those of 8-hydroxyquinoline-2-carboxaldehyde. However, the more negative peak of INHHQ at  $-1267 \text{ mV}$  appears at a less negative potential than the value for isoniazid equal to  $-1288 \text{ mV}$ . The anodic scan of INHHQ included two peaks at  $-47$  and  $+209 \text{ mV}$  that may be correlated to those from 8-hydroxyquinoline-2-carboxaldehyde at  $+16 \text{ mV}$  and  $+286 \text{ mV}$ , which typical of 8-

hydroxyquinoline as seen in Fig. 5.4D or isoniazid at +148 mV. However, the INHHQ analyte provides a smaller oxidation peak at +926 mV that seems to be a signature of the compound as its precursors do not present this peak in the far positive region.

### 5.2.3

#### Square-wave voltammetry for INHHQ using the GC/MWCNTs electrode

The square-wave voltammetry of INHHQ in  $0.02 \text{ mol L}^{-1}$  Britton-Robinson buffer with  $0.25 \text{ mol L}^{-1}$  KCl at pH 11.0 was performed in the anodic direction (Fig. 5.5A) in order to take advantage of the more intense anodic peak observed in the cyclic voltammogram. The explored range was from  $-200 \text{ mV}$  to  $+800 \text{ mV}$  and a profile was observed in the cyclic voltammogram consisting of two peaks: one at  $-67 \text{ mV}$  and another, more intense at  $+303 \text{ mV}$  which are related to peak 1 at  $-47 \text{ mV}$  and peak 2 at  $+209 \text{ mV}$ .

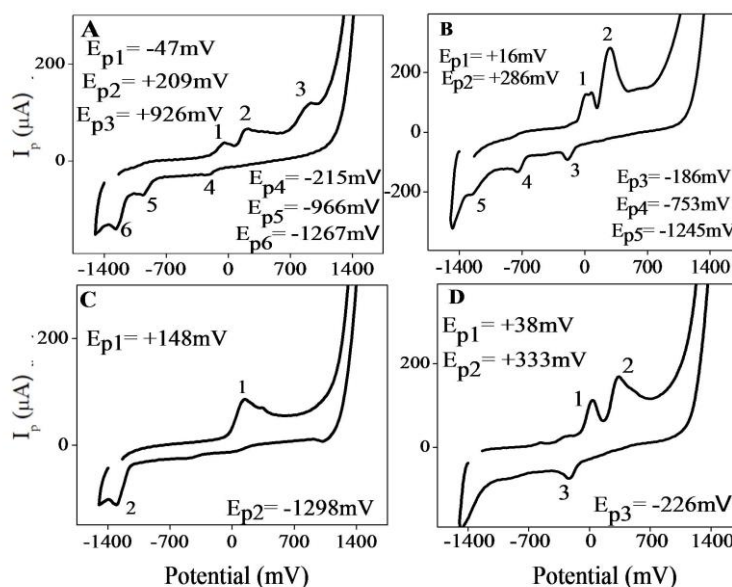


**Figure 5.4.** Cyclic voltammograms of (A) INHHQ at  $6 \times 10^{-4} \text{ mol L}^{-1}$ . (B) 8-hydroxyquinoline-2-carboxaldehyde at the  $6 \times 10^{-4} \text{ mol L}^{-1}$ . (C) isoniazid at  $6 \times 10^{-4} \text{ mol L}^{-1}$ . (D) 8-hydroxyquinoline at the  $6 \times 10^{-4} \text{ mol L}^{-1}$  using BR Buffer (pH 11.0;  $0.02 \text{ mol L}^{-1}$  with KCl  $0.25 \text{ mol L}^{-1}$ ) and scan rate at  $100 \text{ mV s}^{-1}$ .

The choice of the pH was made based on the comparison of intensities obtained for the peak at +303 mV selected for quantitative purposes within the pH range between 7.0 and 12.0 where maximum anodic peak current achieved at pH 11.0 (Fig. 5.5B). The relationship between peak current ( $I_p$ ) and the applied frequency ( $f$ ) for the main square-wave voltammetry oxidation peak was found to be linear as the determination coefficient ( $R^2$ ) is 0.997, which indicates that the oxidation that occurs is irreversible (Fig. 5.5C). Irreversible reactions are also characterized by the linear relationship ( $R^2 = 0.990$ ) between maximum peak potential ( $E_p$ ) and the  $\log(f)$  as seen in Fig. 5.5D for the main oxidation square-wave voltammetry peak.

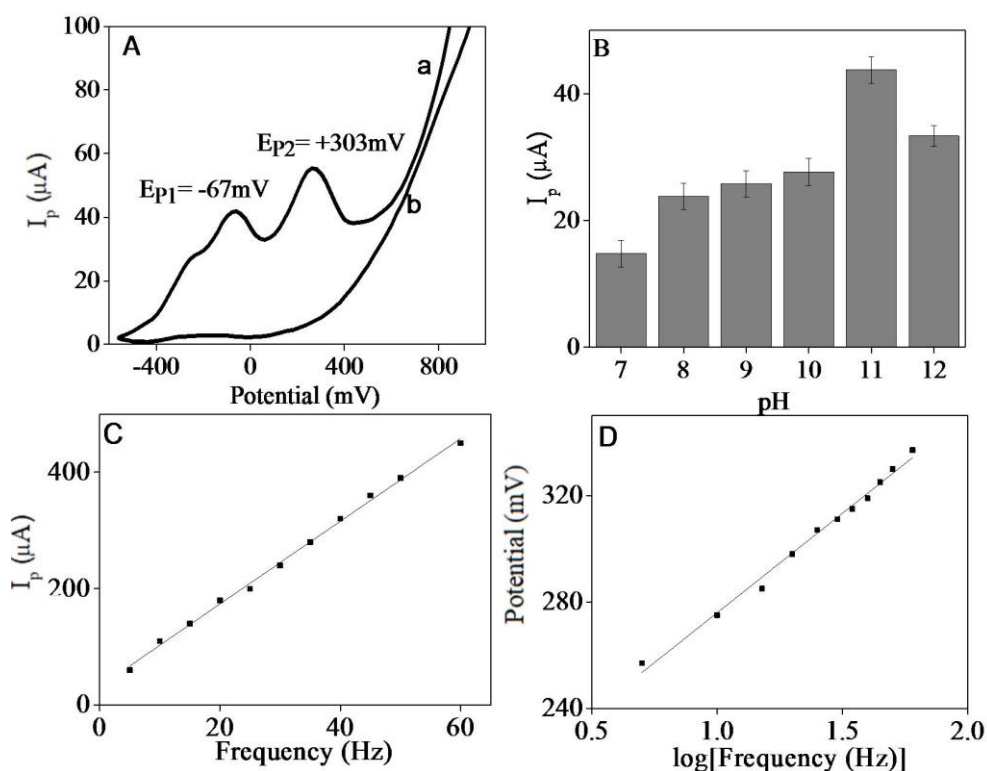


**Figure 5.5.** (A) Anodic square-wave voltammogram of INHHQ at  $4 \times 10^{-5} \text{ mol L}^{-1}$  at  $f = 30 \text{ Hz}$ . (B) Histogram of the effect of pH on the INHHQ SWV peak current at +303 mV at  $f = 30 \text{ Hz}$ . (C)  $I_p$  in function of  $f$  for the peak at +303 mV ( $R^2 = 0.997$ ). (D)  $E_p$  in function of the  $\log f$  ( $R^2 = 0.990$ ). Britton-Robinson Buffer  $0.02 \text{ mol L}^{-1}$  with KCl  $0.25 \text{ mol L}^{-1}$  at pH 11.0 and sweep rate was  $100 \text{ mV s}^{-1}$ .

In order to obtain additional information concerning the main square-wave voltammetry oxidation peak at +303 mV at 30 Hz, a cyclic voltammetric investigation at various scan rates ( $\nu$ ) was performed on the MWCNT-modified glassy carbon electrode for the INHHQ peak at +209 mV corresponding to the +303 mV peak by SWV. A linear relationship was present between  $I_p$  and  $\nu$  as  $R^2$  was equal to 0.995 (Fig. 5.6A) at higher scan rates from 100 to 1000  $\text{mV s}^{-1}$ , which shows that the oxidation is probably an adsorption-controlled process. In contrast, at a low  $\nu$  values from 10 to 100  $\text{mV s}^{-1}$ , the peak current values remain reasonably constant (Fig. 5.6B).

This mixed behavior may occur because the peak at +209 mV of INHHQ is probably a mixture of oxidation events concerning chemical groups from isoniazid and 8-hydroxyquinoline-2-carboxaldehyde. At lower  $\nu$  values, strong adsorption of the oxidized species onto the MWCNTs may also be causing the poisoning of the electrode modified surface, thereby preventing the electron transfer process [111]. This hypothesis is reinforced because when a similar study was performed using a bare glassy carbon electrode, linear relationships are found between  $I_p$  and  $\nu$  at both high ( $R^2 = 0.988$ ) and low ( $R^2 = 0.988$ ) values as shown in Fig. 5.6C and D.

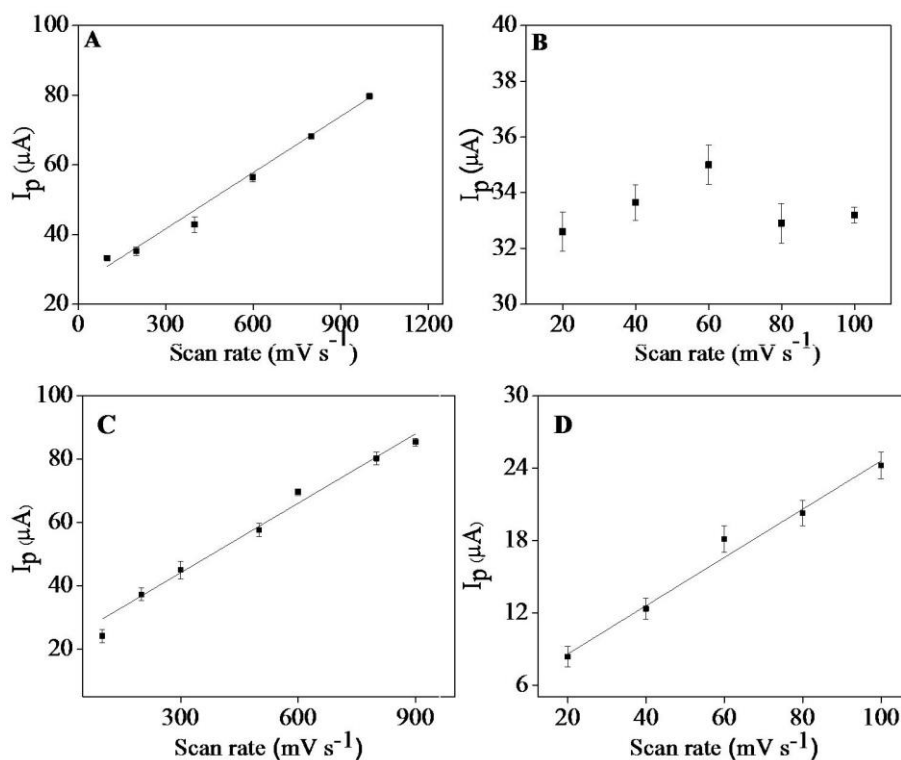


**Figure 5.6.**  $I_p$  versus scan rate of INHHQ (peak at +209 mV or peak 2 of Fig. 3B) at higher (A) and at lower (B) scan rates, using GC/MWNTCs.  $I_p$  versus scan rate of (peak at +418 mV or peak 1' of Fig. 3C) at higher (C) and at lower (D) scan rates, using bare GC electrode. Solution containing  $2 \times 10^{-4} \text{ mol L}^{-1}$  of INHHQ. BR Buffer  $0.02 \text{ mol L}^{-1}$  with KCl  $0.25 \text{ mol L}^{-1}$  and sweep rate was  $100 \text{ mV s}^{-1}$  and pH 11.

## 5.2.4 Analytical performance

As the square-wave voltammetry studies on the oxidation of INHHQ on the MWCNT modified glassy carbon electrode have indicated that the most intense current is achieved at pH 11 with a peak current of approximately +303 mV, quantitative measurements were made by adding sample into the supporting electrolyte at pH 11;  $0.02 \text{ mol L}^{-1}$  Britton-Robinson buffer containing  $0.25 \text{ mol L}^{-1}$  KCl. In order to identify the conditions providing the largest analytical response using square-wave voltammetry using the MWCNT-modified glassy carbon electrode, the instrumental parameters were studied. The signal intensity at +303 mV using a frequency of 30 Hz steadily increased as the pulse amplitude was varied

from 30 to 100 mV. A pulse amplitude of 40 mV was deemed to be optimum due to the better relationship between peak sharpness and intensity. The pulse frequency ( $f$ ) of 30 Hz was also a compromise between peak current and peak width within the 5 to 200 Hz range. The potential step was directly proportional to the peak current up to 20 mV and remained constant above 30 mV.

The analytical curve was constructed using the selected experimental conditions using INNHQ concentrations up to  $64 \mu\text{mol L}^{-1}$  (Fig. 5.7A) with the sequence of square-wave voltammograms shown in Fig. 5.7B. The analytical curve equation,  $I_p$  as a function of analyte concentration (C) was  $I_p (\mu\text{A}) = (1.37 \pm 0.034 \text{ L mol}^{-1}) \times 10^6 C_{\text{INNHQ}} + (0.093 \pm 0.44)$  with dynamic linear range ( $R^2 = 0.996$ ) covering two orders of magnitude and a limit of detection (LOD) equal to  $0.85 \mu\text{mol L}^{-1}$  ( $0.25 \mu\text{g mL}^{-1}$ ) and a limit of quantification (LOQ) equal to  $2.9 \mu\text{mol L}^{-1}$  ( $0.85 \mu\text{g mL}^{-1}$ ). The limits of detection and quantification were calculated by  $3 sb m^{-1}$  and  $10 sb m^{-1}$ , respectively. where  $sb$  is the standard deviation estimated by 10 consecutive measurements of the peak produced by the lowest analyte concentration of the analytical addition curve and  $m$  is the slope of the analytical calibration relationship.

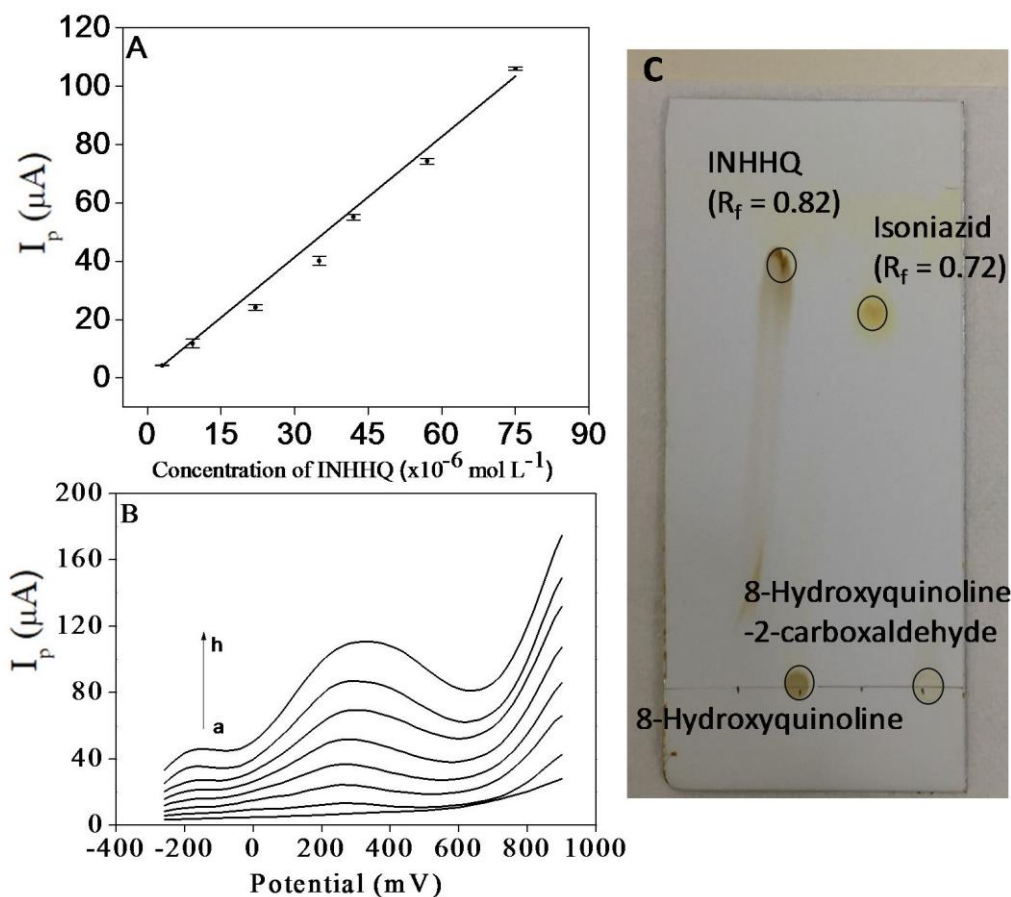


**Figure 5.7.** (A) Analytical curve (peak current at +303 mV) for INHHQ at a GC-MWNTCs electrode ( $R^2 = 0.996$ ). (B) Square-wave voltammetric response of INHHQ using GC-MWNTCs electrode: (a) 0, (b)  $3.0 \times 10^{-6}$  (c)  $9.2 \times 10^{-6}$ , (d)  $2.2 \times 10^{-5}$ , (e)  $3.5 \times 10^{-5}$ , (f)  $4.2 \times 10^{-5}$ , (g)  $5.7 \times 10^{-5}$ , (h)  $6.4 \times 10^{-5} \text{ mol L}^{-1}$ . BR Buffer  $0.02 \text{ mol L}^{-1}$  with KCl  $0.25 \text{ mol L}^{-1}$  at pH 11 and  $100 \text{ mV s}^{-1}$  scan rate. (C) TLC  $R_f$  values of INHHQ and related compounds.

The instrumental precision was determined to be the coefficient of variation of 10 consecutive measurements of the response provided by a  $1 \times 10^{-5} \text{ mol L}^{-1}$  ( $2.9 \mu\text{g mL}^{-1}$ ) analyte standard. Each measurement was performed following a solution agitation step in order to replenish the solution–electrode interface. The obtained instrumental precision was equal to 3%.

The stability of MWCNTs onto the glassy carbon electrode was evaluated by the measurement of 20 repetitive cyclic voltammograms of a  $35 \mu\text{mol L}^{-1}$  INHHQ solution using the same modified electrode. The measured average peak currents for INHHQ were equal to  $40.0 \mu\text{A}$  with a relative standard deviation of 2.3%. These results suggest that the modification of the MWCNTs onto the GC electrode surface had favorable reproducibility and stability for the determination of INHHQ.

### 5.2.5

#### Determination of INHHQ in wistar rats' brains

Before carrying out the analysis of the rat brains fortified with the analyte, a preliminary measurement was performed to evaluate the separation of INHHQ from the precursors (Fig. 5.7C). Although 8-hydroxyquinoline and 8-hydroxyquinoline-2-carboxaldehyde remained near the starting point of the chromatographic plate, both INHHQ and isoniazid were separated as their spots have  $R_f$  values equal to 0.82 and 0.72, respectively. It is important to point out that due to the lower solubility, INHHQ leaves a tail that may influence the recovery of this analyte during the collection of the sample at the  $R_f$  location at  $0.82 \pm 0.04$ .

The separation of INHHQ from the main brain matrix components by thin-layer chromatography (TLC) was also evaluated and no residue of the brain matrix was visually observed at  $R_f$  equal to 0.82 that has been shown to be characteristic for the analyte. Most of the brain matrix was retained at the starting point of the TLC plate. When INHHQ was mixed with either Cu and Zn, a characteristic spot appeared at  $R_f$  equal to 0.26 (Zn-INHHQ) and  $R_f$  equal to 0.36 (Cu-INHHQ) in addition to the spot at  $R_f$  of 0.82 due to INHHQ, indicating that any complexes

formed between metal ions and INHHQ are separated from the residual free INHHQ in the sample.

In order to maximize the amount of sample introduced onto the chromatographic plate, 200  $\mu\text{L}$  of the extracted material were spotted on the TLC plates. 20 spots were introduced per plate with each corresponding to 10  $\mu\text{L}$  by the accumulated additions of five aliquots equal to 2  $\mu\text{L}$ . After the separation was complete, the area of the plate containing the INHHQ at  $0.82 \pm 0.04$  was removed and transferred to a vial to be redissolved in 300  $\mu\text{L}$  of dimethyl sulfoxide and 3 mL of the supporting electrolyte. After vortex mixing, the dispersion was filtered, the filter paper was washed with the supporting electrolyte solution, and the final volume (5.00 mL) was adjusted by further addition of supporting electrolyte solution before the whole contents were transferred to the analytical cell. The same procedure was followed for a plate without INHHQ and no signal was observed, showing that no silica plate components were transferred to the final solution.

The analysis was performed using rat brain extracts composed of three independent samples with a mass of 0.1 g suspended in 2 mL of dimethyl sulfoxide that were fortified with  $5 \times 10^{-5} \text{ mol L}^{-1}$  ( $14.6 \mu\text{g mL}^{-1}$ ) and  $9 \times 10^{-6} \text{ mol L}^{-1}$  ( $2.63 \mu\text{g mL}^{-1}$ ) INHHQ. The recoveries obtained were  $(4.7 \pm 0.6) \times 10^{-5} \text{ mol L}^{-1}$  corresponding to a recovery of  $95 \pm 13.0\%$  and  $(8.6 \pm 1.0) \times 10^{-6} \text{ mol L}^{-1}$  corresponding to a recovery of  $95.4 \pm 11.6\%$ , respectively. The analysis of the blank produced no relevant signals concerning other components of the brain matrix that were carried along INHHQ during the TLC procedure. Considering the complexity of the matrix, a rapid, low-cost and simple TLC procedure was performed to offer more selectivity to the method for the analysis of biological tissues. The achieved

recoveries also indicate the favorable selectivity of the glassy carbon electrode modified with MWCNTS for the electrochemical detection of INHHQ.

The sample with the higher fortification value equal to  $5 \times 10^{-5} \text{ mol L}^{-1}$  was also analyzed by HPLC using a method modified from the literature [60]. The resulting recovery was  $(5.5 \pm 0.1) \times 10^{-5} \text{ mol L}^{-1}$ , corresponding to percent recovery equal to  $110 \pm 1.8\%$ . Despite differences in the mean values of the results, Student's t-test for different variances (confidence limit of 95%; two tails, each with  $\alpha/2 = 0.025$ ) indicated that results are in statistical agreement ( $t_{\text{experimental}} = 2.76 < t_{\text{critical}} = 4.30$ ).

### 5.3

#### Partial conclusion

The MWCNTs afforded amplification of the electrochemical signal measured from INHHQ by square-wave voltammetry due to the increased active area and improved electron-transfer rate. The choice of the pH 11.0 to perform the cyclic voltammetry was selected based on the solubility and stability of INHHQ and the intensity of its electrochemical signal. This electro-analytical method for the determination of INHHQ is reported for the first time. The rapid and easy modification of the glassy carbon electrode with MWCNTs, its sensitivity, reproducibility and the simple pretreatment of the sample, including thin layer chromatography to improve the selectivity of the method, make this an attractive method to determine the anticipated analyte levels in the extracts of the rat brain.

## 6

### **Indirect voltammetric determination of thiomersal in influenza vaccine using photo-degradation and graphene quantum dots modified glassy carbon electrode**

Paper published in *Talanta*, 2020, 120938

DOI: 10.1016/j.talanta.2020.120938

#### 6.1

##### **Thiomersal and analytical methods for its determination**

Thiomersal is an organomercury derivative widely used in topical pharmaceutical preparations and as preservative in vaccines and cosmetics [112]. Thiomersal structure comprises of 49.55 % (w/w) of mercury and its degradation produces thiosalicylic acid, dithiobenzoic acid and ethylmercury [113]. Thiomersal has been used in vaccines against hepatitis B, influenza, Haemophilus influenzae type b, diphtheria, tetanus and whooping cough [114] in typical quantities between 45 to 55 µg per dose (0.50 mL) [115]. Despite the fact that thiomersal is a very effective preservative, its inclusion in vaccines is controversial as some studies indicated the presence of mercury residues in human tissues that could affect the central nervous, cardiovascular, renal and immune systems [115,116]. Therefore, thiomersal concentration in vaccines must be kept at safety levels in order to avoid unnecessary exposition of humans. In this context, analytical methods are required to enable easy determination of thiomersal at trace levels in order to allow, for instance, the quality control of vaccines.

Gil *et al.* photo-decomposed thiomersal in solution using UV and H<sub>2</sub>O<sub>2</sub>. Further reduction of Hg<sup>2+</sup> to Hg was achieved, in a second step, by ultrasound after addition of formic acid. Mercury cold vapor was carried to the quartz cell of an

atomic absorption spectrometer to be detected at levels down to  $40 \mu\text{g L}^{-1}$  ( $0.09 \mu\text{mol L}^{-1}$ ) [117].

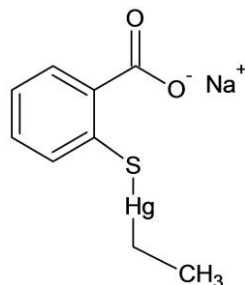


**Figure 6.1.**Thiomersal structure (sodium ethylmercurithiosalicylate).

Reverse-phase high performance liquid chromatography (HPLC) coupled with atomic fluorescence spectrometry was used for the determination of thiomersal. Mercury cold vapor was generated by the post-column reduction of mercury species using UV and in the presence of formic acid. Thimerosal was converted to  $\text{Hg}^{2+}$  then reduced to Hg. The method was applied to the determination of thimerosal in samples of a pharmaceutical industry effluent and in river waters. The limit of detection (LOD) obtained was  $0.09 \text{ g L}^{-1}$  ( $200 \mu\text{mol L}^{-1}$ ) [118]. Xu *et al.* proposed an atomic fluorescence spectrometric method for the determination of thimerosal in the vaccines based on  $\text{Fe}^{3+}$ -induced degradation of thiomersal and LOD of  $0.03 \mu\text{g L}^{-1}$  ( $0.07 \text{ nmol L}^{-1}$ ) was obtained [119]. Wu *et al.* produced mercury cold vapor that was carried to an atomic fluorescence spectrometer. The method was applied for vaccine samples with LOD of  $0.06 \mu\text{g L}^{-1}$  ( $0.1 \text{ nmol L}^{-1}$ ) [120]. Dos Santos *et al.* described the determination of Hg, originally present as thimerosal, in vaccines by photochemical mercury cold vapor generation coupled to inductively coupled plasma optical emission spectrometry (ICP OES) enabling LOD of  $0.6 \mu\text{g L}^{-1}$  ( $1 \text{ nmol L}^{-1}$ ) [121]. He *et al.* also described an ICP OES method to determine

thimerosal in vaccines by photochemical cold vapor generation (LOD of  $0.17 \mu\text{g L}^{-1}$  or  $0.4 \text{ nmol L}^{-1}$ ) [122]. Campanella *et al.* used flow injection analysis (FIA) for the determination of thiomersal based on the UV/microwave induced online oxidation of organic mercury, followed by atomic fluorescence detection [123]. The method produced LOD of  $0.003 \mu\text{g mL}^{-1}$  ( $7 \text{ nmol L}^{-1}$ ) and it was applied to ophthalmic solutions. Miranda-Andrades *et al.* reported a method for quantification of thiomersal, after photo-degradation assisted by graphene quantum dots (GQDs), converting thiomersal into ethylmercury then to  $\text{Hg}^{2+}$ , using visible radiation [61]. Detection was made after chemical reduction to produce mercury cold vapor using a dedicated mercury portable atomic absorption spectrometer. The method enabled LOD of  $20 \text{ ng L}^{-1}$  ( $0.049 \text{ nmol L}^{-1}$ ) in aqueous effluents of pharmaceutical industry and in urine samples.

Meyer *et al.* used HPLC with absorption photometric detection to determine thiomersal in ophthalmic solutions and vaccines detecting values as low as  $0.025 \mu\text{g}$  ( $0.06 \text{ nmol}$ ) in  $50 \mu\text{L}$  of sample [124]. Thiomersal was derivatized with dithizone before carrying out the analysis by HPLC [125]. Acosta *et al.* used HPLC with fluorimetric detection ( $315/442 \text{ nm}$ ) to determine thimerosal in pharmaceutical industry effluents after it was converted (in an on-line UV reactor) to thiosalicylic acid enabling LOD of  $0.72 \mu\text{g mL}^{-1}$  ( $1.8 \mu\text{mol L}^{-1}$ ) [126]. Shivastaw *et al.* developed a colorimetric method (measurement at  $538 \text{ nm}$ ) based on the reaction between thiomersal and dithizone in basic medium to analyze vaccines, obtaining LOD of  $200 \mu\text{g L}^{-1}$  ( $0.49 \mu\text{mol L}^{-1}$ ) [127]. Fredj *et al.* used a FIA system to produce mercury cold vapor from thiomersal, which was separated in a gas diffusion cell then passing through a permanganate solution where Hg was oxidized to  $\text{Hg}^{2+}$  with the

decreasing the permanganate absorbance at 528 nm. The method was applied for vaccine samples with LOD of  $70 \mu\text{g L}^{-1}$  ( $0.17 \mu\text{mol L}^{-1}$ ) [128].

A limited number of works has been dedicated to the electro-analytical determination of thiomersal. Birner *et al.* proposed the use of polarography to determine thiomersal in aqueous solution and in vaccines where the analyte was present in amounts above  $20 \mu\text{g g}^{-1}$  [129]. Da Silva *et al.* applied cyclic voltammetry (CV) with glassy carbon (GC) electrode (acetate buffer; pH 4.0) to determine thiomersal measuring the oxidation peak at +760 mV. Analyses of contact lens care solutions were made with LOD of  $0.09 \mu\text{g mL}^{-1}$  ( $0.22 \mu\text{mol L}^{-1}$ ) [113]. Differential pulse voltammetry was used by Piech *et al.* for thiomersal determination in vaccines using a mercury film silver-based electrode (phosphate buffer; pH 7.0) enabling LOD of  $0.36 \mu\text{g L}^{-1}$  ( $0.9 \text{ nmol L}^{-1}$ ) based on the peak at -555 mV [130]. Gonzalez *et al.* reported a method for determination of thiomersal by square-wave voltammetry (SWV) using a screen-printed electrode modified with chitosan (phosphate buffer; pH 3.2), enabling LOD of  $15.3 \mu\text{g L}^{-1}$  ( $0.038 \mu\text{mol L}^{-1}$ ). The sensor was used to analyze human urine and commercial vaccines. The modified electrode promoted the oxidation of thiomersal with peak at +240 mV [115].

Penagos-Llanos *et al.* applied SWV for determination of thiomersal in vaccines and in pharmaceuticals using a carbon-paste modified electrode decorated with  $\text{La}_2\text{O}_3$  (using phosphate buffer at pH 3.1), enabling detection limit of  $36 \mu\text{g L}^{-1}$  ( $0.09 \mu\text{mol L}^{-1}$ ). The anodic scan produced a thiomersal peak in the range between +800 and +900 mV [131]. Wei *et al.* developed a molecularly imprinted electrochemical sensor based on a microporous metal–organic-framework for the detection of thiomersal. A monolayer of 4-aminothiophenol (4-ATP) was self-

assembled on the surface of a gold electrode, followed by electro-polymerization of the 4-ATP-functionalized gold nanoparticles in the presence of template (thiomersal), forming a microporous molecularly imprinted polymeric film [132]. Thimerosal was determined in ophthalmic solutions and LOD was  $0.014 \text{ ng L}^{-1}$  ( $0.035 \text{ pmol L}^{-1}$ ).

In this work, an electro-analytical method for thiomersal was developed using GQDs as a surface modifier of a GC electrode. GQDs are nanometric fragments of graphene where electron transport is confined in their dimensions. GQDs present special optical and catalytic properties, due to quantum confinement, that can be accessed in the visible range the electromagnetic spectrum. The research presents a new approach for the determination of thiomersal in influenza vaccines using SWV and GQDs-modified GC (GC/GQDs) electrode, exploring the synergistic effect between GQDs, visible radiation and the applied potential in producing very intense Hg oxidation peak during anodic scan.

## 6.2

### Results and discussion

#### 6.2.1

##### Characterization of GQDs in aqueous dispersion and modification of the GC

The GQDs in aqueous dispersion (pH 6.4) were characterized using different techniques. The GQDs dispersion showed photoluminescence emission with maximum at 445 nm (Fig. 6.2A), when excited at 357 nm, indicating quantum confinement. There is no change in emission maximum as the excitation was varied by  $\pm 20$  nm. Raman spectra of GQDs is shown in Fig. 6.2B, exhibiting typical graphene D and G-bands at  $1349 \text{ cm}^{-1}$  and  $1607 \text{ cm}^{-1}$  respectively. Characteristic

Raman features (bands D and G) indicated  $sp^2$  carbon in graphitic nanostructures. The total carbon content in the original aqueous GQDs dispersion, prepared by hydro-exfoliation of 2 g of citric acid, was about  $580 \text{ mg L}^{-1}$ .

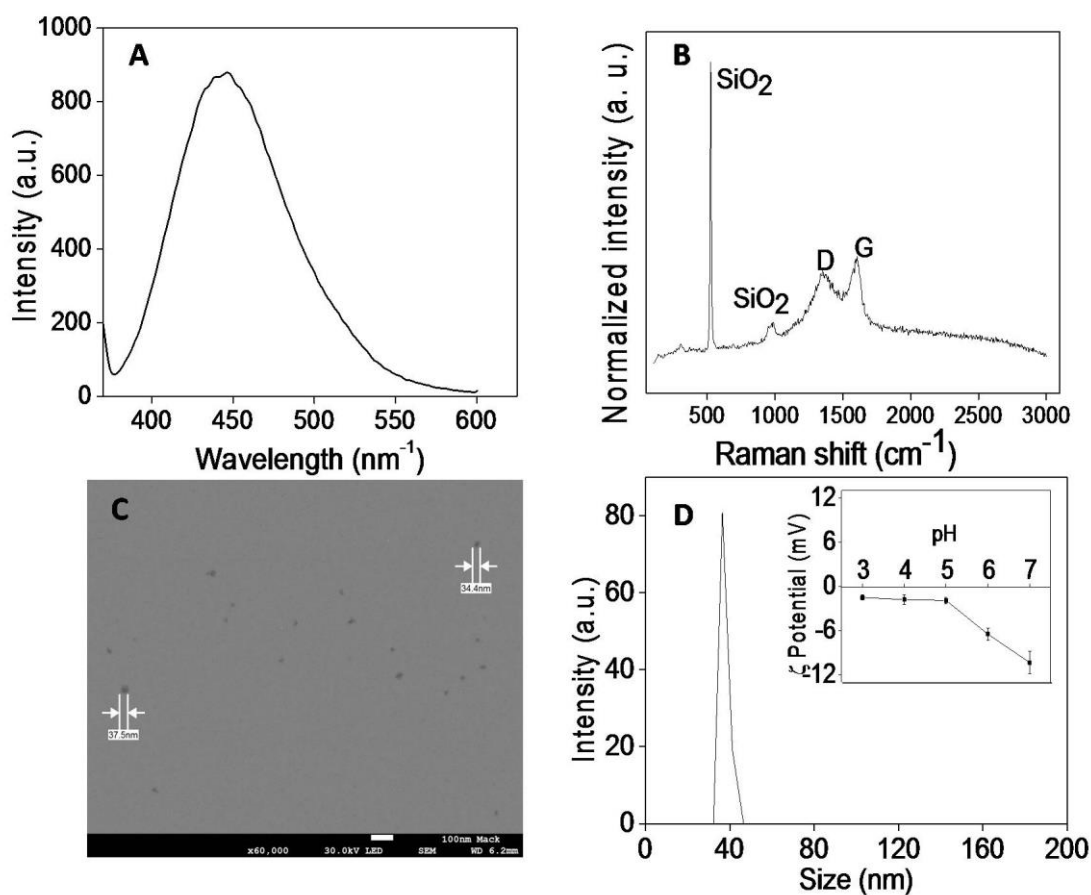


**Figure 6.2.** (A) Photoluminescence spectrum emission GQDs in aqueous dispersion (excitation at 357 nm). (B) Raman spectra of GQDs. (C) Scanning transmission electronic microscopy image of GQDs. (D) Size distribution of GQDs in aqueous dispersion obtained by DLS with insert showing  $\zeta$ -potential of GQDs in aqueous dispersion in function of pH.

As the GQDs original aqueous dispersion is somewhat viscous, a dilution with water (3 parts water to 1 part of GQDs original dispersion, in volume) was required to obtain the STEM images (Fig. 6.2C). It was observed nanomaterials

with an average diameter of  $35.9 \pm 2.2$  nm. DLS confirmed this diameter value with a hydrodynamic size of  $34.0 \pm 3.4$  nm (Fig. 6.2D). The closer estimated sizes (by the image analysis and by DLS) is explained as GQDs are not surface modified with any ligands as usually are the inorganic semiconductor QDs. The negative charge of the GQDs in aqueous dispersion increases as the pH value increases, as seen by  $\zeta$ -potential values in insert in Fig. 6.2D, indicating lower aggregation of nanomaterials as the pH of the aqueous dispersion increases. This is due probably to the  $-\text{COOH}$  groups, at the border of the GQDs, losing protons and becoming negatively charged.

### 6.2.2

#### **Cyclic voltammogram of thiomersal onto the GQDs-modified GC electrode**

A preliminary study, using GQDs dispersion prepared with 2 g of citric acid, was made to evaluate the effect of GQDs modification onto glassy carbon (GC) on the electrochemical response of thiomersal (at  $3.5 \times 10^{-4}$  mol L<sup>-1</sup>). Cyclic voltammograms were obtained comparing the use of bare GC and the GC modified with 10  $\mu\text{L}$  of the GQDs dispersion (re-suspended in 1,4-dioxane). Using a supporting electrolyte at pH 4.0 (BR buffer solution at 0.02 mol L<sup>-1</sup>/KCl at 0.25 mol L<sup>-1</sup>) it was observed two anodic peaks, one with maximum potential ( $E_p$ ) at +189 mV and a large one with  $E_p$  at +1004 mV, as well as one cathodic peak, in the reversed scan, with  $E_p$  at -33 mV (Fig. 6.3). The position of these peaks remains the same no matter the GC was modified with GQDs or not. However, the intensity of these peaks increased when surface of GC was modified with GQDs. For instance, the main peak, observed at  $E_p = +189$  mV (related to the oxidation of  $\text{Hg}^0$  to  $\text{Hg}^{2+}$ ) was about 3.3 times more intense using the GC/GQDs electrode. The modification with GQDs might have improved contact between electrode and

analyte in solution, leading to a larger measured current from the redox processes concerning thiomersal. As potential shifts were not observed, there is no evidence of electrocatalytic effect induced by the nanomaterial when on the surface of the electrode. It is important to point out that blank solution presents none of these electrochemical peaks (Fig. 6.4).

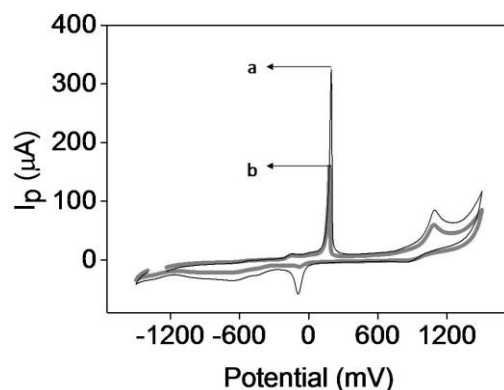


**Figure 6.3.** Cyclic voltammograms of thiomersal (at  $3.5 \times 10^{-4} \text{ mol L}^{-1}$ ) using a) GC/GQDs electrode and bare b) GC electrode: Peak 1 at +189 mV; peak 2 at +1004 mV; peak 3 at -33 mV. BR buffer pH 4.0 ( $0.02 \text{ mol L}^{-1}$ ; KCl  $0.25 \text{ mol L}^{-1}$ ) and  $100 \text{ mV s}^{-1}$  scan rate.

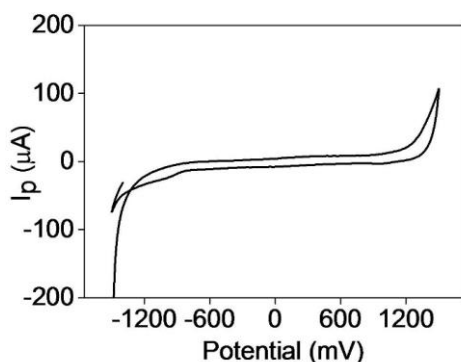


**Figure 6.4.** Cyclic voltammogram of the blank solution using the GC/GQDs electrode. BR buffer ( $0.02 \text{ mol L}^{-1}$ ; pH 4.0 in KCl  $0.25 \text{ mol L}^{-1}$ ) and  $100 \text{ mV s}^{-1}$  scan rate.

Da Silva *et al.* [113] reported the oxidation mechanism of thiomersal using acetate buffer (pH 4.0) in aqueous solutions with initial formation of thiosalicylic acid and ethylmercury [133,134]. Thiosalicylic acid is subsequently oxidized to dithiobenzoic acid while ethylmercury(II) hydroxide is reduced to elemental mercury (scheme in Fig. 6.5) [133,134]. Ethylmercury may form complex ions such as  $\text{CH}_3\text{CH}_2\text{Hg}_2\text{OH}^+$  or  $\text{CH}_3\text{CH}_2\text{HgOH}$  depending upon pH [135] affecting  $\text{Hg}/\text{Hg}^{2+}$  the redox process. Experiments performed with these chemical species using cyclic voltammetry and the GC/GQDs electrode are shown in Fig. 6.5.

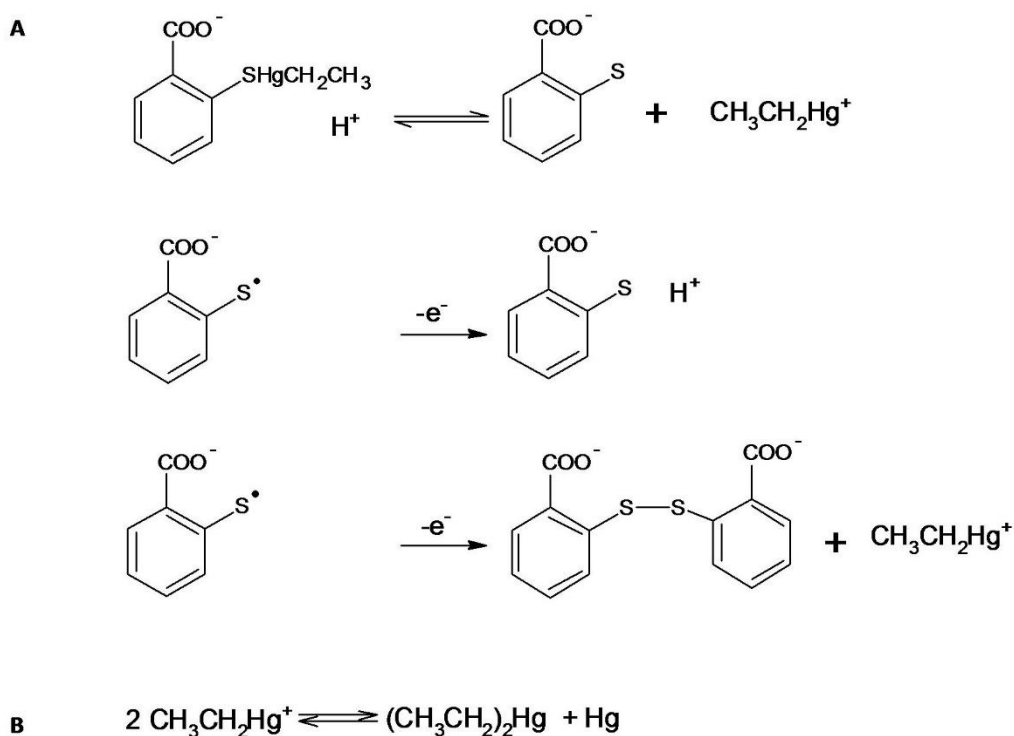


**Figure 6.5.** (A) Mechanism oxidation of thiomersal reported by Silva *et al.* [113] (B) Redox process concerning ethylmercury.

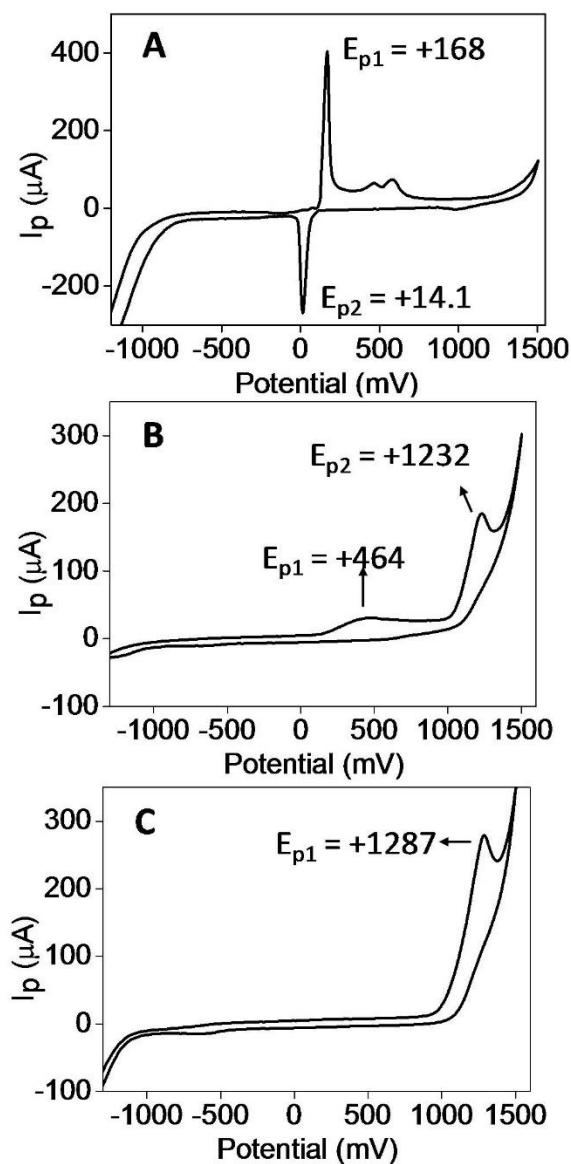


**Figure 6.6.** Cyclic voltammograms using GC/GQDs electrode. (A)  $\text{Hg}^{2+}$  ( $2 \times 10^{-4} \text{ mol L}^{-1}$ ). (B) Thiosalicylic acid ( $3 \times 10^{-3} \text{ mol L}^{-1}$ ). (C) Dithiobenzoic acid ( $3 \times 10^{-3} \text{ mol L}^{-1}$ ). BR buffer pH 4.0 ( $0.02 \text{ mol L}^{-1}$ ;  $\text{KCl}$   $0.25 \text{ mol L}^{-1}$ ) and  $100 \text{ mV s}^{-1}$  scan rate.

The cyclic voltammogram of an  $\text{Hg}^{2+}$  ( $2 \times 10^{-4} \text{ mol L}^{-1}$ ) standard solution produced a redox pair ( $E_{\text{anodic}}/E_{\text{cathodic}} = +168/+14 \text{ mV}$ ) that corresponds to the redox pair observed for thiomersal at  $E_{\text{anodic}}/E_{\text{cathodic}} = +189/-33 \text{ mV}$ . The large peak of thiomersal at  $+1004 \text{ mV}$  is probably a mixture of anodic events concerning

thiosalicylic acid ( $E_p$  at +464 mV and also at +1233 mV) and the one of dithiobenzoic acid ( $E_p = +1287$  mV).

### 6.2.3

#### Stability of the GC/GQDs electrode

The stability of a modified electrode is dependent on achieving homogeneous distribution of the modifying material on the surface of the electrode [136]. Therefore, finding the appropriate solvent to produce the ink used to be added on the surface of the GC allows greater durability as well as stability and reproducibility of the electrode response. Modification by adding 10  $\mu$ L of the dispersion (re-suspended in 1,4-dioxane) was found adequate since good coverage of GC surface was obtained. Solvent might favor high adhesion strength between the ink and the electrode, affecting the descent of modifying material on the electrode surface [137]. Aside from electrode/solvent interactions, electrode/modifying material and solvent/modifying material interactions govern the aggregation size, modifying material arrangement that influences electron transport in an electrode system [136].

A contact angle measurement (Fig. 6.7) has been made to evaluate the interaction between the ink of GQDs, dispersed in either 1,4-dioxane or water, and the GC electrode surface. The contact angle between the surface of the GC and the GQD dispersed in 1,4-dioxane is significantly smaller, when compared to the aqueous GQDs dispersion. A smaller contact angle provides better surface coverage and stability of the GQDs-solvent on the electrode surface. The hydrophobic interactions of 1,4-dioxane with the electrode surface are greater than the interactions of water with the surface electrode, that is, the GQDs-1,4-dioxane has a better adhesion to the electrode surface. In addition, 1,4-dioxane has high vapor

pressure in relation to water, making it an excellent solvent to be used in the preparation of the ink as rapid evaporation (Fig 6.7A) promotes better adhesion of GQDs on the electrode surface. Sequential electrochemical measurements ( $n = 20$ ) were made at  $E_p = +158$  mV using anodic SWV (relative to the anodic peak at  $E_p = +189$  mV obtained by cyclic voltammetry) of a thiomersal solution (at  $2.4 \times 10^{-5}$  mol L<sup>-1</sup>) using modified GQDs/GC electrodes (Fig 6.7B). It was found that the response obtained from the electrode modified using ink of GQDs dispersed in 1,4-dioxane was 1.5 times more intense than the one observed using ink of GQDs dispersed in water. Relative standard deviation of the measured signals was also significantly better using ink of GQDs dispersed in 1,4-dioxane (4.9 %) when compared with the one observed using ink of GQDs dispersed in water (28.3 %).

A comparative evaluation was made by GC modification with the original GQDs dispersions prepared by hydro-exfoliation using different masses of citric acid (1, 2 and 3 g). After concentration (through evaporation) and re-dispersion in 1,4-dioxane, it was found that the electrode modified with the dispersion, originally prepared using 2 g of citric acid, produced a signal (measured at  $E_p = +189$  mV using cyclic voltammetry) about twice the intensity of the one observed using the electrode modified with dispersion prepared using 1 g of citric acid (Fig. 6.7C). The GC modification using the dispersion obtained from hydro-exfoliation of 3 g of citric acid produced greater variation of results besides the fact that the ink did not properly dried on the surface of the electrode after evaporation of 1,4-dioxane. The GC modification with dispersion obtained originally from hydro-exfoliation of 2 g of citric acid produced surface modification with mechanical stability and reproducible response over time.

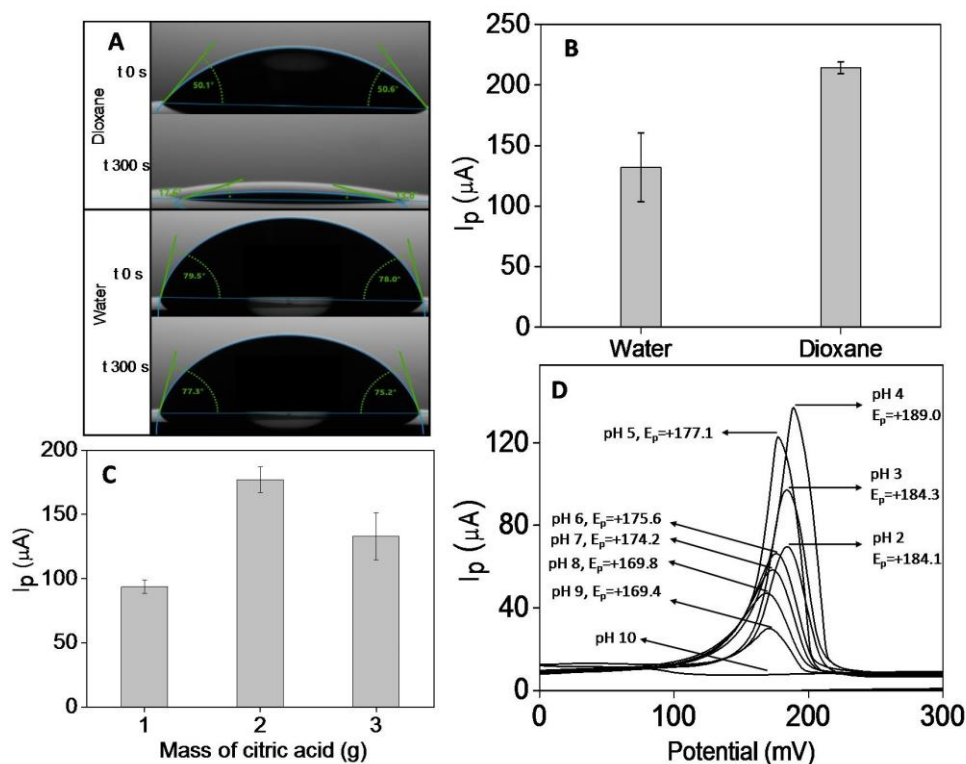


**Figure 6.7.** (A) Contact angle image of the surface of glassy carbon electrode modified with GQDs dispersed in water and in 1,4-dioxane. (B) Histogram of the electrochemical response of thiomersal ( $n = 4$ ) using GC electrode modified with GQDs obtained by hydro-exfoliation in water and then dispersed in either 1,4-dioxane and in water. (C) Peak current (at +189 mV) in function of the amount of GQDs, produced by hydro-exfoliation of different masses of citric acid, deposited onto the GC. (D) Cyclic voltammograms of thiomersal at different pH. a) pH 2,  $E_p = +184.1$  mV, b) pH 3,  $E_p = +184.3$  mV, c) pH 4,  $E_p = +189.0$  mV, d) pH 5,  $E_p = +177.1$  mV, e) pH 6,  $E_p = +175.6$  mV, f) pH 7,  $E_p = +174.3$  mV, g) pH 8,  $E_p = +169.8$  mV, h) pH 9,  $E_p = +169.4$  mV, i) pH 10, no signal. BR buffer  $0.02 \text{ mol L}^{-1}/\text{KCl } 0.25 \text{ mol L}^{-1}$  (scan rate at  $100 \text{ mV s}^{-1}$ ).

The choice of the pH to perform voltammetry was made based on the intensity of the  $\text{Hg}/\text{Hg}^{2+}$  oxidation peak measured from thiomersal ( $4.7 \times 10^{-5} \text{ mol L}^{-1}$ ) varying the pH of the BR buffer of the supporting electrolyte from 2.0 to 10.0. Voltammograms in Fig. 6.7D show that the anodic peak concerning mercury oxidation to  $\text{Hg}^{2+}$  is affected due to the favorable formation of  $\text{Hg}(\text{OH})_2$  or mercuric

hydroxi-complexes at pH above 7.0. As pH decreased from 6.0 to 4.0, the measured current increased and  $E_p$  slightly shifted from +175.6 mV to +189.0 mV. Then, at more acidic conditions, peak intensity decreases, therefore pH 4.0 was chosen for quantitative studies concerning thiomersal.

### 6.2.5

#### Electrochemical behavior of thiomersal on GC/GQDs electrode

By means of the GC/GQDs electrode, the intensity of the main anodic peak, obtained from the cyclic voltammetry of thiomersal (at  $E_p = +189$  mV), increases proportionally with the increase of the square root of the scan rate ( $v^{1/2}$ ), as seen in Fig. 6.8A. The equation modeling this response, obtained using least squares linear regression (Fig. 6.8B), was  $I_p = (35.2 \pm 1.16) - (1.04 \pm 0.21) \times 10^{-4}$  ( $R^2 = 0.990$ ). This result indicated that the process is controlled by diffusion.

The dependency between the sharp and most intense anodic peak,  $E_p = +189$  mV, and the one obtained in the reversed scan, at  $E_p = -33$  mV, was proven by performing a cyclic voltammetry within the potential range between  $-200$  and  $+600$  mV (Fig. 6.8C). The *quasi*-reversible nature of this Hg/Hg<sup>2+</sup> redox pair was confirmed based on the criteria proposed by Nicholson and Shain [138] considering the ratio of current intensities ( $I_{p1}/I_{p3}$ ), where  $I_{p1}$  is the anodic peak current and  $I_{p3}$  is the cathodic peak current. As  $I_{p1}/I_{p3}$  decreases exponentially as the scanning rate ( $v$ ) is increased, the *quasi*-reversibility of the electrochemical process is proven (Fig. 6.8D). This is in agreement with Rhadi *et al.* [139] who reported *quasi*-reversibility of the Hg/Hg<sup>2+</sup> redox process at relatively high scan velocities.

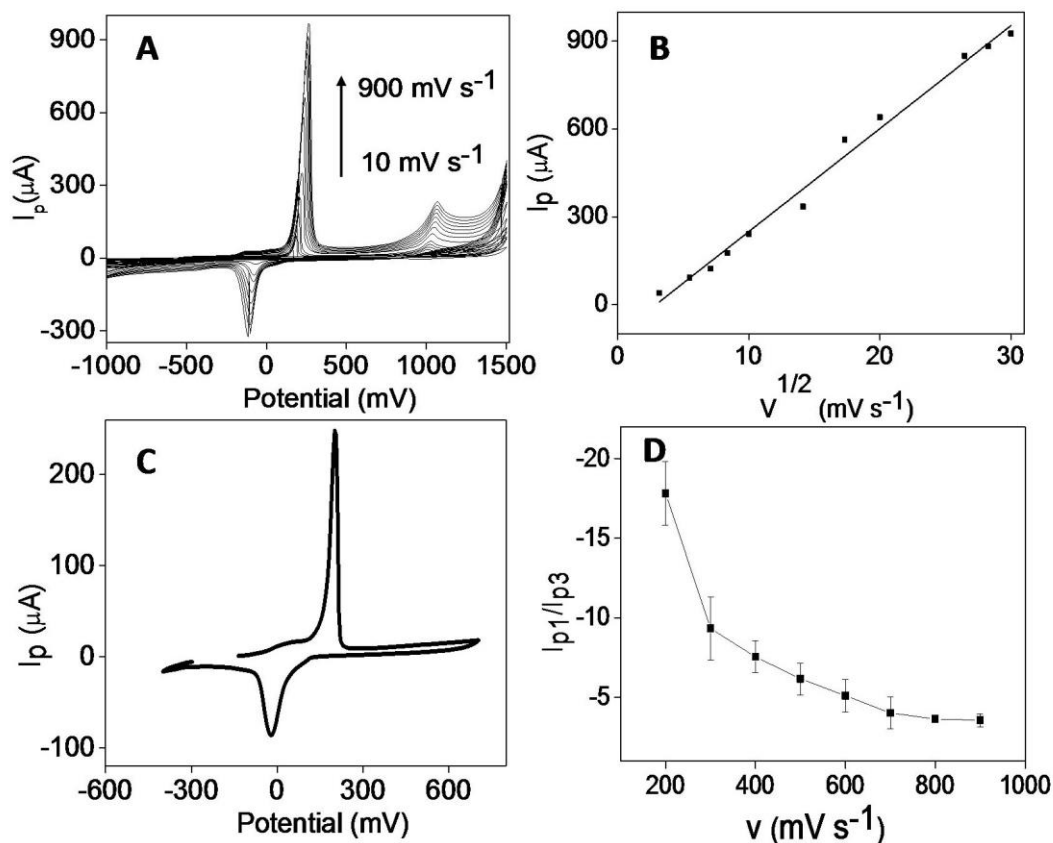


**Figure 6.8.** (A) Cyclic voltammograms of thiomersal (at  $2 \times 10^{-4} \text{ mol L}^{-1}$ ) using the GC/GQDs electrode at different scan rates (10 to  $900 \text{ mV s}^{-1}$ ). (B) peak current ( $I_p$ ) in function of square root of the scan rate ( $v^{1/2}$ ) with  $R^2 = 0.990$ . (C) Cyclic voltammogram of thiomersal performed within the limited potential range between  $-200$  and  $+600 \text{ mV}$ . (D)  $I_{p1}/I_{p3}$  ratio in function of the scanning rate for the redox pair (peak 1 and 3) obtained in CV. Experiments made with BR buffer pH 4.0 ( $0.02 \text{ mol L}^{-1}$ /  $\text{KCl } 0.25 \text{ mol L}^{-1}$ ).

### 6.2.6

#### Square-wave voltammetry using the GC/GQDs electrode: study of synergetic effect between applied potential and sample irradiation

For quantitative purposes, thiomersal was determined by measuring the sharp  $\text{Hg}/\text{Hg}^{2+}$  redox peak that appears at  $E_p = +158 \text{ mV}$ . As literature reports that GQDs, under exposition to visible spectral radiation, favors rapid photo-degradation of thiomersal into  $\text{Hg}^{2+}$  [61], SWV experiments were also made inside a photo-reactor in order to evaluate a synergetic effect between applied potential

and radiation that could lead to a larger analytical signals. In Fig. 6.9A the SWV response of thiomersal measured using the GC/GQDs electrode in an electrochemical cell inside a photo-reactor is shown. The signal, measured was only 18 % higher when voltammetric scanning was made after 20 min of exposition to visible light when compared to the one measured with the electrochemical cell in the dark (Fig. 6.9A). This indicates that visible light was not very effective in promoting the direct degradation of thiomersal when GQDs is immobilized onto the surface of GC.

A second experiment was performed by applying a sequence of 20 voltammetric cycles (at  $100 \text{ mV s}^{-1}$  within  $\pm 300 \text{ mV}$ ) under exposition of light, before applying the square-wave voltammetric scan to read the  $\text{Hg}/\text{Hg}^{2+}$  peak. Cyclic voltammograms were applied without solution stirring in order to minimize mass transport of analyte away from the electrode/solution interface, allowing accumulation of produced  $\text{CH}_3\text{CH}_2\text{Hg}$  from thiomersal [113]. Contrary to what was observed with thiomersal, it was found that the influence of visible radiation improved the GQDs mediated degradation of  $\text{CH}_3\text{CH}_2\text{Hg}$  into  $(\text{CH}_3\text{CH}_2)_2\text{Hg}$  and  $\text{Hg}$  then to  $\text{Hg}^{2+}$ , leading to an improvement of 2.8 times of the signal measured when performing the direct SWV scan without exposition to light (Fig. 6.9B). A comparative of analytical signals obtained by SWV using different experimental conditions is shown in Fig. 6.9C. It was found that the SWV signal, acquired using the GC/GQDs after 20 voltammetric cycles and under light exposition, was respectively 4.5 and 2.8 times more intense than the ones observed after the direct SWV scan in the dark using GC and GC/GQDs electrode. The influence of the previous voltammetric cycles and the incidence of light became evident as the signal achieved under such circumstances was 2.3 times more intense than the one

observed under exposition of radiation but without the voltammetric cycles and 1.4 times more intense than the one using previous voltammetric cycles but performed in the dark. Experiments using bare GC exposed to radiation and applied potential were also performed. The results showed that there was no significant increasing in the signal measured at  $E_p = +158$  mV, without the presence of GQDs.

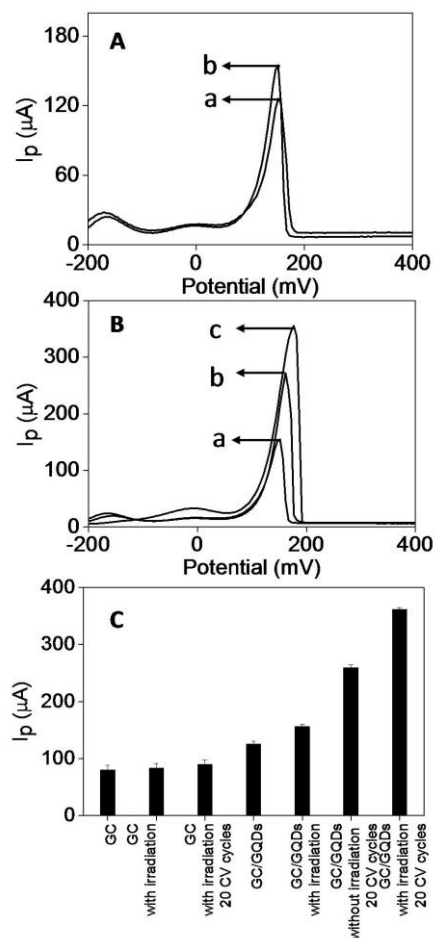


**Figure 6.9.** SWV response from thiomersal ( $2 \times 10^{-4}$  mol L $^{-1}$ ) using GC/GQDs electrode. (A) Measurements made (a) in the dark and (b) under exposition to visible radiation. (B) Measurements made (a) in the dark, (b) in the dark after 20 cyclic voltammetric cycles and (c) under exposition to visible radiation after 20 cyclic voltammetric cycles. (C) Comparative of analytical signals obtained by SWV using different experimental conditions. BR Buffer 0.02 mol L $^{-1}$  (pH 4.0) with KCl 0.25 mol L $^{-1}$ ; SWV scanning rate at 100 mV s $^{-1}$  and CV cycles at 100 mV s $^{-1}$  from  $\pm 300$  mV.

The number of voltammetric cycles required prior to produce the SWV signal, under light exposure, was studied and results are shown in Fig. 6.10, indicating 20 CV cycles as the number to produce better results. A larger number of cycles was not attempted since it would increase analysis time also allowing significant diffusion of produced mercury species away from the electrode/solution interface.

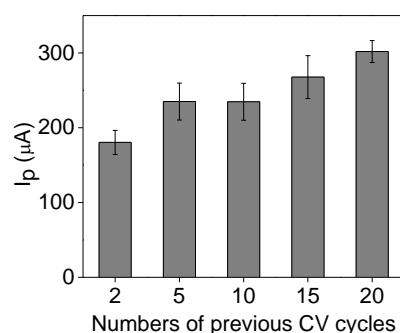


**Figure 6.10.** Square-wave voltammetric signal measured under sample irradiation using different number of previous voltammetric cycles.

A further experiment was made using cold vapor-AAS with multi-path length detection cell in order to evaluate the production of Hg and  $\text{Hg}^{2+}$  under different experimental conditions in the electrochemical cell (Fig. 6.11). Aliquots of solutions (supporting electrolyte with and without the addition of thiomersal) and solutions of thiomersal, in supporting electrolyte, submitted to different treatments in the electrochemical cell were collected, diluted and introduced into de reaction cell (containing  $\text{SnCl}_2$ ) connected to the cold vapor-AAS system. Background mercury level ( $7 \text{ ng L}^{-1}$ ) was found when the diluted supporting electrolyte was added to the cell, increasing to  $12 \text{ ng L}^{-1}$  as thiomersal was added to the supporting electrolyte solution before dilution and analysis by cold vapor-AAS. This indicates that a trace level residue of  $\text{Hg}^{2+}$  is found in thiomersal solution as consequence of

natural degradation. It was also found that a larger amount (more than 3 times) of mercury was measured after applying 20 voltammetric cycles (under stirring of solution) and one SWV scan using GC/GQDs than using bare GC. It is important to point out that most of the elemental mercury generated during the electrochemical process is lost during the time to perform sample cycling under stirring, sample collection from cell, dilution, and transferring to the cold vapor-AAS system. Therefore, the mercury measured by cold vapor-AAS in the experiments made with solutions from the electrochemical cell is the fraction of mercury formed as  $\text{Hg}^{2+}$ . The importance of exposition to light in the electrode modified with GQDs is also demonstrated as the measured mercury was about 2 times the one observed without incidence of light.

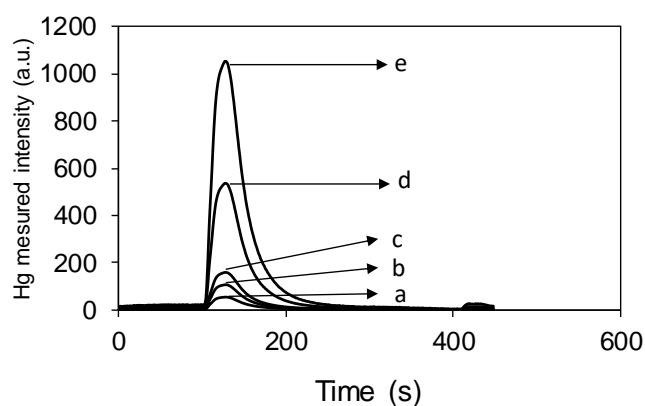


**Figure 6.11.** Absorption time profiles and concentrations of measured mercury cold vapor obtained from solutions added to the reaction cell ( $\text{SnCl}_2$  20 %) coupled to the cold vapor-AAS system: a) BR buffer solution ( $7 \text{ ng L}^{-1}$ ); b) thiomersal in BR buffer solution ( $12 \text{ ng L}^{-1}$ ); c) thiomersal in BR buffer solution after voltammetric cycles and SWV using bare GC electrode ( $17 \text{ ng L}^{-1}$ ); d) thiomersal in buffer solution after voltammetric cycles and SWV using GC/GQDs electrode in the dark

(58 ng L<sup>-1</sup>); e) thiomersal in buffer solution after voltammetric cycles and SWV using GC/GQDs electrode and exposition to visible radiation (112 ng L<sup>-1</sup>).

### 6.2.7

#### Analytical performance

Experimental conditions to perform electrochemical measurement of thiomersal using the GC/GQDs electrode were studied. Pulse amplitude was varied (from 30 to 90 mV) with 40 mV selected due to the better relationship between peak sharpness and intensity. Pulse frequency ( $f$ ) of 25 Hz was also a compromise between peak current and peak width within the 5 to 200 Hz range. Potential step was studied within the 2 to 20 mV with 2 mV preferred considering the higher intensity achieved.

The analytical curve was constructed by sequential addition of increasing concentration of analyte into the electrochemical cell with SWV voltammograms shown in Fig. 6.12A and analytical curve displayed in Fig. 6.12B. Analytical curve equation in terms of peak current ( $I_p$ ) was  $I_p = (6.47 \pm 0.23) \times 10^5 C_{thiomersal} + (11.1 \pm 4.4)$ , where  $I_p$  is in  $\mu\text{A}$  and  $C_{thiomersal}$  is the analyte concentration in mol L<sup>-1</sup>. Determination coefficient ( $R^2$ ) was 0.991 and linear dynamic range expanded up to 32  $\mu\text{mol L}^{-1}$  (12.9  $\mu\text{g mL}^{-1}$ ). Instrumental LOD and LOQ were calculated respectively as  $3sb m^{-1}$  and  $10sb m^{-1}$ , where  $s_b$  is the standard deviation ( $n=10$ ) of the  $I_p$  measured for the lowest concentration of the analytical curve and  $m$  is the sensitivity of the curve. For the GC/GQDs electrode, the instrumental LOD was 0.9  $\mu\text{mol L}^{-1}$  (0.34  $\mu\text{g mL}^{-1}$ ) and the instrumental LOQ was 2.8  $\mu\text{mol L}^{-1}$  (1.1  $\mu\text{g mL}^{-1}$ ) of thiomersal. Instrumental precision was obtained as the coefficient of variation from 10 consecutive measurements of the signal produced by the analyte standard at  $1 \times 10^{-5}$  mol L<sup>-1</sup> (4.0  $\mu\text{g mL}^{-1}$ ) with each one of the measurements made after

solution agitation to replenish the solution-electrode interface. Instrumental precision obtained was 3.2%.

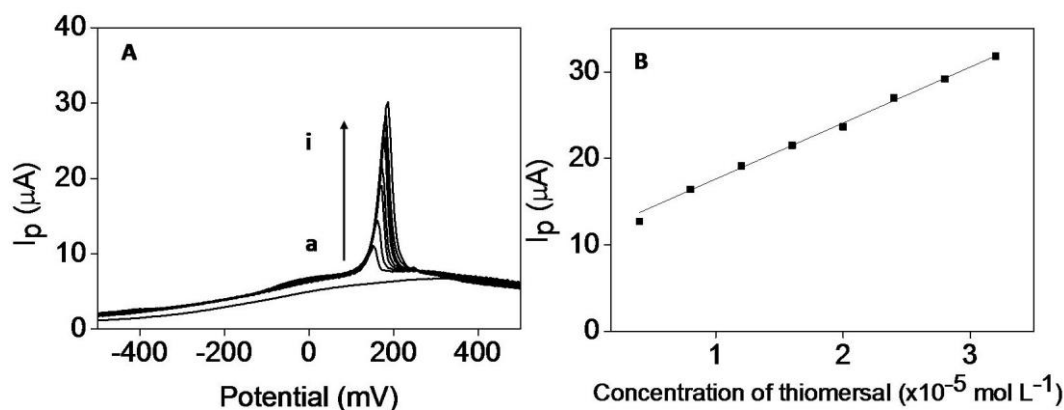


**Figure 6.12.** (A) SWV of thiomersal using GC/GQDs electrode: a) 0, b)  $4 \times 10^{-6}$ , c)  $8 \times 10^{-6}$ , d)  $1.2 \times 10^{-5}$ , e)  $1.6 \times 10^{-5}$ , f)  $2 \times 10^{-5}$ , g)  $2.4 \times 10^{-5}$ , h)  $2.8 \times 10^{-5}$ , i)  $3.2 \times 10^{-5} \text{ mol L}^{-1}$ , and (B) analytical curve:  $I_p = (6.47 \pm 0.23) \times 10^5 C_{\text{thiomersal}} + (11.1 \pm 4.4)$  ( $R^2=0.991$ ).

### 6.2.8

#### Determination of thiomersal in influenza vaccines

The quantitation of thiomersal in vaccines was performed using the proposed method. One of the influenza vaccines, the one without thiomersal, was fortified with the analyte at  $247 \mu\text{mol L}^{-1}$  ( $97.1 \mu\text{g mL}^{-1}$ ). The other one was directly analyzed to access the level of thiomersal originally present. Three aliquots of these samples were analyzed. The recoveries obtained were  $91.9 \pm 2.0 \%$  for the fortified vaccine and  $92.4 \pm 2.7 \%$  for the vaccine originally containing thiomersal (equivalent to  $100 \mu\text{g mL}^{-1}$  as reported by manufacturer). As the composition of vaccines, besides the virus antigens and water, consists of sodium and potassium chlorides and sodium and potassium dihydrogen phosphates [140], interference studies were not conducted as the salt content added from sample is less than the one of the supporting electrolyte in the cell.

These same samples were also analyzed by cold vapor-AAS using the method reported by Miranda-Andrades [61] and recoveries were  $87.8 \pm 1.3$  % for the fortified vaccine and  $99.2 \pm 1.3$  % for the vaccine with thiomersal in its composition. Despite differences in the mean values, the *Student t-test* for similar variances (confidence limit of 95%; two tails, each with  $\alpha/2 = 0.025$ ) indicated that results are in statistical agreement (Table 6.1). The obtained results lead to the conclusion that the proposed method can be use for a simple, selective and sensitive determination of thiomersal in vaccines samples.

**Table 6. 1.** Analysis results of thiomersal in vaccines using the proposed SWV method and by using cold vapor-AAS. Standard deviation for  $n = 3$ . Confidence limit of 95%; two tails, each with  $\alpha/2 = 0.025$ .

Technique	fortified vaccine		vaccine	
	Obtained result ( $\mu\text{mol L}^{-1}$ )	% recovery	Obtained result ( $\mu\text{mol L}^{-1}$ )	% recovery
SWV	$227.0 \pm 4.9$	$91.9 \pm 2.0$	$228.2 \pm 6.6$	$92.4 \pm 2.7$
CV-AAS	$216.8 \pm 3.2$	$87.8 \pm 1.3$	$245.0 \pm 3.2$	$99.2 \pm 1.3$
t-test	$t_{exp}=3.0 < Critical=4.3$		$t_{exp}=3.9 < Critical=4.3$	

### 6.3.

#### Partial conclusion

The proposed method allowed sensitive indirect determination of thiomersal using GQDs as a modifier of a GC electrode. By combining exposition of light with the applied potential promoted a significant degradation of thiomersal and the increasing of the  $\text{Hg}/\text{Hg}^{2+}$  redox peak used as analytical signal measured by SWV. The GQDs is an attractive nanomaterial for sensing devices due to their easy

preparation, photo-catalytic properties, high thermal stability, and low cost. Modification of GC is easy and the adaptation of the electro-analytical cell into a photochemical reactor is very simple. The method was successfully applied for the determination of thiomersal concentration in vaccines and proven as sensitive as the commonly used methods. A linear voltammetric response was obtained in the concentration range from  $3.0 \mu\text{mol L}^{-1}$  ( $1.2 \mu\text{g mL}^{-1}$ ) to  $32 \mu\text{mol L}^{-1}$  ( $12 \mu\text{g mL}^{-1}$ ), with a detection limit of  $0.9 \mu\text{mol L}^{-1}$  ( $0.34 \mu\text{g mL}^{-1}$ ). Acceptable recoveries confirms the usefulness of the method for quality control.

## 7

### Voltammetric determination of creatinine using a gold electrode modified with Nafion mixed with graphene quantum dots/copper

Paper submitted in *Electroanalytical Chemistry*

#### 7.1

##### Creatinine and analytical methods for its determination

Creatinine (2-amino-1-methyl-5H-imidazol-4-one) is a decomposition product from creatine phosphate in muscles [141]. Creatinine is excreted at a relatively constant rate that has been shown to be proportional to the individual's muscle mass. It is removed from circulation by glomerular filtration and excreted in the urine [141]. Creatinine levels can be used for the diagnosis of renal, thyroid, muscle malfunction [142], biomedical diagnosis of acute heart attack, and the quantitative evaluation of the hemodialysis therapy [143]. The normal concentration of creatinine in human urine is in the range from 0.5 to 1.5 mg dL<sup>-1</sup> and from 0.7 to 1.2 mg dL<sup>-1</sup> in blood serum [144].

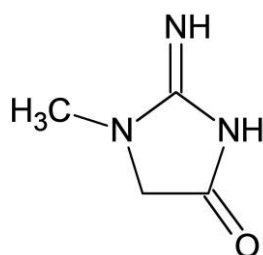


**Figure 7.1.** Creatinine structure (2-Amino-1-methyl-5H-imidazol-4-one).

As one of the most important biomarkers it is extensively used as internal standard in the metabolomic studies [145], therefore, it is crucial to develop reliable and simple analytical methods to monitor creatine in body fluids. The methods most

frequently used to measure creatinine are based on the Jaffe's reaction, first described in 1886, based on the reaction of creatinine with picric acid in an alkaline solution to form a red-orange chromogen. This method has subsequently been shown to be nonspecific and subject to positive interference by a large number of compounds, such as ascorbate, pyruvate, acetone, and glucose.

Another method to determine creatinine has been through the color developed when creatinine reacts with 3,5-dinitrobenzoic acid or its derivatives, being successfully adapted as a test strip diagnosis. However, the color produced is less stable than that of the Jaffee chromogen [141].

In order to increase the accuracy and diminish interferences from innumerable metabolites and drugs in biological samples, several methods based on liquid chromatography have been introduced. Zuo *et al.* used hydrophilic interaction liquid chromatography with photometric detection (absorbance at 205 nm) to determine creatinine in milk and orange juice. The limit of detection (LOD) was  $0.39 \mu\text{mol L}^{-1}$  [146]. Yokoyama *et al.* presented a high performance liquid chromatography (HPLC) method, using a weak-acid cation-exchange column, for the determination of creatinine in urine samples. The LOD obtained using absorption photometric detection was  $0.34 \mu\text{mol L}^{-1}$  with linear dynamic range from 5 to  $500 \mu\text{mol L}^{-1}$  [147]. Fraselle *et al.* used high resolution HPLC-tandem mass spectrometry to determined creatinine in urine samples with  $44.2 \mu\text{mol L}^{-1}$  [148]. Ponghong *et al.* employed flow injection analysis to determine creatinine in urine samples with linear dynamic range from 5.3 to  $884 \mu\text{mol L}^{-1}$ [149]. Using a portable microfluidic system, Songjaroen *et al.* proposed a method to determine creatinine in urine samples enabling LOD of  $29.2 \mu\text{mol L}^{-1}$ [150]. However, all of

the methods mentioned requires time-consuming sample preparation. A summary of other reported analytical methods for creatinine are in Table 7.1.

Electro-analytical techniques have also been used for the detection of creatinine [151]. De Araujo *et al.* used differential pulse voltammetry (DPV) for the indirect quantification of creatinine from urine samples based on the electrochemical monitoring the reduction of the picrate anion at a glassy carbon electrode in an alkaline medium before and after reaction of creatinine (Jaffe's reaction). A LOD of  $380 \text{ nmol L}^{-1}$  was achieved based on the peak measured at  $-650 \text{ mV}$  [152]. Yadav *et al.* proposed a biosensor for creatinine using a mixture of three enzymes: amidohydrolase, creatine amidinohydrolase and sarcosine oxidase. These enzymes were covalently immobilized via N-ethyl-N-(3-dimethylaminopropyl) carbodiimide and N-hydroxy succinimide onto carboxylated multi-walled carbon nanotube/polyaniline nanocomposite film electrodeposited over the surface of a Pt electrode. The LOD was  $0.1 \text{ }\mu\text{mol L}^{-1}$  with response up to  $750 \text{ }\mu\text{mol L}^{-1}$  using Tris-HCl buffer (pH 4.7) and amperometric measurement at  $+200 \text{ mV}$  [153].

Several types of electrode-based non-enzymatic creatinine sensors are reported in the literature using copper as a means to indirectly determine creatinine. Raveendran *et al.* electrodeposited copper on a screen-printed carbon electrode with measured signal based on the formation of a soluble copper-creatinine complex. In the presence of creatinine, the cyclic voltammogram obtained, using the modified electrode, presented an anodic peak at  $+200 \text{ mV}$  whereas a cathodic peak was observed around  $-400 \text{ mV}$ . The quantification of creatinine considered the anodic peak, enabling LOD of  $0.075 \text{ }\mu\text{mol L}^{-1}$  with a linear dynamic range up to 378

$\mu\text{mol L}^{-1}$  (in phosphate buffer, pH 7.4) [154]. Pandey *et al.* developed a creatinine sensor based on polymethylene blue nanofilm onto copper-carbon nanofiber nanocomposite and used DPV for the quantification of creatinine in blood serum and saliva by monitoring the oxidation peak at +200 mV. A linear dynamic range up to  $7.9 \mu\text{mol L}^{-1}$  concentration range and LOD of  $1.7 \text{ nmol L}^{-1}$  were achieved using phosphate buffer (pH 7.2). The DPV response of creatinine was attributed to the formation of creatinine-Cu complex, with Cu acting as the electrocatalyst for the oxidation of creatinine [143]. Han *et al.* used cyclic voltammetry (CV) to determine creatinine in urine samples using poly(ethyleneimine)/phosphotungstic acid multi-layer modified electrode with  $\text{Cu}^{2+}$  added into the supporting electrolyte solution ( $\text{NH}_4\text{-HCl}$  buffer, pH 5.4). Creatinine was determined by measuring the redox peak current of Cu(II)-creatinine complex/Cu(I)-creatinine complex. A linear response from 0.125 to  $62.5 \mu\text{mol L}^{-1}$  was obtained with a LOD of  $0.06 \mu\text{mol L}^{-1}$  [155].

Recently, Gao *et al.* developed an electrochemical sensor for creatinine based on graphene oxide modified with copper nanoparticles. Hydrothermal reaction of graphene oxide with dopamine hydrochloride was conducted to prepare reduced graphene oxide (rGO), together with self-polymerization of polydopamine (PDA) attaching on rGO. Nile blue (NB) was loaded on rGO under ultrasonication. The resulting PDA rGO-NB complex was deposited on the surface of glassy carbon electrode under cyclic voltammetry scanning. Copper nanoparticles (CuNPs) were prepared through electrochemical reduction of  $\text{Cu}^{2+}$  ions and electrodeposited on PDA-rGO-NB surface. The concentration range from 0.01 to  $100 \mu\text{mol L}^{-1}$  was achieved, with a detection limit of  $2 \text{ nmol L}^{-1}$  [156]. Characteristics of other electro-

analytical methods reported for the determination of creatinine are summarized in Table 7.2.

In this work, a square-wave voltammetric method was developed for the determination of creatinine using a gold electrode modified with a film (ink) of Nafion containing graphene quantum dots produced by hydro-exfoliation of a molten of citric acid and  $\text{Cu}(\text{NO}_3)_2$ , (Nafion-GQDs-Cu). GQDs are nanometric fragments of graphene, where electron transport is confined in their dimensions. As GQDs are carbon-based nanostructures they are bio-compatible and present low toxicity. It is also possible to modify them during production or after produced. This new sensor was simple to prepare and the method was used to determine creatinine, based on the formation of copper-creatinine complex on the surface of GQDs-Cu, enabling enough detection capability for urine samples.

**Table 7. 1.** Summary of characteristics of analytical methods for creatinine.

Sample	Technique	Range	LOD	Reference
Urine and serum	UV-VIS spectrophotometric using sodium gluconate-capped AgNPs	0.0003 – 0.05 $\mu\text{mol L}^{-1}$	0.0002 $\mu\text{mol L}^{-1}$	[157]
Urine	Quantitative spectral deconvolution $^1\text{HNMR}$	1250 – 10000 $\mu\text{mol L}^{-1}$	6 $\mu\text{mol L}^{-1}$	[158]
Urine	FIA-MS	270-31000 $\mu\text{mol L}^{-1}$	20 $\mu\text{mol L}^{-1}$	[159]
Urine	HPLC with UV detection	2802 – 29900 $\mu\text{mol L}^{-1}$	-	[160]
Urine	Microfluidic paper-based analytical devices	200-1000 $\mu\text{mol L}^{-1}$	80 $\mu\text{mol L}^{-1}$	[161]
Urine	Capillary electrophoresis with contactless conductivity detector	88.4 – 1300 $\mu\text{mol L}^{-1}$	-	[162]
Saliva	RP-HPLC with tandem mass spectrometry	22.9 – 115 $\mu\text{mol L}^{-1}$	Diverse	[163]
Urine	HPLC tandem MS	0.008 – 17.6 $\mu\text{mol L}^{-1}$	0.002 $\mu\text{mol L}^{-1}$	[164]
Urine	Isotope dilution extractive electrospray ionization tandem mass spectrometry	0.44 – 88.4 $\mu\text{mol L}^{-1}$	0.44 $\mu\text{mol L}^{-1}$	[165]
Urine and serum	UV-Vis spectrophotometry of a copper/creatinine complex	8.8 – 530 $\mu\text{mol L}^{-1}$	2.5 $\mu\text{mol L}^{-1}$	[166]
Urine	Surface-enhanced Raman spectroscopy upon silver colloidal suspensions	884 – 24750 $\mu\text{mol L}^{-1}$	88 $\mu\text{mol L}^{-1}$	[167]
Urine	HPLC with UV and fluorimetric detection	1768 – 17680 $\mu\text{mol L}^{-1}$	1.8 $\mu\text{mol L}^{-1}$	[168]

Continuation of table 1

Sample	Technique	Range	LOD	Reference
Urine	Low-capacity cation-exchange chromatography	1 – 1000 $\mu\text{mol L}^{-1}$	0.02 $\mu\text{mol L}^{-1}$	[147]
Serum	Capillary zone electrophoresis with reduced capillary length	17 – 1768 $\mu\text{mol L}^{-1}$	4.42 $\mu\text{mol L}^{-1}$	[169]
Blood	Micellar electrokinetic chromatography with UV detection	10 – 1000 $\mu\text{mol L}^{-1}$	5 $\mu\text{mol L}^{-1}$	[170]
Creatine supplement formulations	LC with UV detection	20 – 900 $\mu\text{mol L}^{-1}$	1.5 $\mu\text{mol L}^{-1}$	[171]
Urine and blood serum	HPLC	0.004 – 17 $\mu\text{mol L}^{-1}$	0.0017 $\mu\text{mol L}^{-1}$	[172]
Bovine serum albumin	Ion-sensitive field effect transistor (biosensor) utilizing creatine deiminase	up to 5000 $\mu\text{mol L}^{-1}$	10 $\mu\text{mol L}^{-1}$	[173]
Urine	HPLC with UV detection	2.2 – 221 $\mu\text{mol L}^{-1}$	1.38 $\mu\text{mol L}^{-1}$	[174]
Urine	Kinetic spectrophotometric (Jaffe techniques)	8.1 – 442 $\mu\text{mol L}^{-1}$	2.6 $\mu\text{mol L}^{-1}$	[175]
Urine	FIA-UV (Jaffe techniques)	265 – 530 $\mu\text{mol L}^{-1}$	26.5 $\mu\text{mol L}^{-1}$	[175]
Urine	HPLC	10 – 300 $\mu\text{mol L}^{-1}$	3 $\mu\text{mol L}^{-1}$	[176]
Urine	Capillary electrophoresis	23 – 200 $\mu\text{mol L}^{-1}$	-	[177]

**Table 7.2.** Summary of characteristics of electrochemical methods for creatinine in different samples

Sample	Technique electrochemical	Electrode	Range	LOD	Reference
Grapes juice	CV	AgNPs/Polyoxometalate functionalized reduced graphene oxide (rGO) modified GCE	0.05 – 1.5 nmol L <sup>-1</sup>	0.0151 nmol L <sup>-1</sup>	[178]
-	Amperometry	Ammonium ion-selective Cu-polyaniline nanocomposite	1 – 100 μmol L <sup>-1</sup>	0.5 μmol L <sup>-1</sup>	[179]
-	CV	Copper platinum electrode	2.21 – 132.6 μmol L <sup>-1</sup>	0.60 μmol L <sup>-1</sup>	[180]
Serum	Amperometry	Array of 16 gold electrodes on polypyrrole matrix	up to 1.0 mmol L <sup>-1</sup>	4 μmol L <sup>-1</sup>	[181]
Urine	Potentiometric	β-cyclodextrin incorporated poly-3,4-ethylene dioxythiophene modified GCE	100 – 100 000 μmol L <sup>-1</sup>	60 μmol L <sup>-1</sup>	[182]
-	Impedance spectroscopy	Molecular imprinted polymer on gold electrode	0.44 – 1.76 μmol L <sup>-1</sup>	0.35 μmol L <sup>-1</sup>	[183]
-	Choroamperometry	Organic nickel (II) complex modified GCE	50 – 1000 μmol L <sup>-1</sup>	27 μmol L <sup>-1</sup>	[184]
Urine	SWV	Enzymeless-screen-printed carbon electrode	0.37 – 3.6 mmol L <sup>-1</sup>	8.6 μmol L <sup>-1</sup>	[185]
-	Potentiometric	Metallic electrode/ion selective electrode	-	-	[186]
Serum	Amperometry	PbO <sub>2</sub> film on Pt	1 – 1000 μmol L <sup>-1</sup>	0.8 μmol L <sup>-1</sup>	[187]
-	Amperometry	Thick-film hydrogen peroxide electrode system, 3 enzymes	0.2 – 2 mmol L <sup>-1</sup>	-	[188]
Serum	Amperometry	Enzyme composite with a polyimide film; screen printed electrode	0.9 – 1.2 mmol L <sup>-1</sup>	10 – 20 μmol L <sup>-1</sup>	[189]

## 7.2

### Results and discussion

#### 7.2.1

#### Characterization of GQDs and GQDs-Cu in aqueous dispersion

The GQDs and GQDs-Cu, in aqueous dispersions, were characterized using different techniques in order to evaluate their size distribution, structural and optical characteristics. The GQDs and the GQDs-Cu showed photoluminescence emission with maximum respectively at 445 nm and 452 nm, under excitation at 357 nm (Fig. 7.2A). The photoluminescence of GQDs is about 3 times more intense than the one of GQDs-Cu, therefore it seems that photoluminescence intensity of GQDs was quenched in the presence of copper probably due to either the coordination to carboxyl groups on the edges and defects of GQDs or by direct reduction of  $\text{Cu}^{2+}$  to Cu, in this way removing electrons from the conductance band and affecting excitonic recombination [190]. The red-shift of 7 nm also indicate decreasing in energy bandgap.

The Raman spectra of the GQDs and GQDs-Cu are shown in the Fig. 7.2B. GQDs spectrum exhibited typical G and 2D-bands at  $1349\text{ cm}^{-1}$  and  $1607\text{ cm}^{-1}$  respectively. Characteristic Raman features (bands D and G) indicated  $\text{sp}^2$  carbon in graphitic nanostructures. In contrast, Raman spectra of GQD-Cu presented three Raman peaks at 272, 322, and  $607\text{ cm}^{-1}$ . Three Raman active modes can be considered, assigning the peak at  $272\text{ cm}^{-1}$  to the  $A_g$  and the peaks at 322 and  $607\text{ cm}^{-1}$  to the  $B_g$  modes. These wavenumbers are close to those reported in the literature ( $288, 330$  and  $621\text{ cm}^{-1}$ ) [191,192]. The total carbon content in the original aqueous GQDs dispersion, prepared by hydro-exfoliation of 0.5 g of citric acid, was about  $143\text{ mg L}^{-1}$ .

Since the nanomaterials original aqueous dispersions present themselves as viscous samples, a dilution with water (3:1 water:original nanomaterial dispersion, in volume) was required to obtain the STEM images of GQDs (Fig. 7.2C) and GQDs-Cu (Fig. 7.2D). It was observed an average diameter of  $35.9 \pm 2.2$  nm for GQDs and  $27.6 \pm 4.2$  nm for GQDs-Cu, respectively, also confirmed by dynamic light scattering (DLS) that indicated hydrodynamic sizes of  $34.0 \pm 3.4$  nm (for GQDs in Fig. 7.2E) and  $24.0 \pm 3.1$  (for GQDs-Cu in Fig. 7.2F). The slightly higher hydrodynamic size for GQDs than for GQDs-Cu is in agreement with the results reported by Teymourinia *et al.* and it is attributed to the charge of copper atoms hindering more effectively the aggregation of nanomaterial [193].

The surface of the GQDs is negatively charged due to the presence of carboxylic acid groups. At the range of pH 3.0-5.0 the negative surface of the GQDs is efficiently neutralized by  $H^+$  ions and  $\zeta$ -potential values above  $-4$  mV were obtained (inserted in Fig. 7.2E). As the pH was increased to 6.0, the surface became more negative due to the lower availability of  $H^+$  ions. For the aqueous dispersion of GQDs-Cu, at pH 3.0 and 4.0,  $\zeta$ -potential values about  $-9$  mV were obtained, and as pH was increased to 5.0 and 6.0, a  $\zeta$ -potential value about  $-15$  mV was measured due to the lower availability of  $H^+$  ions, which makes the surface more negative. These results are in agreement with the ones reported by Lei *et al.*, [194] and showed that a higher negative surface charge in the GQDs-Cu was obtained (insert in Fig. 7.2F) when compared to GQDs. This also explains the high stability that copper confers on GQDs, minimizing aggregation of nanoparticles.

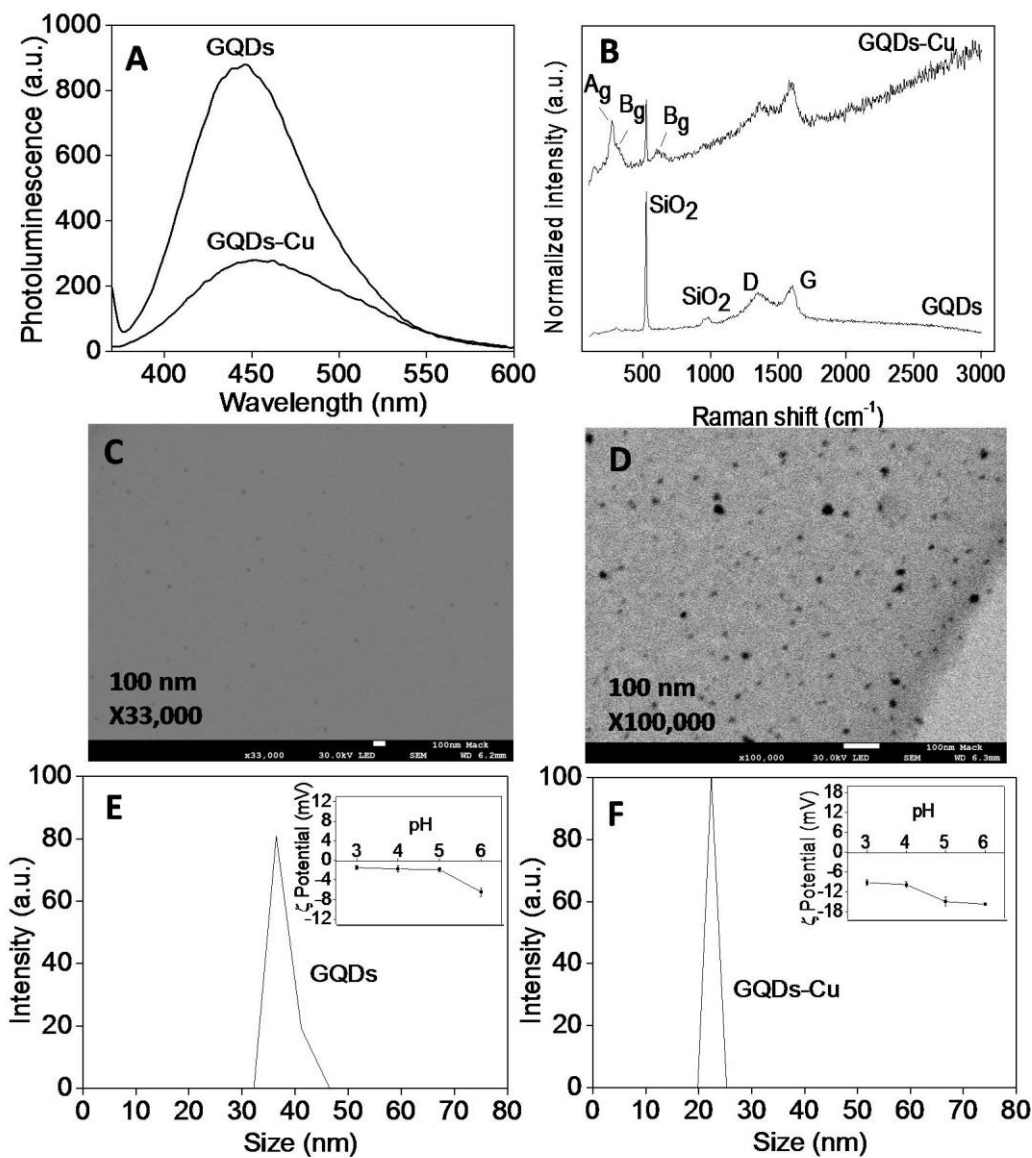


**Figure 7.2.** (A) Photoluminescence emission GQDs and GQDs-Cu (excitation at 337 nm). (B) Raman spectra of GQDs and GQDs-Cu. (C) STEM image of GQDs, (D) STEM image of GQDs-Cu. (E) Size distribution obtained by DLS for GQDs and  $\zeta$ -potential of GQDs in function of pH. (F) Size distribution obtained by GQDs-Cu and  $\zeta$ -potential of GQDs-Cu in function of pH.

X-ray photoelectron spectroscopy (XPS) indicated the presence of copper in the GQDs structure. In Fig. 7.3A were presented the survey spectra and the peaks for carbon 1s (~285eV) and oxygen 1s (~535eV) regions. The survey spectra

showed the presence of copper (0.3 at%), oxygen (30.7 at%), and nitrogen (1.3 at%) and carbon (67.7 at%) in the sample. No other elements were found at the limit of the resolution. The spectrum showed C 1s peaks at  $284.8 \pm 0.1$  eV and  $288.7 \pm 0.1$  eV (Fig. 7.3B), which can be assigned to the contributions of C-C  $sp^2$  and  $sp^3$ , and the C=O respectively. Spectra also shows Cu 2p peak (Fig. 7.3C) at binding energy 935 and 955 eV. Cu (I) oxide and Cu metal profiles are similar [195], therefore, the presence of copper(I) oxide or Cu metal or a mixture of both can be considered. Those XPS spectral features strongly indicated the functionalization of GQDs with copper.

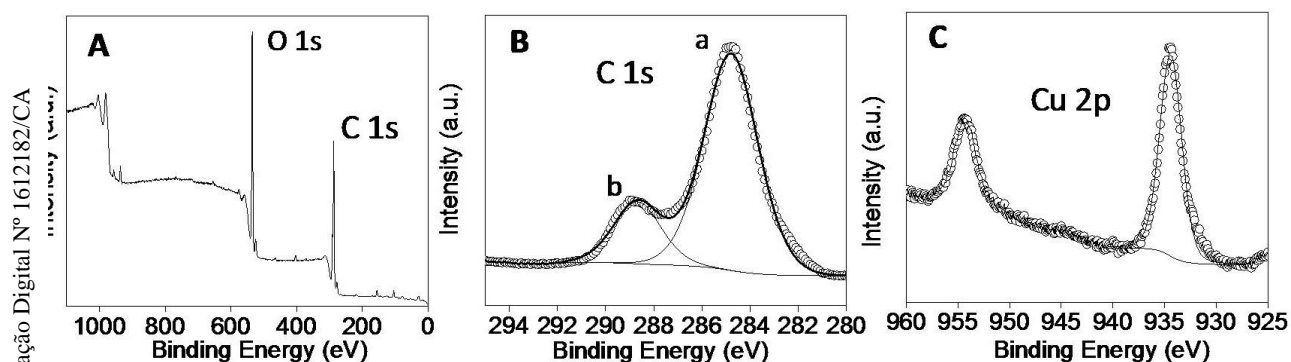


**Figure 7.3.** (A) XPS general survey spectra of GQDs-Cu. (B) High resolution C 1s peaks with a and b corresponding to C-C  $sp^2$  e  $sp^3$ , and COOH groups, respectively. (C) High resolution Cu 2p peaks with profile corresponding to copper(I) oxide or Cu metal.

### 7.2.2

#### Cyclic Voltammograms of creatinine using a gold electrode modified with Nafion-GQDs-Cu

Initially, different electrodes as glassy carbon (GC), gold and platinum were used to evaluate the redox properties of creatinine at  $2.0 \times 10^{-4}$  mol L<sup>-1</sup> (using different supporting electrolytes such as ammonium chloride; pH 4.5 and Britton Robinson buffer; pH 3 to 7) by performing a cyclic voltammograms within  $\pm 1500$

mV. In all cases no electrochemical activity was observed. According to literature, creatinine appears not to present significant electrochemical activity, which means that the direct transfer of electrons between creatinine and the electrode is not favorable [155]. In fact, most studies reported in literature proposes the electrochemical determination of creatinine using a mediator such as enzymes [152,153,156,188,189], copper in solution or as a modifier in the surface of electrodes [154,155,180]. When using copper, the determination of creatinine is based on the chelation property of the analyte rather than its redox behavior [155], which means that creatinine is probed in terms of how it affects the redox response of copper. Taking advantage from this, the modification of GQDs using  $\text{Cu}(\text{NO}_3)_2$  seemed to be adequate as a sensor for creatinine. Therefore, different electrode substrates (GC, Au and Pt) were modified (deposition of the GQDs-Cu dispersion, dried at room temperature) and only Au seemed to provide some stability to the deposited film and enable electrochemical response in terms of the redox signal concerning copper.

In order to produce an improved mechanical stability for the GQDs-Cu on the surface of Au electrode and a reliable reproducible response, Nafion was mixed to the dispersion of GQDs-Cu prior to deposition. Without the use of Nafion, a poorly reproducible response was obtained. As an inert polymeric film, Nafion provides a mechanical barrier that minimizes leaching of the modifier material from the electrode surface. Thus, Nafion was mixed GQDs-Cu dispersion in a 1 to 1 volume proportion (Nafion-GQDs-Cu dispersion 1/1 in volume) for the development of all analyses.

Cyclic voltammograms using the Au electrode modified with a mixture of Nafion-GQDs-Cu were obtained in presence and in absence of creatinine in the measured solution (Fig. 7.4). The CV obtained for the supporting electrolyte (BR buffer  $0.02 \text{ mol L}^{-1}$ ; pH 4 in KCl  $0.25 \text{ mol L}^{-1}$ ) without creatinine and using the Au/Nafion-GQDs-Cu electrode presented one anodic peak (peak 1) with peak potential  $E_p = +350 \text{ mV}$  and two cathodic peaks, as the scan was reversed, with  $E_p = +824 \text{ mV}$  (peak 2) and  $E_p = +632 \text{ mV}$  (peak 3).

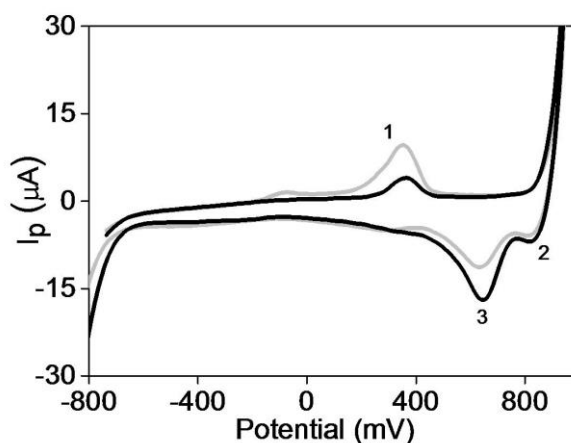


**Figure 7.4.** Cyclic voltammograms using Au/Nafion-GQDs-Cu electrode for a solution without creatinine (grey) and with creatinine (black). Experimental conditions: BR buffer ( $0.02 \text{ mol L}^{-1}$ ; pH 4.0 in KCl  $0.25 \text{ mol L}^{-1}$ ) and  $100 \text{ mV s}^{-1}$  scan rate. Creatinine at  $4 \times 10^{-5} \text{ mol L}^{-1}$ .

The anodic peak (peak 1) is attributed to  $\text{Cu}/\text{Cu}^{2+}$  oxidation process and the cathodic ones are probable due to the reduction of  $\text{Cu}^{2+}$  to  $\text{Cu}^+$  (peak 2) and the reduction of  $\text{Cu}^+$  to  $\text{Cu}$  (peak 3). This experimental observation is similar to the previously reported by Shaikh *et al.* [196] when studying the reduction of  $\text{Cu}^{2+}$  in Britton-Robinson (BR) aqueous buffer (at various pH values) using a glassy carbon electrode. Peak 2 due to the  $\text{Cu}^{2+}/\text{Cu}^+$  electron transfer couple is less intense than peak 3 for the  $\text{Cu}^+/\text{Cu}$  reduction couple. This can be explained considering the

relative stability of  $\text{Cu}^{2+}$  and  $\text{Cu}^+$  ions which depends highly on solvent Shaikh *et al.* [196]. Stability under aqueous conditions is significantly affected by the hydration energy of the ions coordinated with the water. The  $\text{Cu}^{2+}$  ion possess a greater charge density than the  $\text{Cu}^+$ , hence, forms a much stronger coordination, exempting more energy [196]. In contrast,  $\text{Cu}^+$  is significantly stable in non-aqueous media [197] and with ligands such as  $\text{Cl}^-$  [198]. In non-aqueous solvents, the relative higher stability of  $\text{Cu}^+$ , is owing that these solvents tend to solvate  $\text{Cu}^{2+}$  in a lesser effective way than it does water, solvating  $\text{Cu}^+$  more effectively than water [196].

In the presence of creatinine, a decreasing in current of peak 1 and a shifting towards more positive potentials (to  $E_p = +363$  mV) were observed whereas the currents measured from both cathodic peaks increased with a more significant increasing for peak 3. It can be proposed that during anodic scan, Cu is oxidized to  $\text{Cu}^{2+}$  and the  $\text{Cu}^{2+}$ -creatinine complex forms on the surface of the electrode, as it is reported to occur in solution [199]. Thus, the decreasing in anodic peak current can be attributed to the formation of such a complex. In the reverse scan, the formation of the creatinine complex with  $\text{Cu}^+$  seems to be hindered as sequential additions of creatinine in the electrochemical cell produces no further significant changes in peak current (Fig. 7.5). In polar solvents,  $\text{Cu}^{2+}$  complexes are predominantly coordinated to five or six ligands. However,  $\text{Cu}^+$  complexes are expected to favor four (tetrahedral) or lower coordination numbers. Therefore, electron transfer involving  $\text{Cu}^{2+}$  and  $\text{Cu}^+$  would be accompanied by major structural and stereochemical changes [196]. In addition, the reduction of  $\text{Cu}^+$  to Cu implies in losing all ligands. For this reason, in the reverse scan there was no significant change in peak intensities as there is no complexation taking place.

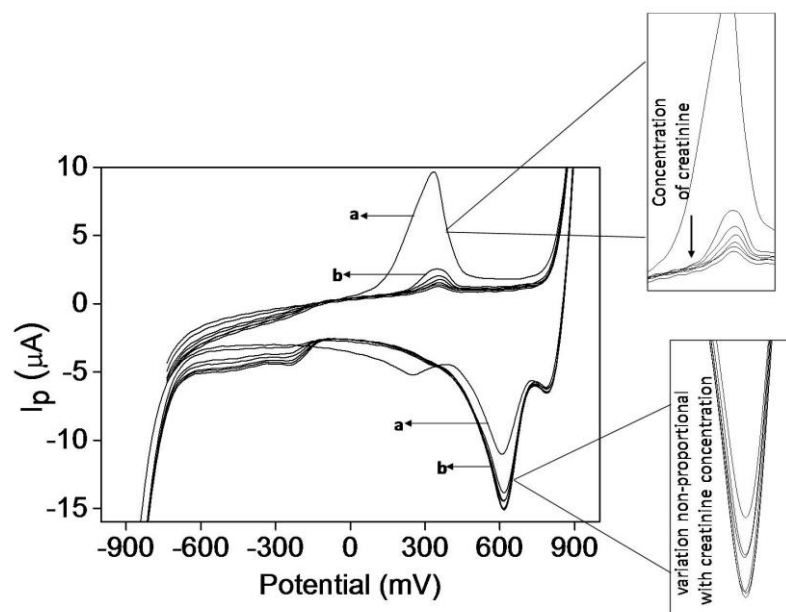


**Figure 7.5.** Cyclic voltammograms using the Au/Nafion-GQDs-Cu electrode and sequential additions of creatinine. (a) blank, (b) creatinine addition. Experimental conditions: BR buffer ( $0.02 \text{ mol L}^{-1}$ ; pH 4.0 in KCl  $0.25 \text{ mol L}^{-1}$ ) and  $100 \text{ mV s}^{-1}$  scan rate.

### 7.2.3

#### Effect of Nafion and graphene quantum dots on the electrode surface

In order to evaluate the role of GQDs in the nanocomposite as a modifier of the Au electrode, additions of increasing concentration of creatinine into the electrochemical cell were also made using an Au electrode modified only with a mixture of  $\text{Cu}(\text{OH})_2$  and Nafion, 1/1 v/v (1  $\mu\text{L}$  onto the surface of the electrode and dried under infrared lamp). Results obtained by cyclic voltammetry showed a new anodic peak (at  $-20.9 \text{ mV}$ ) besides the one (at  $+424.9 \text{ mV}$ ) already reported, and the two cathodic peaks in the reverse scan (Fig. 7.6A). The anodic peaks probably correspond respectively to the species  $\text{Cu}^+$  and  $\text{Cu}^{2+}$  from  $\text{Cu}(\text{OH})_2$  and  $\text{CuOH}$  formed during the  $\text{Cu}(\text{OH})_2$  synthesis. The  $\text{Cu}^{2+}$  peak potential obtained using the Au Nafion-GQDs-Cu electrode was about  $75 \text{ mV}$  smaller than the

potential observed for  $\text{Cu}^{2+}$  using the Au electrode modified with Nafion- $\text{Cu}(\text{OH})_2$ , demonstrating that GQDs facilitate electro-oxidation of copper. When increasing creatinine concentrations were added to the cell, monitored by the Au electrode modified with Nafion- $\text{Cu}(\text{OH})_2$ , no changes in the current after the first addition of creatinine was observed (Fig. 7.6A). This indicates that the participation of GQDs is relevant, mediating oxidation of Cu and the electron transfer also probably increasing active area that favors formation of the creatinine- $\text{Cu}^{2+}$ -complex.

Nafion formed a well-dispersed suspension of GQDs-Cu, allowing a uniform coating of the surface of the Au electrode, also providing mechanical stability to the modifier. Without the use of Nafion, leaching of the modifying material from the electrode surface occurs. Thus mixtures of Nafion and GQDs-Cu dispersion at proportions of 1/1 and 1/2 (in volume) were tested. The response in terms of peak current ( $I_p$ ) of blank (without creatinine) was more reproducible using Nafion-GQDs-Cu dispersion 1/1 v/v (Fig 7.6B).

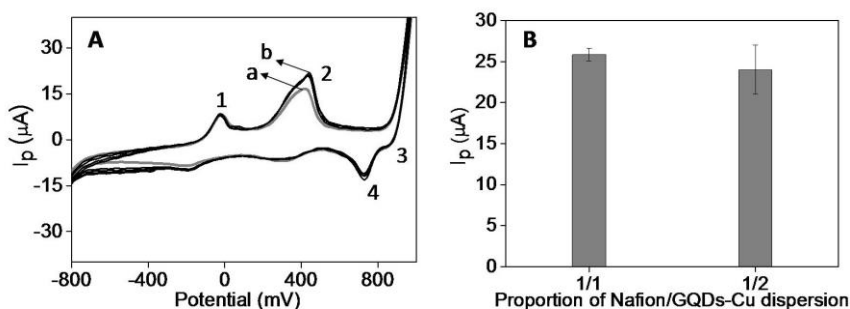


**Figure 7.6.** (A) Cyclic voltammograms using the Au/Nafion-GQDs-Cu electrode and sequential additions of creatinine. (a) blank, (b) creatinine addition. (B) Study of proportion of Nafion: GQDs-Cu dispersion. Experimental conditions: BR buffer ( $0.02 \text{ mol L}^{-1}$ ; pH 4.0 in  $\text{KCl } 0.25 \text{ mol L}^{-1}$ ) and  $100 \text{ mV s}^{-1}$  scan rate.

The relationship between scan rate and anodic peak current ( $E_p = +350$  mV) can be used to obtain valuable information regarding electrochemical behavior of creatinine on the Au/Nafion-GQDs-Cu electrode. A sequence of cyclic voltammograms of creatinine (at  $4 \times 10^{-5}$  mol L<sup>-1</sup>) was recorded using the Au/Nafion-GQDs-Cu electrode, in BR buffer (pH 4.0; 0.02 mol L<sup>-1</sup> in KCl 0.25 mol L<sup>-1</sup>), at different scan rates (from 10 to 800 mVs<sup>-1</sup>) as seen in Fig. 7.7A. An increasing in  $I_p$  was found to be directly proportional to the increase of scan rate, with a determination coefficient ( $R^2$ ) of 0.990 (Fig. 7.7B), which reveals an adsorption-controlled process.

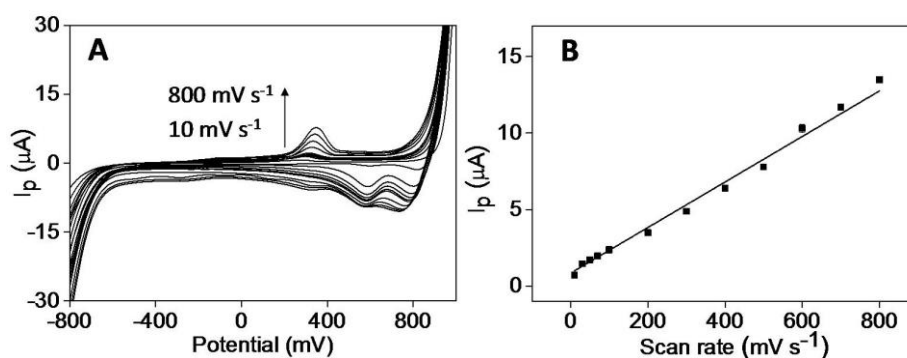


**Figure 7.7.** (A) Cyclic voltammograms of creatinine at different scan rates (10 to 800 mV s<sup>-1</sup>), using Au/Nafion-GQDs-Cu electrode. Experimental conditions: BR Buffer pH 4.0; 0.02 mol L<sup>-1</sup> in KCl 0.25 mol L<sup>-1</sup>. Solution containing  $4 \times 10^{-5}$  mol L<sup>-1</sup> of creatinine. (B) Peak current ( $I_p$ ) measured at  $E_p = +350$  mV in function of the scan rate.

#### 7.2.4 Influence of pH

The choice of the pH to perform the voltammetric measurements was made based on the intensity of the measured Cu/Cu<sup>2+</sup> oxidation peak and its behavior in the presence of creatinine. Square-wave voltammetry (SWV) was chosen to

perform quantitative measurements using a mixture of BR buffer (at  $0.02 \text{ mol L}^{-1}$ ) and KCl (at  $0.25 \text{ mol L}^{-1}$ ) and anodic scanning from  $\pm 1000 \text{ mV}$  (Fig. 7.8).

The creatine-creatinine equilibrium was reported to be essentially independent upon temperature, between  $22$  and  $40^\circ\text{C}$ , but to be strongly dependent on pH [200]. Literature suggests that at lower pH ( $\text{pH} < 2$ ) creatine in a creatine-creatinine mixture will be ultimately converted to creatinine [200]. At  $\text{pH} > 6.0$ , approximately equimolar ratios of creatine and creatinine will be established, but at pH  $3.5$ - $4.0$ , the equilibrium favors the formation of creatinine ( $> 90\%$ ). Therefore, the study was performed in the pH range of  $3.0$  to  $7.0$  and based on the comparison of intensities obtained for the peak at  $E_p = +415 \text{ mV}$  by SWV. The maximum anodic peak current was achieved at pH  $3.0$  -  $5.0$  (Fig. 7.8A). Changing the pH of the electrolyte was found to influence and affect the peak position (shift to less positive potentials).

As pH values increased from  $4.0$  to  $7.0$ , both  $E_p$  values of the redox process and  $I_p$  decreases probably due to influence of creatine and also to the formation of  $\text{Cu}(\text{OH})_2$  on the surface of the electrode which is indicated by the enlargement of the voltammetric peaks toward less positive potentials. At pH  $3.0$  and  $4.0$ , a sharp voltammetric peak is obtained and better relative responses were found as creatinine was added to the electrochemical cell (Fig. 7.8B-F). The supporting electrolyte at pH  $4.0$  was selected for further studies.

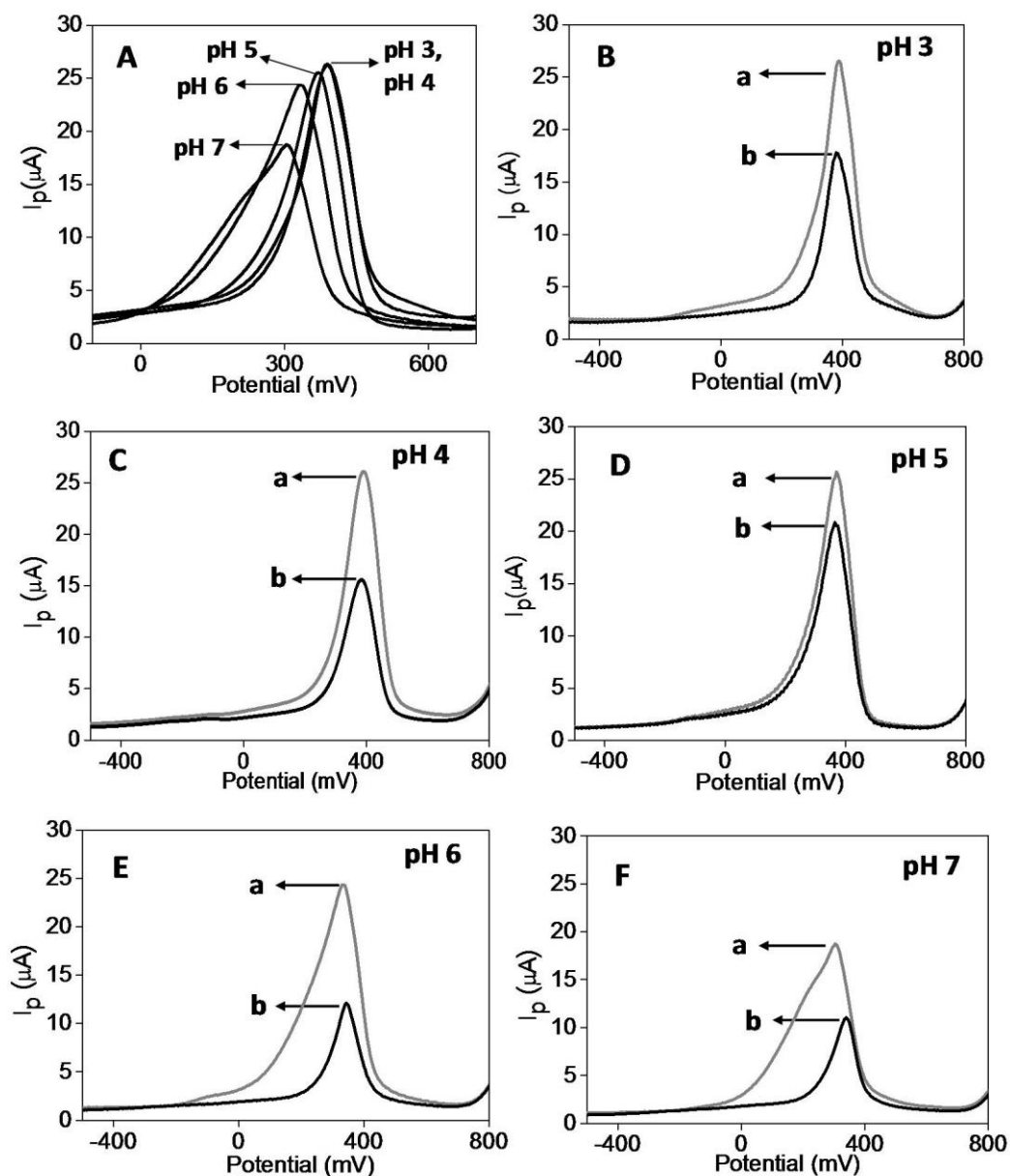


**Figure 7.8.** Voltammetric responses using SWV) and the Au/Nafion-GQDs-Cu electrode. (A) without addition of creatinine at different pH values. (B) at pH 3 without (a) and with (b) creatinine. (C) at pH 4 without (a) and with (b) creatinine. (D) at pH 5 without (a) and with (b) creatinine. (E) at pH 6 without (a) and with (b) creatinine. (F) at pH 7 without (a) and with (b) creatinine. BR Buffer  $0.02 \text{ mol L}^{-1}$  with KCl  $0.25 \text{ mol L}^{-1}$  with creatinine addition ( $4 \times 10^{-5} \text{ mol L}^{-1}$ ).

Since Cu/Cu<sup>2+</sup> oxidation proceeds probably through adsorption, the catalytic surface area of Au/Nafion-GQDs-Cu electrode is sufficient to allow complexation with creatinine at lower concentrations but, at higher concentrations of analyte, the modifier composition should be adjusted in order to allow enough contact area to proceed interaction with the analyte, thus expanding analytical response range. Therefore, a voltammetric study (using SWV) was conducted using electrodes containing different GQDs-Cu amount prepared using different amounts of Cu(NO<sub>3</sub>)<sub>2</sub>·3H<sub>2</sub>O (0.03, 0.06 and 0.09 g) and 0.6 grams of citric acid, also keeping the proportion of GQDs-Cu and Nafion constant at 1/1 v/v. It was observed that as the amount of Cu(NO<sub>3</sub>)<sub>2</sub> in the composite increased, the peak current in absence of creatinine ( $I_{p0}$ ) measured by the Au/Nafion-GQDs-Cu electrode also increased. However, it is decided to use 0.06 g of copper since larger amounts (0.09 g) produce low reproducibility at the analyte response.

The amount of the Nafion-GQDs-Cu to be added onto the surface of the Au electrode was also evaluated. Different amounts of the modifier (from 1  $\mu$ L to 4  $\mu$ L) were added on the electrode surface and the amount of creatinine added into the electrochemical cell was the same in all the experiments. The best condition was chosen based on the ratio between the signal of blank ( $I_{p0}$ ) and the signal measured in the presence of creatinine ( $I_{p(cre)}$ ) at  $1 \times 10^{-5}$  mol L<sup>-1</sup>. The best response (lower  $I_{p0}/I_{p(cre)}$  ratio) was found using deposition of 1  $\mu$ L of the modifier (Fig. 7.9). A lower  $I_{p0}/I_{p(cre)}$  means that electrode saturation would be achieved at higher concentrations of creatinine. The use of the lower amount of modifier also benefited the drying process, making it faster under the infrared lamp and enabling better mechanical stability of the modification onto the Au electrode surface.

The stability of Au/Nafion-Au-GQDs-Cu electrode was evaluated by obtaining 20 repetitive cyclic voltammograms using  $4 \times 10^{-5} \text{ mol L}^{-1}$  of creatinine. The measured average peak currents for creatinine were  $16.4 \mu\text{A}$  with the relative standard deviation of 1.8 %.

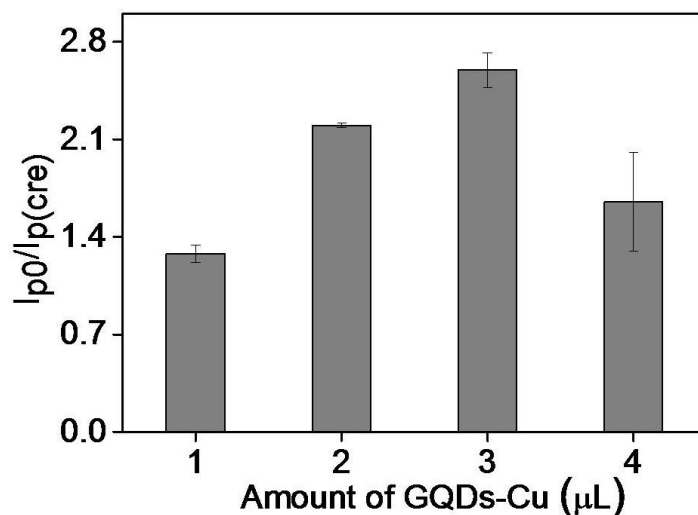


**Figure 7.9.** Effect of Nafion-GQDs-Cu on the Au electrode surface in terms of the relative current produced in absence and in the presence of creatinine. Experimental conditions: BR Buffer pH 4.0;  $0.02 \text{ mol L}^{-1}$  in KCl  $0.25 \text{ mol L}^{-1}$ .

### 7.2.5 Analytical performance

A study was performed aiming to achieve experimental and instrumental conditions appropriated to determine creatinine using the Au/Nafion-GQDs-Cu electrode by SWV. The chosen supporting electrolyte was the BR buffer (pH 4.0;  $0.02 \text{ mol L}^{-1}$ ) and KCl ( $0.25 \text{ mol L}^{-1}$ ) and signal intensity was measured at  $E_p = +415 \text{ mV}$ . Pulse amplitude steadily increased the voltammetric peak measured using the electrode without creatinine as it was varied (from 30 to 90 mV) with 20 mV selected due to the better relationship between peak sharpness and intensity. Frequency ( $f$ ) of 20 Hz was a compromise between peak current and peak width

within the 5 to 100 Hz range and potential step chosen was 10 mV. These studies were made in the presence of creatinine.

It is considered that on applying potential, copper undergoes electrochemical oxidation and the formed  $\text{Cu}^{2+}$  ions combine with the creatinine at the electrode surface, forming the  $\text{Cu}^{2+}$ -creatinine complex. The formation of the complex decreases the concentration of free  $\text{Cu}^{2+}$  formed and released by the electrode surface thus decreasing the characteristic  $\text{Cu}/\text{Cu}^{2+}$  current and leading to an analytical response inversely proportional to the increasing concentration of creatinine in the electrochemical cell.

The normalized analytical curve was constructed by sequential additions of analyte into the electrochemical cell (Fig. 7.10A and Fig. 7.10B), based on the  $I_{p0}/I_{p(\text{cre})}$  ratio, where,  $I_{p0}$  is the peak current of the blank and  $I_{p(\text{cre})}$  is the peak current measured in the presence of creatinine. There are two linear ranges relating measured peak current and creatinine concentration: range 1 (Fig.7.10B curve *a*, from  $5 \times 10^{-8}$  to  $1 \times 10^{-6}$  mol L<sup>-1</sup>) and range 2 (Fig.7.10B curve *b* from  $1 \times 10^{-6}$  to  $4.5 \times 10^{-4}$  mol L<sup>-1</sup>). However, the linear range covering the higher concentration range was chosen for quantitative purposes as it is enough to guarantee determination of creatinine levels in urine samples. In such range of concentrations, the response is modeled by the equation  $I_{p0}/I_{p(\text{cre})} = (6.56 \pm 0.16) \times 10^3 C_{\text{creatinine}} + (1.48 \pm 0.03)$  with  $R^2$  of 0.990. The  $C_{\text{creatinine}}$  is the analyte concentration in mol L<sup>-1</sup>

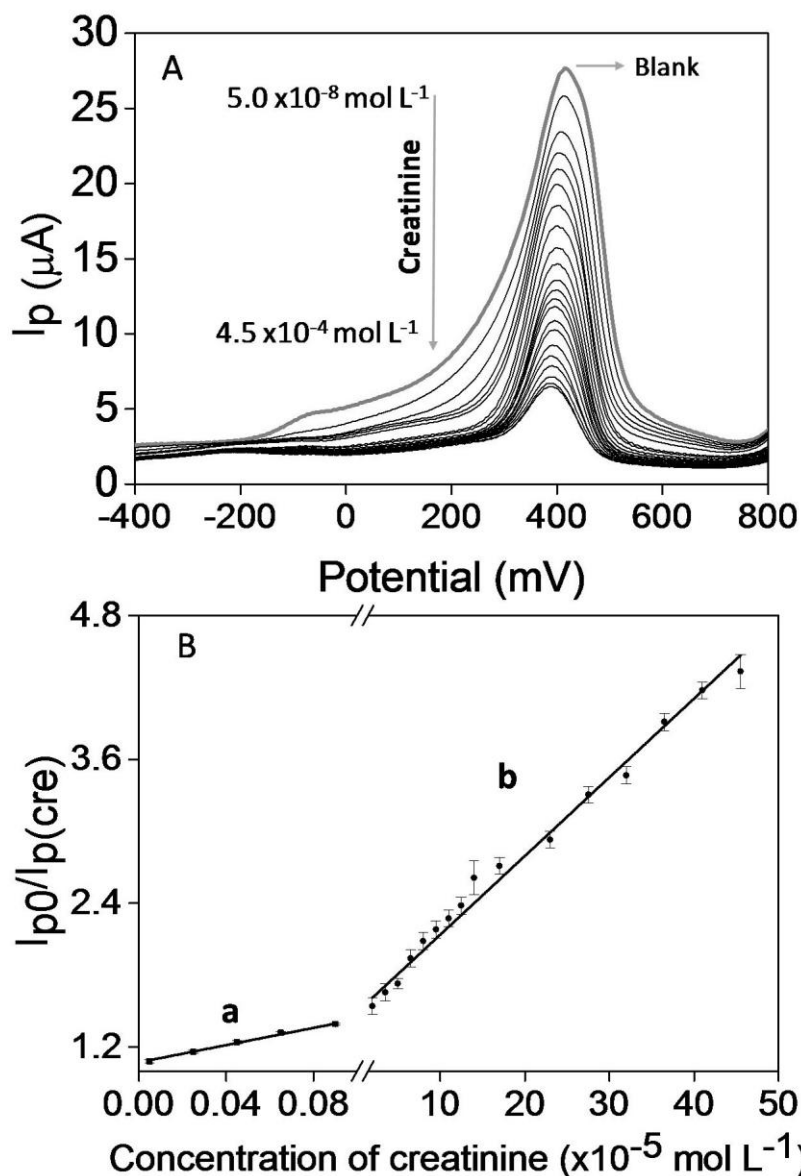


**Figure 7.10.** (A) Square-wave voltammetric responses of creatinine using Au/Nafion-GQDs-Cu electrode (peak current at  $E_P = +415$  mV). (B) Blank (in grey) and linear responses for creatinine (in black): (a) Lower concentration range ( $5 \times 10^{-8}$  to  $1 \times 10^{-6}$  mol L $^{-1}$ ) and (b) higher concentration range ( $5 \times 10^{-6}$  to  $4.5 \times 10^{-4}$  mol L $^{-1}$ ) with  $I_{p0}/I_{p(cre)} = (6.56 \pm 0.16) \times 10^3 C_{creatinine} + (1.48 \pm 0.03)$  and  $R^2 = 0.990$ . Experimental conditions: BR Buffer pH 4.0; 0.02 mol L $^{-1}$  in KCl 0.25 mol L $^{-1}$ .

Instrumental limit of quantification (LOQ) was considered as the lower concentration ( $5 \times 10^{-8} \text{ mol L}^{-1}$ ) in this range that still keep the linear response at least at  $R^2 = 0.990$ . The Pearson's correlation coefficient ( $\rho$ ) was calculated to test the linear response of this instrumental LOQ. A  $\rho$  value of 0.993 indicated a strong correlation and linearity for  $1 \times 10^{-6} \text{ mol L}^{-1}$ .

The instrumental precision was obtained as the variation coefficient of 10 consecutive measurements of the signal produced by the analyte concentration of  $1.0 \times 10^{-5} \text{ mol L}^{-1}$  and  $1.2 \times 10^{-4} \text{ mol L}^{-1}$ . Each measurement was made after a solution agitation step to replenish the solution-electrode interface and the precision at  $1.0 \times 10^{-5} \text{ mol L}^{-1}$  was 2.7% while at  $1.2 \times 10^{-4}$  was 1.9%.

Accuracy of the method was evaluated by determining two different concentration levels of creatinine in control solutions (fortifications at  $5 \times 10^{-5} \text{ mol L}^{-1}$  and  $5 \times 10^{-6} \text{ mol L}^{-1}$ ). The recoveries obtained ( $n = 3$ ) were  $(4.6 \pm 0.1) \times 10^{-5} \text{ mol L}^{-1}$  ( $93 \pm 3.1\%$ ) and  $(4.4 \pm 0.2) \times 10^{-6} \text{ mol L}^{-1}$  ( $89 \pm 4.2\%$ ) showing the potential of the Au/Nafion-GQDs-Cu electrode as an electrochemical sensor for the detection of creatinine.

### 7.2.6

#### Interference study

Studies were conducted to evaluate the possible interferences imposed by some of the components of urine on the electroanalytic creatinine signal measured using the Au/Nafion-GQDs-Cu electrode. Biological interferents from human urine samples were tested: urea, uric acid, glucose, potassium ions and sulfate ions. Creatinine concentration was kept at  $5.0 \times 10^{-6} \text{ mol L}^{-1}$  and tests were executed using two different molar ratios of creatinine/mixture of interferents at 1:1 and 1:2

proportions. The concentration of each of the interferers in the mixture is: urea ( $2.0 \times 10^{-4} \text{ mol L}^{-1}$ ), uric acid ( $2.5 \times 10^{-5} \text{ mol L}^{-1}$ ), glucose ( $5.0 \times 10^{-6} \text{ mol L}^{-1}$ ), potassium ions ( $5.0 \times 10^{-6} \text{ mol L}^{-1}$ ), and sulfate ions ( $5.0 \times 10^{-6} \text{ mol L}^{-1}$ ).

SWV response of creatinine and creatinine/mixture of interferents (at 1:1 and 1:2 proportions). The addition of  $5.0 \times 10^{-6} \text{ mol L}^{-1}$  of creatinine (without interferents) in the electrochemical cell induced a value to  $I_{p0}/I_{pcre}$  of 1.10, while, the molar ratio of 1:1 and 1:2 caused values of 1.04 and 1.05, respectively. That is, there was an increase of the creatinine signal around 5%, due to the interference. Hence, most of the major substances that compose urine matrix imposed negligible influence on the variation of signal produced by creatinine. This indicated a good selectivity of the Au/Nafion-GQDs-Cu electrode toward creatinine.

### 7.2.7

#### Determination of creatinine in urine

In order to demonstrate the applicability of the SWV method based on the use of the Au/Nafion-GQDs-Cu electrode, three fresh urine samples were analyzed. Urine samples were provided from three healthy volunteers, including two adult females and one male adult. One female and the male volunteer were under a diet high in animal protein while the other female volunteer whose diet is mostly vegetables and low in animal protein.

A volume of 60 mL of urine sample was submitted to a procedure to remove most of protein content and insoluble residues by adding 10 mL of methanol/acetonitrile (50/50% v/v). Urine samples were fortified with creatinine at three levels:  $10 \mu\text{mol L}^{-1}$  ( $1.1 \text{ mg L}^{-1}$ ),  $150 \mu\text{mol L}^{-1}$  ( $16.9 \text{ mg L}^{-1}$ ),  $300 \mu\text{mol L}^{-1}$  ( $33.9 \text{ mg L}^{-1}$ ). The average analyte original contents, calculated by the average

recovery achieved using the fortification values are indicated in Table 7.3. The values obtained from the analyte fortification procedure enabled estimation of the original contents of creatinine that agreed with the original values quantified in samples using HPLC. The results are presented in the Table 7.4. The *Student t*-test for similar variances (previously verified using the *Fisher-Snedecor* test) was used to compare the mean values of the results of each method. The statistical test considered a confidence limit of 95% (two tails, each with  $\alpha/2=0.025$ ). The test indicated that results are in statistical agreement ( $t_{\text{experimental}} < t_{\text{critical}}$ ). Considering the complexity of the matrix, the result can be considered satisfactory.

**Table 7.3.** Quantification study after urine samples fortification with creatinine for the estimation of the original analyte content.

Human urine samples	Creatinine fortification level ( $\mu\text{mol L}^{-1}$ )	Creatinine concentration in the electrochemical cell ( $\mu\text{mol L}^{-1}$ )	Creatinine found <sup>a</sup> ( $\mu\text{mol L}^{-1}$ )	Original creatinine recovered in the fortification experiment <sup>b</sup> ( $\mu\text{mol L}^{-1}$ )	Average original creatinine <sup>c</sup> ( $\mu\text{mol L}^{-1}$ )
<b>Woman A</b>	10	1.6	85.0 ±	83.4	
	150	25	0.9	81.2	84.1 ±
	300	50	106.2 ±	87.7	2.6
<b>Man A</b>			1.5		
			137.7 ±		
			1.0		
<b>Man A</b>	10	1.6	92.1 ±	90.5	
	150	25	1.1	93.2	92.8 ±
	300	50		94.7	1.7

			118.2 ±		
			0.7		
			144.7 ±		
			1.1		
	10	1.6	60.7 ±	59.1	62.7 ±
<b>Woman</b>	150	25	0.9	64.9	2.5
<b>B</b>	300	50	89.9 ±	64.1	
			0.8		
			114.1±		
			1.3		

<sup>a</sup> Standard deviation based on the three total creatinine values found per sample.

<sup>b</sup> Values discounting the creatinine fortification concentration and the found concentration in fortified sample

<sup>c</sup> Average values computing all fortification levels.

**Table 7.4.** Analysis results of creatinine in urine samples using the proposed SWV method and by HPLC. Standard deviation for  $n = 3$ . Confidence limit of 95%; two tails, each with  $\alpha/2 = 0.025$ .

Human urine samples	SWV C ( $\mu\text{mol L}^{-1}$ )	HPLC C ( $\mu\text{mol L}^{-1}$ )	t-test
Woman A	84.1 ± 2.6	81.9 ± 1.0	$t_{\text{exp}}=1.4 < t_{\text{critical}}$
Man A	92.8 ± 1.7	89.0 ± 0.5	$t_{\text{exp}}=3.7 < t_{\text{critical}}$
Woman B	62.7 ± 2.5	60.3 ± 1.2	$t_{\text{exp}}=1.5 < t_{\text{critical}}$

$t_{\text{critical}} = 4.3$ .

### 7.3

#### Partial conclusion

Various works [143,151–156] has been dedicated to the electro-analytical determination of creatinine; however, many require laborious procedures for

electrode modification as well as time consuming sample treatment or the use of expensive reagents. In this work, a simple pyrolysis reaction of citric acid with a small amount of  $\text{Cu}(\text{NO}_3)_2$  was used to produce a nanocomposite which was used to create a non-enzymatic electrochemical sensor of creatinine. A simple electrode modification procedure provided a sensing for creatinine in urine after only a simple sample pre-treatment, covering a concentration range enough to allow determination of typical concentrations of creatinine in urine. Reproducible results and proper recoveries besides LOD, which correspond to the same or lower order of magnitude of the best ones reported in literature (Table 7.2), are features that indicate advantages of the proposed sensor.

## 8 General Conclusion

Voltammetry methods using sensors based on carbon nanomaterial were developed. Carbon nanotubes (CNTs) and graphene quantum dots (GQDs) showed differentiated electrochemical responses towards the chosen analytes when used alone, after functionalization or as composites. The modification of electrodes with nanomaterials was fundamental to enable a sensitive, reproducible and selective analytical responses, providing advantages to analytical detection when compared to traditional electrodes.

The modification of the GC using a layer of MWCNTs provided amplification of the electrochemical signal measured from primaquine and INHHQ

by SWV due to the increased active area and improved electron-transfer rate. GC/MWCNTs also provided, when working on a proper pH, higher resolution in detecting the different electrochemical steps involved in the redox process of primaquine. The electrode enabled low LOD ( $28 \text{ nmol L}^{-1}$ ) for primaquine and when associated with a simple developed procedure, relying on LLE associated with TLC, enabled selectivity and capability to determine the lower levels expected in urine samples. The electro-analytical method for the determination of INHHQ is reported for the first time. The simple pretreatment of the sample, involving LLE and TLC, make this an effective method to determine the expected analyte levels in the extracts of the rat brain.

GQDs as a modifier of a GC electrode allowed the sensitive indirect determination of thiomersal. By combining the exposition of light with the applied potential promoted a significant degradation of thiomersal and the increasing of the  $\text{Hg}/\text{Hg}^{2+}$  redox peak used as an analytical signal measured by SWV. The GQDs are an attractive nanomaterial for sensing devices due to their easy preparation, photocatalytic properties, high thermal stability, and low cost. The method was successfully applied for the determination of thiomersal concentration in vaccines and proven as sensitive as the commonly used methods. A detection limit of  $0.85 \text{ } \mu\text{mol L}^{-1}$  was obtained. Acceptable recoveries confirm the usefulness of the method for quality control.

Several works reported the electro-analytical determination of creatinine, but many require laborious procedures for electrode modification as well as time-consuming sample treatment or the use of expensive reagents. In this work, a simple procedure was used to produce a nanocomposite based on GQDs and copper, which

was used as an electrochemical sensor for creatinine as the analyte decreased the characteristic  $\text{Cu}/\text{Cu}^{2+}$  oxidation peak of the nanocomposite. The method was applied in the analysis of urine samples, after only a simple sample pre-treatment, covering a concentration range enough to allow determination of typical concentrations of creatinine in urine. Good sensitivity, reproducible results, adequate recoveries and the overall performance achieved are characteristics that indicate advantages of the sensors used in this work.

## 9 Future work

- Develop an electro-analytical method using *f*-MWCNTs doped with copper as an electrode modifier for the determination of creatinine and its application in urine samples.
- Apply the developed method for the monitoring of INHHQ using GC/MWCNTs in samples of brain, kidney and, liver tissues.
- Develop a biosensor or enzyme-sensor for INHHQ determination, aiming to obtain an even more selective method and lower detection limits.
- Evaluate the use of Covalent organic frameworks (COF) along with MWCNTs or GQDs as sensors to determine different analytes of biological or pharmaceutical interest.

## 10 Reference

- [1] K.Y. Goud, M. Satyanarayana, A. Hayat, K.V. Gobi, J.L. Marty, Nanomaterial-based electrochemical sensors in pharmaceutical applications, Elsevier Inc., 2019.
- [2] S. Cheemalapati, Chemically modified electrodes-metal nanoparticles., 2 (2018) 2017–2018.
- [3] R.W. Murray, A.G. Ewing, R.A. Durst, Chemically Modified Electrodes: Molecular Design for Electroanalysis, *Anal. Chem.* 59 (1987).
- [4] M. Opallo, A. Lesniewski, A review on electrodes modified with ionic liquids, *J. Electroanal. Chem.* 656 (2011) 2–16.
- [5] G. March, T.D. Nguyen, B. Piro, Modified electrodes used for electrochemical detection of metal ions in environmental analysis, *Biosensors.* 5 (2015) 241–275.
- [6] E.E.L. Tanner, R.G. Compton, How can Electrode Surface Modification Benefit Electroanalysis?, *Electroanalysis.* 30 (2018) 1336–1341.

- [7] M. De Fátima Brito Souza, Chemically modified electrodes applied to electroanalysis: A brief presentation | Eletrodos quimicamente modificados aplicados à eletroanálise: Uma breve abordagem, *Quim. Nova.* 20 (1997) 191–195.
- [8] A.C. Pereira, A.D.S. Santos, L.T. Kubota, Tendências em modificação de eletrodos amperométricos para aplicações eletroanalíticas, *Quim. Nova.* 25 (2002) 1012–1021.
- [9] A. Walcarius, Analytical Applications of Silica-Modified Electrodes –A Comprehensive Review, *Electroanalysis.* 10 (1998) 1217–1235.
- [10] M. Alvarez-Icaza, U. Bilitewski, Mass Production of Biosensors, *Anal. Chem.* 65 (1993) 525–533.
- [11] G.G. Wallace, M. Smyth, H. Zhao, Conducting electroactive polymer-based biosensors, *TrAC - Trends Anal. Chem.* 18 (1999) 245–251.
- [12] B.D. Ratner, Surface modification of polymers: chemical, biological and surface analytical challenges, *Biosens. Bioelectron.* 10 (1995) 797–804.
- [13] N. Jadon, R. Jain, S. Sharma, K. Singh, Recent trends in electrochemical sensors for multianalyte detection – A review, *Talanta.* 161 (2016) 894–916.
- [14] A.K. Geim, K.S. Novoselov, The rise of graphene, *Nanosci. Technol. A Collect. Rev. from Nat. Journals.* (2009) 11–19.
- [15] M. Pumera, A. Ambrosi, A. Bonanni, E.L.K. Chng, H.L. Poh, Graphene for electrochemical sensing and biosensing, *TrAC - Trends Anal. Chem.* 29 (2010) 954–965.
- [16] J. Wang, Nanomaterial-based electrochemical biosensors, *Analyst.* 130 (2005) 421–426.
- [17] C. Li, E.T. Thostenson, T.-W. Chou, Sensors and actuators based on carbon nanotubes and their composites: A review, *Compos. Sci. Technol.* 68 (2008) 1227–1249.
- [18] G. Zhao, H. Wang, G. Liu, Recent advances in chemically modified electrodes, microfabricated devices and injection systems for the electrochemical detection of heavy metals: A review, *Int. J. Electrochem. Sci.* 12 (2017) 8622–8641.
- [19] L. Agüí, P. Yáñez-Sedeño, J.M. Pingarrón, Role of carbon nanotubes in electroanalytical chemistry. A review, *Anal. Chim. Acta.* 622 (2008) 11–47.
- [20] N.S. Lawrence, R.P. Deo, J. Wang, Comparison of the electrochemical reactivity of electrodes modified with carbon nanotubes from different sources, *Electroanalysis.* 17 (2005) 65–72.
- [21] G. Liu, S.L. Riechers, M.C. Mellen, Y. Lin, Sensitive electrochemical detection of enzymatically generated thiocholine at carbon nanotube modified glassy carbon electrode, *Electrochem. Commun.* 7 (2005) 1163–1169.
- [22] A. Salimi, M. Izadi, R. Hallaj, M. Rashidi, Simultaneous determination of ranitidine and metronidazole at glassy carbon electrode modified with single wall carbon nanotubes, *Electroanalysis.* 19 (2007) 1668–1676.
- [23] R.N. Goyal, A. Tyagi, N. Bachheti, S. Bishnoi, Voltammetric determination

- of bisoprolol fumarate in pharmaceutical formulations and urine using single-wall carbon nanotubes modified glassy carbon electrode, *Electrochim. Acta.* 53 (2008) 2802–2808.
- [24] O.E. Fayemi, A.S. Adekunle, E.E. Ebenso, Electrochemical determination of serotonin in urine samples based on metal oxide nanoparticles/MWCNT on modified glassy carbon electrode, *Sens. Bio-Sensing Res.* 13 (2017) 17–27.
- [25] K. Sipa, M. Brycht, A. Leniart, P. Urbaniak, A. Nosal-Wiercińska, B. Pałecz, S. Skrzypek,  $\beta$ -Cyclodextrins incorporated multi-walled carbon nanotubes modified electrode for the voltammetric determination of the pesticide dichlorophen, *Talanta.* 176 (2018) 625–634.
- [26] F.F. Hudari, J.C. Souza, M.V.B. Zanoni, Adsorptive stripping voltammetry for simultaneous determination of hydrochlorothiazide and triamterene in hemodialysis samples using a multi-walled carbon nanotube-modified glassy carbon electrode, *Talanta.* 179 (2018) 652–657.
- [27] S.X. dos Santos, É.T.G. Cavalheiro, Determination of Hydroquinone with a Carbon Nanotube/Polyurethane Resin Composite Electrode, *Anal. Lett.* 49 (2016) 1513–1525.
- [28] B. Dogan-Topal, B. Bozal-Palabiyik, B. Uslu, S.A. Ozkan, Multi-walled carbon nanotube modified glassy carbon electrode as a voltammetric nanosensor for the sensitive determination of anti-viral drug valganciclovir in pharmaceuticals, *Sensors Actuators, B Chem.* 177 (2013) 841–847.
- [29] J.M. Costa-Fernández, R. Pereiro, A. Sanz-Medel, The use of luminescent quantum dots for optical sensing, *TrAC - Trends Anal. Chem.* 25 (2006) 207–218.
- [30] X. Peng, M.C. Schlamp, A. V. Kadavanich, A.P. Alivisatos, Epitaxial growth of highly luminescent CdSe/CdS core/shell nanocrystals with photostability and electronic accessibility, *J. Am. Chem. Soc.* 119 (1997) 7019–7029.
- [31] S. Huang, W. Li, P. Han, X. Zhou, J. Cheng, H. Wen, W. Xue, Carbon quantum dots: Synthesis, properties, and sensing applications as a potential clinical analytical method, *Anal. Methods.* 11 (2019) 2240–2258.
- [32] S. Hu, A. Trinchi, P. Atkin, I. Cole, Tunable photoluminescence across the entire visible spectrum from carbon dots excited by white light, *Angew. Chemie - Int. Ed.* 54 (2015) 2970–2974.
- [33] X. Sun, C. Brückner, Y. Lei, One-pot and ultrafast synthesis of nitrogen and phosphorus co-doped carbon dots possessing bright dual wavelength fluorescence emission, *Nanoscale.* 7 (2015) 17278–17282.
- [34] L. Li, G. Wu, G. Yang, J. Peng, J. Zhao, J.J. Zhu, Focusing on luminescent graphene quantum dots: Current status and future perspectives, *Nanoscale.* 5 (2013) 4015–4039.
- [35] J. Shen, Y. Zhu, C. Chen, X. Yang, C. Li, Facile preparation and upconversion luminescence of graphene quantum dots, *Chem. Commun.* 47 (2011) 2580–2582.

- [36] R. Liu, D. Wu, X. Feng, K. Müllen, Bottom-up fabrication of photoluminescent graphene quantum dots with uniform morphology, *J. Am. Chem. Soc.* 133 (2011) 15221–15223.
- [37] F. Faridbod, A.L. Sanati, Graphene Quantum Dots in Electrochemical Sensors/Biosensors, *Curr. Anal. Chem.* 15 (2018) 103–123.
- [38] S. Dong, Q. Bi, C. Qiao, Y. Sun, X. Zhang, X. Lu, L. Zhao, Electrochemical sensor for discrimination tyrosine enantiomers using graphene quantum dots and  $\beta$ -cyclodextrins composites, *Talanta*. 173 (2017) 94–100.
- [39] N.R. Nirala, G. Khandelwal, B. Kumar, Vinita, R. Prakash, V. Kumar, One step electro-oxidative preparation of graphene quantum dots from wood charcoal as a peroxidase mimetic, *Talanta*. 173 (2017) 36–43.
- [40] S. Zhuo, M. Shao, S.T. Lee, Upconversion and downconversion fluorescent graphene quantum dots: Ultrasonic preparation and photocatalysis, *ACS Nano*. 6 (2012) 1059–1064.
- [41] D. Jiang, Y. Chen, N. Li, W. Li, Z. Wang, J. Zhu, H. Zhang, B. Liu, S. Xu, Synthesis of luminescent graphene quantum dots with high quantum yield and their toxicity study, *PLoS One*. 10 (2015) 5–7.
- [42] F. Liu, M.H. Jang, H.D. Ha, J.H. Kim, Y.H. Cho, T.S. Seo, Facile synthetic method for pristine graphene quantum dots and graphene oxide quantum dots: Origin of blue and green luminescence, *Adv. Mater.* 25 (2013) 3657–3662.
- [43] A. Bayat, E. Saievar-Iranizad, Synthesis of green-photoluminescent single layer graphene quantum dots: Determination of HOMO and LUMO energy states, *J. Lumin.* 192 (2017) 180–183.
- [44] Y. Dong, J. Shao, C. Chen, H. Li, R. Wang, Y. Chi, X. Lin, G. Chen, Blue luminescent graphene quantum dots and graphene oxide prepared by tuning the carbonization degree of citric acid, *Carbon N. Y.* 50 (2012) 4738–4743.
- [45] X. Wu, F. Tian, W. Wang, J. Chen, M. Wu, J.X. Zhao, Fabrication of highly fluorescent graphene quantum dots using L-glutamic acid for *in vitro/in vivo* imaging and sensing, *J. Mater. Chem. C*. 1 (2013) 4676–4684.
- [46] B. Zheng, Y. Chen, P. Li, Z. Wang, B. Cao, F. Qi, J. Liu, Z. Qiu, W. Zhang, Ultrafast ammonia-driven, microwave-assisted synthesis of nitrogen-doped graphene quantum dots and their optical properties, *Nanophotonics*. 6 (2017) 259–267.
- [47] M. Roushani, Z. Abdi, Novel electrochemical sensor based on graphene quantum dots/riboflavin nanocomposite for the detection of persulfate, *Sensors Actuators, B Chem.* 201 (2014) 503–510.
- [48] P. Pang, F. Yan, H. Li, H. Li, Y. Zhang, H. Wang, Z. Wu, W. Yang, Graphene quantum dots and Nafion composite as an ultrasensitive electrochemical sensor for the detection of dopamine, *Anal. Methods*. 8 (2016) 4912–4918.
- [49] S.L. Ting, S.J. Ee, A. Ananthanarayanan, K.C. Leong, P. Chen, Graphene quantum dots functionalized gold nanoparticles for sensitive electrochemical detection of heavy metal ions, *Electrochim. Acta*. 172 (2015) 7–11.

- [50] M. Arvand, S. Hemmati, Magnetic nanoparticles embedded with graphene quantum dots and multiwalled carbon nanotubes as a sensing platform for electrochemical detection of progesterone, *Sensors Actuators, B Chem.* 238 (2017) 346–356.
- [51] J. Cai, B. Sun, X. Gou, Y. Gou, W. Li, F. Hu, A novel way for analysis of calycosin via polyaniline functionalized graphene quantum dots fabricated electrochemical sensor, *J. Electroanal. Chem.* 816 (2018) 123–131.
- [52] N. Aristov, A. Habekost, Cyclic Voltammetry - A Versatile Electrochemical Method Investigating Electron Transfer Processes, *World J. Chem. Educ.* Vol. 3, 2015, Pages 115-119. 3 (2015) 115–119.
- [53] N. Elgrishi, K.J. Rountree, B.D. McCarthy, E.S. Rountree, T.T. Eisenhart, J.L. Dempsey, A Practical Beginner's Guide to Cyclic Voltammetry, *J. Chem. Educ.* 95 (2018) 197–206.
- [54] E.S. Rountree, B.D. McCarthy, T.T. Eisenhart, J.L. Dempsey, Evaluation of homogeneous electrocatalysts by cyclic voltammetry, *Inorg. Chem.* 53 (2014) 9983–10002.
- [55] V. Mirceski, R. Gulaboski, M. Lovric, I. Bogeski, R. Kappl, M. Hoth, Square-Wave Voltammetry: A Review on the Recent Progress, *Electroanalysis.* 25 (2013) 2411–2422.
- [56] D. De Souza, S.A.S. Machado, L.A. Avaca, Voltametria de onda quadrada. Primeira parte: Aspectos teóricos, *Quim. Nova.* 26 (2003) 81–89.
- [57] V. Mirceski, S. Skrzypek, L. Stojanov, Square-wave voltammetry, *ChemTexts.* 4 (2018)
- [58] R. Moscoso, Electrodo Modificados Com Nanotubos De Carbono y Nitrocompuestos. Thesis, Universidad de Chile, 2015.
- [59] A.K. Dwivedi, D. Saxena, S. Singh, HPLC and HPTLC assays for the antimalarial agents Chloroquine, Primaquine and Bulaquine, *J. Pharm. Biomed. Anal.* 33 (2003) 851–858.
- [60] D.S. Cukierman, A.B. Pinheiro, S.L.P. Castiñeiras-Filho, A.S.P. da Silva, M.C. Miotto, A. De Falco, T. de P. Ribeiro, S. Maisonette, A.L.M.C. da Cunha, R.A. Hauser-Davis, J. Landeira-Fernandez, R.Q. Aucélio, T.F. Outeiro, M.D. Pereira, C.O. Fernández, N.A. Rey, A moderate metal-binding hydrazone meets the criteria for a bioinorganic approach towards Parkinson's disease: Therapeutic potential, blood-brain barrier crossing evaluation and preliminary toxicological studies, *J. Inorg. Biochem.* 170 (2017) 160–168.
- [61] J.R. Miranda-Andrades, S. Khan, C.A.T. Toloza, E.C. Romani, F.L. Freire Júnior, R.Q. Aucélio, Thiomersal photo-degradation with visible light mediated by graphene quantum dots: Indirect quantification using optical multipath mercury cold-vapor absorption spectrophotometry, *Spectrochim. Acta - Part B At. Spectrosc.* 138 (2017) 81–89.
- [62] S.K. George, M.T. Dipu, U.R. Mehra, P. Singh, A.K. Verma, J.S. Ramgaokar, Improved HPLC method for the simultaneous determination of allantoin, uric acid and creatinine in cattle urine, *J. Chromatogr. B Anal.*

- Technol. Biomed. Life Sci. 832 (2006) 134–137.
- [63] World Health Organization (WHO), World Malaria Report 2008, Geneva, <http://www.who.int/malaria/publications/atoz/9789241563697/en/index.html>, (2008),  
Accessed date: 20 March 2019.
- [64] Compendium of WHO Malaria Guidance – Prevention, Diagnosis, Treatment, Surveillance and Elimination, World Health Organization, Geneva, 2019.
- [65] M.L.P.M. Arguelho, M.V.B. Zanoni, N.R. Stradiotto, Electrochemical oxidation and voltammetric determination of the antimalaria drug primaquine, *Anal. Lett.* 38 (2005) 1415–1425.
- [66] Primaquine Phosphate, The American Society of Health-System Pharmacists, <https://web.archive.org/web/20161220060718/https://www.drugs.com/monograph/primaquine-phosphate.html>, Accessed date: 22 March 2019.
- [67] N. Vale, M. Prud, C.A. Marques, M.S. Collins, J. Gut, J. Matos, P.J. Rosenthal, M.T. Cushion, E. Ros, M.M. Mota, R. Moreira, P. Gomes, Imidazoquinones as Antimalarial and Antipneumocystis Agents †, (2009) 7800–7807.
- [68] P. Arguin, K. Tan, Malaria - chapter 3, in: Gary W. Brunette (Ed.), CDC Health Information for International Travel (Yellow Book), CDC and Oxford University Press, 2016, <https://wwwnc.cdc.gov/travel/yellowbook/2018/infectious-diseasesrelated-to-travel/malaria#1939>.
- [69] S. Kristensen, A.-L. Grislingaas, J. V. Greenhill, T. Skjetne, J. Karlsen, H.H. Tønnesen, Photochemical stability of biologically active compounds: V. Photochemical degradation of primaquine in an aqueous medium, *Int. J. Pharm.* 100 (1993) 15–23.
- [70] Brasil. Ministerio da Saude, Agencia Nacional de Vigilancia Sanitaria (ANVISA), *Farmacopeia Brasileira*, (2010), <https://doi.org/10.1590/S0102-33062006000100002>.
- [71] A.P. Cruz, C.D. Bertol, F.S. Murakami, M.A.S. Silva, Development and validation of RP- HPLC method for determination of primaquine in extended release tablets, *Lat. Am. J. Pharm.* 27 (2008) 415–418.
- [72] S.M. Hassan, M.E.-S. Metwally, A.M.A. Cuf, A Sensitive Colour Reaction for the Deterination of Primaquine in Pharmaceutical Preparations, *Anal. Lett.* 15 (1892) 213–219.
- [73] A.M. Nouralla Altigani, A.A. Elbashir, H.Y. Aboul-Enein, Optimization and Validation of a Fluorescence Method for the Determination of Primaquine in Pharmaceutical Formulation, *Curr. Anal. Chem.* 14 (2017) 30–35.

- [74] B. Avula, B.L. Tekwani, N.D. Chaurasiya, P. Fasinu, N.P. Dhammika Nanayakkara, H.M.T. Bhandara Herath, Y.H. Wang, J.Y. Bae, S.I. Khan, M.A. Elsohly, J.D. McChesney, P.A. Zimmerman, I.A. Khan, L.A. Walker, Metabolism of primaquine in normal human volunteers: Investigation of phase I and phase II metabolites from plasma and urine using ultra-high performance liquid chromatography-quadrupole time-of-flight mass spectrometry, *Malar. J.* 17 (2018) 1–14.
- [75] A.G.N.C. Mello, M.V.D.F. Vieira, L.W.P. de Sena, T.P. da Paixão, A.C.G. Pinto, D.P. de A. Grisólia, M.T. Silva, J.L.F. Vieira, A.G.N.C. Mello, M.V.D.F. Vieira, L.W.P. de Sena, T.P. da Paixão, A.C.G. Pinto, D.P. de A. Grisólia, M.T. Silva, J.L.F. Vieira, Levels of primaquine and carboxyprimaquine in patients with malaria vivax from the Brazilian Amazon basin, *Rev. Inst. Med. Trop. Sao Paulo.* 60 (2018).
- [76] G.W. Parkhurst, M. V. Nora, R.W. Thomas, P.E. Carson, High-Performance Liquid Chromatographic-Ultraviolet Determination of Primaquine and Its Metabolites in Human Plasma and Urine, *J. Pharm. Sci.* 73 (1984) 1329–1331.
- [77] V.K. Dua, P.K. Kar, R. Sarin, V.P. Sharma, High-performance liquid Chromatographic determination of primaquine and carboxyprimaquine concentrations in plasma and blood cells in Plasmodium vivax malaria cases following chronic dosage with primaquine, *J. Chromatogr. B Biomed. Appl.* 675 (1996) 93–98.
- [78] J. Lal, N. Mehrotra, R.C. Gupta, Analysis and pharmacokinetics of bulaquine and its major metabolite primaquine in rabbits using an LC-UV method - A pilot study, *J. Pharm. Biomed. Anal.* 32 (2003) 141–150.
- [79] K. Na-Bangchang, E.A. Guirou, A. Cheomung, J. Karbwang, Determination of primaquine in whole blood and finger-pricked capillary blood dried on filter paper using HPLC and LCMS/MS, *Chromatographia.* 77 (2014) 561–569.
- [80] M. Page-Sharp, K.F. Ilett, I. Betuela, T.M.E. Davis, K.T. Batty, Simultaneous determination of primaquine and carboxyprimaquine in plasma using solid phase extraction and LC-MS assay, *J. Chromatogr. B Anal. Technol. Biomed. Life Sci.* 902 (2012) 142–146.
- [81] Y.S. Endoh, H. Yoshimura, N. Sasaki, Y. Ishihara, H. Sasaki, S. Nakamura, Y. Inoue, M. Nishikawa, High-performance liquid chromatographic determination of pamaquine, primaquine and carboxy primaquine in calf plasma using electrochemical detection, *J. Chromatogr. B Biomed. Sci. Appl.* 579 (1992) 123–129.
- [82] M.H. Mashhadizadeh, M. Akbarian, Voltammetric determination of some anti-malarial drugs using a carbon paste electrode modified with Cu(OH) 2 nano-wire, *Talanta.* 78 (2009) 1440–1445.
- [83] N.B. Thapliyal, T.E. Chiwunze, R. Karpoormath, S. Cherukupalli, Fabrication of highly sensitive gold nanourchins based electrochemical sensor for nanomolar determination of primaquine, *Mater. Sci. Eng. C.* 74

- (2017) 27–35.
- [84] B.B. Prasad, A. Kumar, R. Singh, *Molecularly imprinted polymer-based electrochemical sensor using functionalized fullerene as a nanomediator for ultratrace analysis of primaquine*, Elsevier Ltd, 2016.
- [85] X. Qiu, L. Lu, J. Leng, Y. Yu, W. Wang, M. Jiang, L. Bai, An enhanced electrochemical platform based on graphene oxide and multi-walled carbon nanotubes nanocomposite for sensitive determination of Sunset Yellow and Tartrazine, *Food Chem.* 190 (2016) 889–895.
- [86] T. Yang, Y. Gao, J. Xu, L. Lu, Y. Yao, Z. Wang, X. Zhu, H. Xing, Nickel clusters grown on three-dimensional graphene oxide-multi-wall carbon nanotubes as an electrochemical sensing platform for luteolin at the picomolar level, *RSC Adv.* 5 (2015) 64739–64748.
- [87] M.A. La-Scalea, C.M.S. Menezes, G.C. Matsutami, M.C. Polli, S.H.P. Serrano, E.I. Ferreira, Molecular modeling of the voltammetric oxidation at a glassy carbon electrode of the antimalarial drug primaquine and its prodrugs succinylprimaquine and maleylprimaquine, *Electrochim. Acta.* 51 (2006) 5103–5111.
- [88] M.A. La-scalea, C.M. Chin, M.L. Cruz, H.P. Serrano, E.I. Ferreira, Approach To the Study of Anti-Chagas Prodrugs Mechanism of Action, *Bioelectrochemistry.* (2000) 55–59.
- [89] D. K. Gosser, *Book Reviews*, (1993) 96–100.
- [90] D.L. Mount, L.C. Patchen, S.B. Williams, F.C. Churchill, Colorimetric and Thin-Layer Chromatographic Methods for Field Assay of Chloroquine and Its Metabolites in Urine, *Bull. World Health Organ.* 65 (1987) 615–623.
- [91] N.J. White, *Clinical Pharmacokinetics of Antimalarial Drugs*, *Clin. Pharmacokinet.* 10 (1985) 187–215.
- [92] C.L. Masters, R. Cappai, K.J. Barnham, V.L. Villemagne, Molecular mechanisms for Alzheimer’s disease: Implications for neuroimaging and therapeutics, *J. Neurochem.* 97 (2006) 1700–1725.
- [93] R. Brookmeyer, E. Johnson, K. Ziegler-Graham, H.M. Arrighi, Forecasting the global burden of Alzheimer’s disease, *Alzheimer’s Dement.* 3 (2007) 186–191.
- [94] A. Serrano-Pozo, M.P. Frosch, E. Masliah, B.T. Hyman, Neuropathological alterations in Alzheimer disease, *Cold Spring Harb. Perspect. Med.* 1 (2011) 1–24.
- [95] L.E. Scott, C. Orvig, Medicinal inorganic chemistry approaches to passivation and removal of aberrant metal ions in disease, *Chem. Rev.* 109 (2009) 4885–4910.
- [96] A. Budimir, Metal ions, Alzheimer’s disease and chelation therapy, *Acta Pharm.* 61 (2011) 1–14.
- [97] S.Y. Chen, Y. Chen, Y.P. Li, S.H. Chen, J.H. Tan, T.M. Ou, L.Q. Gu, Z.S. Huang, Design, synthesis, and biological evaluation of curcumin analogues as multifunctional agents for the treatment of Alzheimer’s disease, *Bioorganic Med. Chem.* 19 (2011) 5596–5604.

- [98] L. Mucke, D.J. Selkoe, Neurotoxicity of amyloid  $\beta$ -protein: Synaptic and network dysfunction, *Cold Spring Harb. Perspect. Med.* 2 (2012) 1–18.
- [99] T. Kowalik-Jankowska, M. Ruta-Dolejsz, K. Wisniewska, L. Lankiewicz, H. Kozlowski, Possible involvement of Copper(II) in Alzheimer disease, *Environ. Health Perspect.* 110 (2002) 869–870.
- [100] E.L. Sampson, L. Jenagaratnam, R. Meshane, Metal protein attenuating compounds for the treatment of Alzheimer’s dementia, *Cochrane Database Syst. Rev.* 2014 (2014).
- [101] R.A. Hauser-Davis, L. V. De Freitas, D.S. Cukierman, W.S. Cruz, M.C. Miotto, J. Landeira-Fernandez, A.A. Valiente-Gabioud, C.O. Fernández, N.A. Rey, Disruption of zinc and copper interactions with A $\beta$ (1-40) by a non-toxic, isoniazid-derived, hydrazone: A novel biometal homeostasis restoring agent in Alzheimer’s disease therapy?, *Metallomics.* 7 (2015) 743–747.
- [102] A. De Falco, Activity evaluation and toxicological profile of new potential “Metal Protein Attenuating Compounds” in biological models of Alzheimer’s disease, 2017, PhD diss., PUC-Rio.
- [103] L.V. De Freitas, C.C.P. Da Silva, J. Ellena, L.A.S. Costa, N.A. Rey, Structural and vibrational study of 8-hydroxyquinoline-2-carboxaldehyde isonicotinoyl hydrazone - A potential metal-protein attenuating compound (MPAC) for the treatment of Alzheimer’s disease, *Spectrochim. Acta - Part A Mol. Biomol. Spectrosc.* 116 (2013) 41–48.
- [104] J. Kalia, R.T. Raines, Hydrolytic stability of hydrazones and oximes, *Angew. Chemie - Int. Ed.* 47 (2008) 7523–7526.
- [105] M.J. Pedrozo-Peñafiel, J.M.S. Almeida, C.A.T. Toloza, D.G. Larrudé, W.F. Pacheco, R.Q. Aucelio, Square-wave voltammetric determination of primaquine in urine using a multi-walled carbon nanotube modified electrode, *Microchem. J.* 150 (2019) 104201.
- [106] F.H. Wu, G.C. Zhao, X.W. Wei, Electrocatalytic oxidation of nitric oxide at multi-walled carbon nanotubes modified electrode, *Electrochem. Commun.* 4 (2002) 690–694.
- [107] G.C. Zhao, Z.Z. Yin, L. Zhang, X.W. Wei, Direct electrochemistry of cytochrome c on a multi-walled carbon nanotubes modified electrode and its electrocatalytic activity for the reduction of H<sub>2</sub>O<sub>2</sub>, *Electrochem. Commun.* 7 (2005) 256–260.
- [108] J. Claret, C. Muller, J.M. Feliu, J. Virgili, U. De Barcelona, *Polarographic and Voltammetric Studies Solution-Basic Media \**, (1982) 1475–1479.
- [109] M.C. Stević, L.M. Ignjatović, G. Ćirić-Marjanović, S.M. Stanišić, D.M. Stanković, J. Zima, Voltammetric behaviour and determination of 8-hydroxyquinoline using a glassy carbon paste electrode and the theoretical study of its electrochemical oxidation mechanism, *Int. J. Electrochem. Sci.* 6 (2011) 2509–2525.
- [110] E. Hammam, A.M. Beltagi, M.M. Ghoneim, Voltammetric assay of rifampicin and isoniazid drugs, separately and combined in bulk,

- pharmaceutical formulations and human serum at a carbon paste electrode, *Microchem. J.* 77 (2004) 53–62.
- [111] P. Zanello, C. Nervi, F. F. De Biani, *Inorganic Electrochemistry: Theory, Practice and Application*, 2012, 2nd ed. Cambridge: Royal Society of Chemistry.
- [112] WHO, World Health Organization 2020, <https://www.who.int/biologicals/areas/vaccines/thiomersal/en/> (accessed 06 January 2020).
- [113] M.P. Da Silva, J. Rodriguez, L. Hernández, Electrochemical oxidative determination of thimerosal in soft contact lens care solutions by cyclic voltammetry, *Analyst.* 119 (1994) 1971–1974.
- [114] WHO, Global Advisor Committee on Vaccine Safety Statement on Thiomersal, 2020, [https://www.who.int/vaccine\\_safety/committee/topics/thiomersal/questions/en/](https://www.who.int/vaccine_safety/committee/topics/thiomersal/questions/en/) (accessed 06 January 2020).
- [115] C. Gonzalez, O. García-Beltrán, E. Nagles, A new and simple electroanalytical method to detect thiomersal in vaccines on a screen-printed electrode modified with chitosan, *Anal. Methods.* 10 (2018) 1196–1202.
- [116] J. Rodrigues, V. Branco, J. Lu, A. Holmgren, C. Carvalho, Toxicological effects of thiomersal and ethylmercury: Inhibition of the thioredoxin system and NADP<sup>+</sup>-dependent dehydrogenases of the pentose phosphate pathway, *Toxicol. Appl. Pharmacol.* 286 (2015) 216–223.
- [117] S. Gil, I. Lavilla, C. Bendicho, Greener analytical method for determination of thiomersal (sodium ethylmercurithiosalicylate) in ophthalmic solutions using sono-induced cold vapour generation-atomic absorption spectrometry after UV/H<sub>2</sub>O<sub>2</sub> advanced oxidation, *J. Anal. At. Spectrom.* 22 (2007) 569–572.
- [118] G. Acosta, A. Spisso, L.P. Fernández, L.D. Martinez, P.H. Pacheco, R.A. Gil, Determination of thimerosal in pharmaceutical industry effluents and river waters by HPLC coupled to atomic fluorescence spectrometry through post-column UV-assisted vapor generation, *J. Pharm. Biomed. Anal.* 106 (2015) 79–84.
- [119] Q. Xu, Z. Wang, L. Jin, P. Liu, Y. Tian, S. Zhang, C. Zhang, Non-chromatographic separation and determination of thimerosal and inorganic mercury in vaccines by Fe<sup>3+</sup>-induced degradation with cold vapor atomic fluorescence spectrometry, *Anal. Methods.* 10 (2018) 2144–2150.
- [120] Q. Wu, Z. Zhu, Z. Liu, H. Zheng, S. Hu, L. Li, Dielectric barrier discharge-plasma induced vaporization for the determination of thiomersal in vaccines by atomic fluorescence spectrometry, *J. Anal. At. Spectrom.* 27 (2012) 496–500.
- [121] E.J. Dos Santos, A.B. Herrmann, A.B. Dos Santos, L.M. Baika, C.S. Sato, L. Tormen, R.E. Sturgeon, A.J. Curtius, Determination of thimerosal in human and veterinarian vaccines by photochemical vapor generation coupled to ICP OES, *J. Anal. At. Spectrom.* 25 (2010) 1627–1632.

- [122] H. He, Z. Zhu, H. Zheng, Q. Xiao, L. Jin, S. Hu, Dielectric barrier discharge micro-plasma emission source for the determination of thimerosal in vaccines by photochemical vapor generation, *Microchem. J.* 104 (2012) 7–11.
- [123] B. Campanella, M. Onor, M.C. Mascherpa, A. D'Ulivo, C. Ferrari, E. Bramanti, Determination of thiomersal by flow injection coupled with microwave-assisted photochemical online oxidative decomposition of organic mercury and cold vapor atomic fluorescence spectroscopy, *Anal. Chim. Acta.* 804 (2013) 66–69.
- [124] R.C. Meyer, L.B. Cohn, Thimerosal determination by high-pressure liquid chromatography, *J. Pharm. Sci.* 67 (1978) 1636–1638.
- [125] M. Zaręba, P.T. Sanecki, R. Rawski, Simultaneous determination of thimerosal and aluminum in vaccines and pharmaceuticals with the use of HPLC method, *Acta Chromatogr.* 28 (2016) 299–311.
- [126] G. Acosta, S. Torres, M. Kaplan, L.P. Fernández, P.H. Pacheco, R.A. Gil, Liquid chromatography coupled to molecular fluorescence with postcolumn UV sensitization for thimerosal and derivative compounds monitoring in environmental samples, *Electrophoresis.* 37 (2016) 2531–2537.
- [127] K.P. Shrivastaw, S. Singh, A new method for spectrophotometric determination of thiomersal in biologicals, *Biologicals.* 23 (1995) 65–69.
- [128] A. Fredj, H. Okbi, N. Adhoum, L. Monser, Gas diffusion flow injection determination of thiomersal in vaccines, *Talanta.* 91 (2012) 47–51.
- [129] Birner, Thimerosal as, (1964) 1264–1265.
- [130] R. Piech, J. Wymazała, J. Smajdor, B. Paczosa-Bator, Thiomersal determination on a renewable mercury film silver-based electrode using adsorptive stripping voltammetry, *Anal. Methods.* 8 (2016) 1187–1193.
- [131] J. Penagos-Llanos, J.A. Calderón, E. Nagles, J.J. Hurtado, Voltammetric determination of thiomersal with a new modified electrode based on a carbon paste electrode decorated with La<sub>2</sub>O<sub>3</sub>, *J. Electroanal. Chem.* 833 (2019) 536–542.
- [132] X. Wei, T. Wu, Y. Yuan, X. Ma, J. Li, Highly sensitive analysis of organometallic compounds based on molecularly imprinted electrochemical sensors, *Anal. Methods.* 9 (2017) 1771–1778.
- [133] C.B. Reader, M.J., Lines, Decomposition of Thimerosal in Aqueous Solution, 72 (1983) 1406–1409.
- [134] J.R. Procopio, M.P. da Silva, M. del Carmen Asensio, M.T. Sevilla, L. Hernandez, HPLC analysis of thimerosal and its degradation products in ophthalmic solutions with electrochemical detection, *Talanta.* 39 (1992) 1619–1623.
- [135] F. McDonald, J.E. Parkin, The effect of disodium edetate and sodium chloride on the stability of ethylmercury arising from the decomposition of thimerosal (thiomersal), *Drug Dev. Ind. Pharm.* 21 (1995) 2403–2410.
- [136] K.B. Hatzell, M.B. Dixit, S.A. Berlinger, A.Z. Weber, Understanding inks for porous-electrode formation, *J. Mater. Chem. A.* 5 (2017) 20527–20533.

- [137] M. Wu, X. Xiao, N. Vukmirovic, S. Xun, P.K. Das, X. Song, P. Olalde-Velasco, D. Wang, A.Z. Weber, L.W. Wang, V.S. Battaglia, W. Yang, G. Liu, Toward an ideal polymer binder design for high-capacity battery anodes, *J. Am. Chem. Soc.* 135 (2013) 12048–12056.
- [138] R.S. Nicholson, I. Shain, Theory of Stationary Electrode Polarography: Single Scan and Cyclic Methods Applied to Reversible, Irreversible, and Kinetic Systems, *Anal. Chem.* 36 (1964) 706–723.
- [139] M.M. Radhi, W.T. Tan, M.Z.B. Ab Rahman, A.B. Kassim, Electrochemical redox of Hg<sup>2+</sup> mediated by activated carbon modified glassy carbon electrode, *Int. J. Electrochem. Sci.* 5 (2010) 615–629.
- [140] WHO, World health organization 2020, [https://www.who.int/immunization\\_standards/vaccine\\_quality/pq\\_259\\_influenza\\_seasonal\\_10dose\\_gc\\_insert.jpg?ua=1](https://www.who.int/immunization_standards/vaccine_quality/pq_259_influenza_seasonal_10dose_gc_insert.jpg?ua=1) (accessed 06 January 2020).
- [141] M.L. Bishop, J.L. Duben-Engelkirk, E.P. Fody, *Clinical Chemistry: Principles, Procedures, Correlations*, 4th Edition, Lippincott Williams & Wilkins (Eds.), Philadelphia, 2000, p. 263-266.
- [142] E.P. Randviir, C.E. Banks, Analytical methods for quantifying creatinine within biological media, *Sensors Actuators, B Chem.* 183 (2013) 239–252.
- [143] I. Pandey, P.K. Bairagi, N. Verma, Electrochemically grown polymethylene blue nanofilm on copper-carbon nanofiber nanocomposite: An electrochemical sensor for creatinine, *Sensors Actuators, B Chem.* 277 (2018) 562–570.
- [144] U. Lad, S. Khokhar, G.M. Kale, Electrochemical creatinine biosensors, *Anal. Chem.* 80 (2008) 7910–7917.
- [145] P. Chen, Y. Peng, M. He, X.C. Yan, Y. Zhang, Y.N. Liu, Sensitive electrochemical detection of creatinine at disposable Screen-Printed carbon electrode mixed with ferrocenemethanol, *Int. J. Electrochem. Sci.* 8 (2013) 8931–8939.
- [146] Y. Zuo, Y. Yang, Z. Zhu, W. He, Z. Aydin, Determination of uric acid and creatinine in human urine using hydrophilic interaction chromatography, *Talanta.* 83 (2011) 1707–1710.
- [147] Y. Yokoyama, S. Tsuji, H. Sato, Simultaneous determination of creatinine, creatine, and UV-absorbing amino acids using dual-mode gradient low-capacity cation-exchange chromatography, *J. Chromatogr. A.* 1085 (2005) 110–116.
- [148] S. Fraselle, K. De Cremer, W. Coucke, G. Glorieux, J. Vanmassenhove, E. Schepers, N. Neiryneck, I. Van Overmeire, J. Van Loco, W. Van Biesen, R. Vanholder, Development and validation of an ultra-high performance liquid chromatography-tandem mass spectrometry method to measure creatinine in human urine, *J. Chromatogr. B Anal. Technol. Biomed. Life Sci.* 988 (2015) 88–97.
- [149] K. Ponghong, N. Teshima, K. Grudpan, J. Vichapong, S. Motomizu, T. Sakai, Successive determination of urinary bilirubin and creatinine employing

- simultaneous injection effective mixing flow analysis, *Talanta*. 133 (2015) 71–76.
- [150] T. Songjaroen, T. Maturros, A. Sappat, A. Tuantranont, W. Laiwattanapaisal, Portable microfluidic system for determination of urinary creatinine, *Anal. Chim. Acta*. 647 (2009) 78–83.
- [151] C.S. Pundir, S. Yadav, A. Kumar, Creatinine sensors, *TrAC - Trends Anal. Chem.* 50 (2013) 42–52.
- [152] W.R. De Araújo, M.O. Salles, T.R.L.C. Paixão, Development of an enzymeless electroanalytical method for the indirect detection of creatinine in urine samples, *Sensors Actuators, B Chem.* 173 (2012) 847–851.
- [153] S. Yadav, A. Kumar, C.S. Pundir, Amperometric creatinine biosensor based on covalently coimmobilized enzymes onto carboxylated multiwalled carbon nanotubes/polyaniline composite film, *Anal. Biochem.* 419 (2011) 277–283.
- [154] J. Raveendran, P.E. Resmi, T. Ramachandran, B.G. Nair, T.G. Satheesh Babu, Fabrication of a disposable non-enzymatic electrochemical creatinine sensor, *Sensors Actuators, B Chem.* 243 (2017) 589–595.
- [155] P. Han, S. Xu, S. Feng, Y. Hao, J. Wang, Direct determination of creatinine based on poly(ethyleneimine)/phosphotungstic acid multilayer modified electrode, *Talanta*. 151 (2016) 114–118.
- [156] X. Gao, R. Gui, H. Guo, Z. Wang, Q. Liu, Creatinine-induced specific signal responses and enzymeless ratiometric electrochemical detection based on copper nanoparticles electrodeposited on reduced graphene oxide-based hybrids, *Sensors Actuators, B Chem.* 285 (2019) 201–208.
- [157] S. Sadeghi, M. Hosseinpour-Zaryabi, Sodium gluconate capped silver nanoparticles as a highly sensitive and selective colorimetric probe for the naked eye sensing of creatinine in human serum and urine, *Microchem. J.* 154 (2020) 104601.
- [158] Maulidiani, F. Abas, R. Rudiyanto, N.M. Hafiz Abdullah, A. Azlan, N.H. Lajis, Application of quantitative spectral deconvolution <sup>1</sup>H NMR (qsd-NMR) in the simultaneous quantitative determination of creatinine and metformin in human urine, *Anal. Methods*. 11 (2019) 5487–5499.
- [159] H. Jurdáková, R. Górová, G. Addová, A. Šalingová, I. Ostrovský, FIA-MS/MS determination of creatinine in urine samples undergoing butylation, *Anal. Biochem.* 549 (2018) 113–118.
- [160] A.R. Fernandes, P.S. De Souza, A.E. De Oliveira, A.R. Chaves, A new method for the determination of creatinine in urine samples based on disposable pipette extraction, *J. Braz. Chem. Soc.* 29 (2018) 695–700.
- [161] S.S. Sununta, P.R. Attanarat, O.C. Hailapakul, N.P. Raphairaksit, 34\_109, 34 (2018) 109–113.
- [162] W. Grochocki, M.J. Markuszewski, J.P. Quirino, Simultaneous determination of creatinine and acetate by capillary electrophoresis with contactless conductivity detector as a feasible approach for urinary tract infection diagnosis, *J. Pharm. Biomed. Anal.* 137 (2017) 178–181.

- [163] M. Suzuki, M. Furuhashi, S. Sesoko, K. Kosuge, T. Maeda, K. Todoroki, K. Inoue, J.Z. Min, T. Toyo'oka, Determination of creatinine-related molecules in saliva by reversed-phase liquid chromatography with tandem mass spectrometry and the evaluation of hemodialysis in chronic kidney disease patients, *Anal. Chim. Acta.* 911 (2016) 92–99.
- [164] H. Hou, W. Xiong, X. Zhang, D. Song, G. Tang, Q. Hu, LC-MS-MS measurements of urinary creatinine and the application of creatinine normalization technique on cotinine in smokers' 24 hour urine, *J. Anal. Methods Chem.* 1 (2012).
- [165] X. Li, X. Fang, Z. Yu, G. Sheng, M. Wu, J. Fu, H. Chen, Direct quantification of creatinine in human urine by using isotope dilution extractive electrospray ionization tandem mass spectrometry, *Anal. Chim. Acta.* 748 (2012) 53–57.
- [166] P. Nagaraja, K. Avinash, A. Shivakumar, H. Krishna, Quantification of creatinine in biological samples based on the pseudoenzyme activity of copper-creatinine complex, *Spectrochim. Acta - Part A Mol. Biomol. Spectrosc.* 92 (2012) 318–324.
- [167] Y. Wang, J. Chen, Y. Wu, Y. Chen, J. Pan, J. Lei, Y. Chen, L. Sun, S. Feng, R. Chen, Surface-enhanced Raman spectroscopy of creatinine in silver colloid, *Tenth Int. Conf. Photonics Imaging Biol. Med. (PIBM 2011)*. 8329 (2012) 83290K.
- [168] J. Zhao, H. Chen, P. Ni, B. Xu, X. Luo, Y. Zhan, P. Gao, D. Zhu, Simultaneous determination of urinary tryptophan, tryptophan-related metabolites and creatinine by high performance liquid chromatography with ultraviolet and fluorimetric detection, *J. Chromatogr. B Anal. Technol. Biomed. Life Sci.* 879 (2011) 2720–2725.
- [169] A. Zinellu, C. Carru, M.F. Usai, S. Sotgia, L. Deiana, Determination of creatinine in human serum by short-end injection capillary zone electrophoresis, *Electrophoresis.* 25 (2004) 1096–1101.
- [170] E. Pobozy, A. Radomska, R. Koncki, S. Głab, Determination of dialysate creatinine by micellar electrokinetic chromatography, *J. Chromatogr. B Anal. Technol. Biomed. Life Sci.* 789 (2003) 417–424.
- [171] A.K. Dash, A. Sawhney, A simple LC method with UV detection for the analysis of creatine and creatinine and its application to several creatine formulations, *J. Pharm. Biomed. Anal.* 29 (2002) 939–945.
- [172] V.F. Samanidou, A.S. Metaxa, I.N. Papadoyannis, Direct simultaneous determination of uremic toxins: Creatine, creatinine, uric acid, and xanthine in human biofluids by HPLC, *J. Liq. Chromatogr. Relat. Technol.* 25 (2002) 43–57.
- [173] A.P. Soldatkin, J. Montoriol, W. Sant, C. Martelet, N. Jaffrezic-Renault, Creatinine sensitive biosensor based on ISFETs and creatinine deiminase immobilised in BSA membrane, *Talanta.* 58 (2002) 351–357.
- [174] J.F. Jen, S.L. Hsiao, K.H. Liu, Simultaneous determination of uric acid and creatinine in urine by an eco-friendly solvent-free high performance liquid chromatographic method, *Talanta.* 58 (2002) 711–717.

- [175] P. Campins Falcó, L.A. Tortajada Genaro, S. Meseger Lloret, F. Blasco Gomez, A. Sevillano Cabeza, C. Molins Legua, Creatinine determination in urine samples by batchwise kinetic procedure and flow injection analysis using the Jaffé reaction: Chemometric study, *Talanta*. 55 (2001) 1079–1089.
- [176] K.J. Shingfield, N.W. Offer, Simultaneous determination of purine metabolites, creatinine and pseudouridine in ruminant urine by reversed-phase high-performance liquid chromatography, *J. Chromatogr. B Biomed. Sci. Appl.* 723 (1999) 81–94.
- [177] R. Gatti, V. Lazzarotto, C.B. De Palo, E. Cappellin, P. Spinella, E.F. De Palo, A rapid urine creatinine assay by capillary zone electrophoresis, *Electrophoresis*. 20 (1999) 2917–2921.
- [178] Z. Zhang, Y. Li, X. Liu, Y. Zhang, D. Wang, Molecular imprinting electrochemical sensor for sensitive creatinine determination, *Int. J. Electrochem. Sci.* 13 (2018) 2986–2995.
- [179] M. Zhybak, V. Beni, M.Y. Vagin, E. Dempsey, A.P.F. Turner, Y. Korpan, Creatinine and urea biosensors based on a novel ammonium ion-selective copper-polyaniline nano-composite, *Biosens. Bioelectron.* 77 (2016) 505–511.
- [180] C.H. Chen, M.S. Lin, A novel structural specific creatinine sensing scheme for the determination of the urine creatinine, *Biosens. Bioelectron.* 31 (2012) 90–94.
- [181] F. Wei, S. Cheng, Y. Korin, E.F. Reed, D. Gjertson, C.M. Ho, H.A. Gritsch, J. Veale, Serum creatinine detection by a conducting-polymer-based electrochemical sensor to identify allograft dysfunction, *Anal. Chem.* 84 (2012) 7933–7937.
- [182] P. Kumar, R. Jaiwal, C.S. Pundir, An improved amperometric creatinine biosensor based on nanoparticles of creatininase, creatinase and sarcosine oxidase, *Anal. Biochem.* 537 (2017) 41–49.
- [183] B. Khadro, C. Sanglar, A. Bonhomme, A. Errachid, N. Jaffrezic-Renault, Molecularly imprinted polymers (MIP) based electrochemical sensor for detection of urea and creatinine, *Procedia Eng.* 5 (2010) 371–374.
- [184] A.N. Kozitsina, S.S. Dedeneva, Z. V. Shalygina, A. V. Okhokhonin, D.L. Chizhov, A.I. Matern, K.Z. Brainina, Determination of urea and creatinine by chronoamperometry, *J. Anal. Chem.* 69 (2014) 758–762.
- [185] J.C. Chen, A.S. Kumar, H.H. Chung, S.H. Chien, M.C. Kuo, J.M. Zen, An enzymeless electrochemical sensor for the selective determination of creatinine in human urine, *Sensors Actuators, B Chem.* 115 (2006) 473–480.
- [186] S.S.M. Hassan, E.M. Elnemma, A.H.K. Mohamed, Novel biomedical sensors for flow injection potentiometric determination of creatinine in human serum, *Electroanalysis*. 17 (2005) 2246–2253.
- [187] J.H. Shin, Y.S. Choi, H.J. Lee, S.H. Choi, J. Ha, I.J. Yoon, H. Nam, G.S. Cha, Employing an Insoluble Oxidizing Agent for Removing Redox-Active Interferences, 73 (2001) 5965–5971.
- [188] E.J. Kim, T. Haruyama, Y. Yanagida, E. Kobatake, M. Aizawa, Disposable

- creatinine sensor based on thick-film hydrogen peroxide electrode system, *Anal. Chim. Acta.* 394 (1999) 225–231.
- [189] M.B. Mădăraș, I.C. Popescu, S. Ufer, R.P. Buck, Microfabricated amperometric creatine and creatinine biosensors, *Anal. Chim. Acta.* 319 (1996) 335–345.
- [190] C.A.T. Toloza, Spectroanalytical methods using graphene quantum dots as photoluminescent probes for the determination of analytes of biological and pharmacological interest, 2018, PhD diss., PUC-Rio.
- [191] J.F. Xu, W. Ji, Z.X. Shen, W.S. Li, S.H. Tang, X.R. Ye, D.Z. Jia, X.Q. Xin, Raman spectra of CuO nanocrystals, *J. Raman Spectrosc.* 30 (1999) 413–415.
- [192] M. Rashad, M. Rusing, G. Berth, K. Lischka, A. Pawlis, CuO and Co<sub>3</sub>O<sub>4</sub> Nanoparticles: Synthesis, Characterizations, and Raman Spectroscopy, *Science (80-. )*. 18 (2013) 556–577.
- [193] H. Teymourinia, M. Salavati-Niasari, O. Amiri, Simple synthesis of Cu<sub>2</sub>O/GQDs nanocomposite with different morphologies fabricated by tuning the synthesis parameters as novel antibacterial material, *Compos. Part B Eng.* 172 (2019) 785–794.
- [194] Y. Lei, J. Hu, Z. Zhang, Z. Ouyang, Z. Jiang, Y. Lin, Photoelectric properties of SnO<sub>2</sub> decorated by graphene quantum dots, *Mater. Sci. Semicond. Process.* 102 (2019) 104582.
- [195] Thermo Scientific XPS. <https://xpssimplified.com/elements/copper.php> (accessed 20 March 2020).
- [196] A.A. Shaikh, J. Firdaws, Badrunnessa, S. Serajee, M.S. Rahman, P.K. Bakshi, Electrochemical studies of the pH dependence of Cu(II) reduction in aqueous britton-robinson buffer solution, *Int. J. Electrochem. Sci.* 6 (2011) 2333–2343.
- [197] M.D. Benari, G.T. Hefter, Electrochemical characteristics of the copper(II)/copper(I) redox couple in dimethyl sulfoxide solutions, *Aust. J. Chem.* 43 (1990) 1791–1801.
- [198] D.M. Soares, S. Wasle, K.G. Weil, K. Doblhofer, Copper ion reduction catalyzed by chloride ions, *J. Electroanal. Chem.* 532 (2002) 353–358.
- [199] M. Mitewa, and P.R. BONTCHEV\*, A four-membered chelate complex creatinine, *Po/Yhedron Vol. 4, No. 7, Pp. I IS%1 161*, 1985 Print. Gt. Britain 0277-5387/85. 4 (1985) 1159–1161.
- [200] N.J. Fuller, M. Elia, Factors influencing the production of creatinine: Implications for the determination and interpretation of urinary creatinine and creatine in man, *Clin. Chim. Acta.* 175 (1988) 199–210.

**11**  
**Attachment**

**A**  
**Published papers**



Contents lists available at [ScienceDirect](https://www.sciencedirect.com)

Microchemical Journal

journal homepage: [www.elsevier.com/locate/microc](http://www.elsevier.com/locate/microc)



## Square-wave voltammetric determination of primaquine in urine using a multi-walled carbon nanotube modified electrode



Marlin J. Pedrozo-Peñañiel<sup>a</sup>, Joseany M.S. Almeida<sup>a</sup>, Carlos A.T. Toloza<sup>b</sup>, Dunieskys G. Larrudé<sup>d</sup>, Wagner F. Pacheco<sup>c</sup>, Ricardo Q. Aucelio<sup>a,\*</sup>

<sup>a</sup> Chemistry Department, Pontifical Catholic University of Rio de Janeiro, Rio de Janeiro, RJ, Brazil

<sup>b</sup> Department of Natural and Exact Sciences, Universidad de la Costa, Barranquilla, Colombia

<sup>c</sup> Institute of Chemistry, Fluminense Federal University, Niterói, RJ, Brazil

<sup>d</sup> MackGráphe, Graphene and Nanomaterial Research Center, Mackenzie Presbyterian University, São Paulo, Brazil



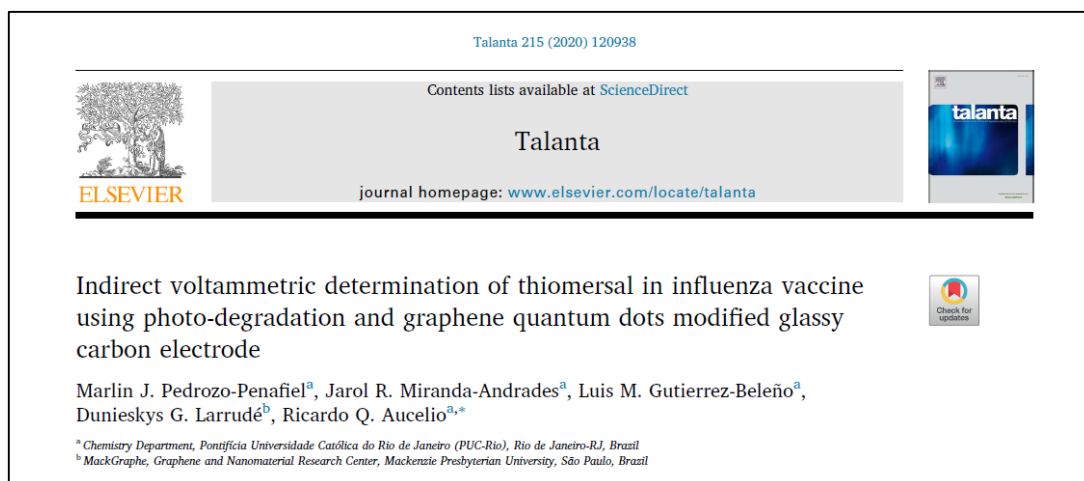
Analytical Letters



ISSN: 0003-2719 (Print) 1532-236X (Online) Journal homepage: <https://www.tandfonline.com/loi/lanl20>

## Square Wave Voltammetric Determination of 8-Hydroxyquinoline-2-Carboxaldehyde Isonicotinoyl Hydrazone (INHHQ), a Promising Metal-Protein Attenuating Compound for the Treatment of Alzheimer's Disease, Using a Multiwalled Carbon Nanotube (MWCNT) Modified Glassy Carbon Electrode (GCE)

Marlin J. Pedrozo-Peñañiel, Anna De Falco, Jarol R. Miranda-Andrades, Joseany M. S. Almeida, Dunieskys G Larrudé, Nicolás A. Rey & Ricardo Q. Aucelio



## B Participation in congress

### Oral presentation

- XXIII CONGRESO DE LA SOCIEDAD IBEROAMERICANA DE ELECTROQUÍMICA, 2018, Cusco-Peru.
- II JORNADA DE PÓS-GRADUAÇÃO E PESQUISA-DQ/PUC-Rio, Rio de Janeiro, 2018, Brazil.
- I JORNADA DE PÓS-GRADUAÇÃO E PESQUISA-DQ/PUC-Rio, Rio de Janeiro, 2017, Brazil.

### Posters

- 5º CONGRESO URUGUAYO DE QUIMICA ANALITICA (CUQA), 2018, Montevideo-Uruguai.
- 42ª REUNIÃO ANUAL DA SOCIEDADE BRASILEIRA DE QUÍMICA (42ª RASQB), 2019, Joinville, Santa Catarina, Brazil.
- III JORNADA DE PÓS-GRADUAÇÃO E PESQUISA-DQ/PUC-Rio, Rio de Janeiro, 2019, Brazil.
- XVII ENCONTRO REGIONAL DA SBQ-RIO, Rio de Janeiro, 2019, Brazil.